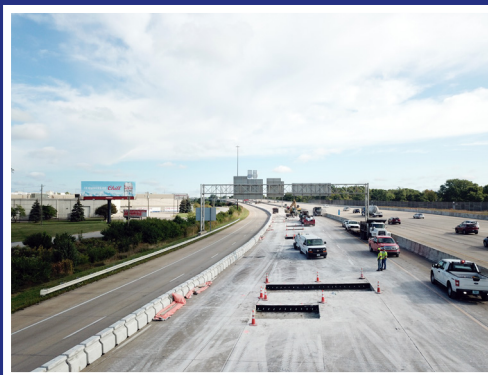


JOINT TRANSPORTATION RESEARCH PROGRAM

INDIANA DEPARTMENT OF TRANSPORTATION
AND PURDUE UNIVERSITY



Determining the Optimal Traffic Opening Timing Through an In-Situ NDT Method for Concrete Early Age Properties



Yen-Fang Su, Guangshuai Han, Na Lu

RECOMMENDED CITATION

Su, Y.-F., Han, G., & Lu, N. (2020). *Determining the optimal traffic opening timing through an in-situ NDT method for concrete early age properties* (Joint Transportation Research Program Publication No. FHWA/IN/JTRP-2020/02). West Lafayette, IN: Purdue University. <https://doi.org/10.5703/1288284317113>

AUTHORS

Yen-Fang Su

Guangshuai Han

Graduate Research Assistants

Lyles School of Civil Engineering

Purdue University

Na (Luna) Lu

ACPA Professor

Lyles School of Civil Engineering

Purdue University

(765) 494-5842

luna@purdue.edu

Corresponding Author

JOINT TRANSPORTATION RESEARCH PROGRAM

The Joint Transportation Research Program serves as a vehicle for INDOT collaboration with higher education institutions and industry in Indiana to facilitate innovation that results in continuous improvement in the planning, design, construction, operation, management and economic efficiency of the Indiana transportation infrastructure. https://engineering.purdue.edu/JTRP/index_html

Published reports of the Joint Transportation Research Program are available at <http://docs.lib.purdue.edu/jtrp/>.

NOTICE

The contents of this report reflect the views of the authors, who are responsible for the facts and the accuracy of the data presented herein. The contents do not necessarily reflect the official views and policies of the Indiana Department of Transportation or the Federal Highway Administration. The report does not constitute a standard, specification or regulation.

TECHNICAL REPORT DOCUMENTATION PAGE

| | | | |
|---|---|---|--|
| 1. Report No. FHWA/IN/JTRP-2020/02 | 2. Government Accession No. | 3. Recipient's Catalog No. | |
| 4. Title and Subtitle Determining the Optimal Traffic Opening Timing Through an In-Situ NDT Method for Concrete Early Age Properties | 5. Report Date February 2020 | | 6. Performing Organization Code |
| | 7. Author(s) Yen-Fang Su, Guangshuai Han, and Na (Luna) Lu | | 8. Performing Organization Report No. FHWA/IN/JTRP-2020/02 |
| 9. Performing Organization Name and Address Joint Transportation Research Program (SPR) Hall for Discovery and Learning Research (DLR), Suite 204 207 S. Martin Jischke Drive West Lafayette, IN 47907 | 10. Work Unit No. | | 11. Contract or Grant No. SPR-4210 |
| | 12. Sponsoring Agency Name and Address Indiana Department of Transportation State Office Building 100 North Senate Avenue Indianapolis, IN 46204 | | 13. Type of Report and Period Covered Final Report |
| 14. Sponsoring Agency Code | | | |
| 15. Supplementary Notes Conducted in cooperation with the U.S. Department of Transportation, Federal Highway Administration. | | | |
| 16. Abstract <p>Developing a reliable in-situ testing method to determine the strength of concrete for traffic opening is a critical need for INDOT, due to the fast-pace construction schedule exposes concrete pavements and/or structures undergoing a substantial loading conditions even at its early ages. Nevertheless, the current methods for determining traffic opening times are inefficient and expensive, often causing construction delays or cost overruns. To address this critical need, we propose to develop an in-situ nondestructive testing (NDT) method that enables an accurate and efficient understanding of early age properties of concrete using electromechanical impedance (EMI) method coupled with piezoelectric sensors.</p> <p>Previous literature has indicated that a piezoelectric sensor coupled with electromechanical impedance (EMI) technique can be a promising method to monitor the concrete properties changes of newly casted concrete and evaluate the condition of existed concrete at the laboratory scale. Based on the direct and indirect effect, piezoelectric materials can act both as a transducer and a receiver to capture the properties change of host structures of which it is attached to. The high frequency detection and fast response of this method will provide an accurate and reliable dataset of early age properties of concrete. This data enables us to monitor the in-situ concrete strength for determining the optimal traffic opening time.</p> <p>In this report, the feasibility of EMI sensing technology for monitoring the compressive strength gain of concrete is systematically investigated. The substantial experiments were conducted from cement paste, various mortar, concrete to field test on the interstate highway. Also, computer modeling work was performed to assist the experimental studies. Finally, the novel EMI technology can be delivered to DOT as one of the optional methods for in-situ concrete strength monitoring to determine the optimal traffic opening time.</p> | | | |
| 17. Key Words concrete, piezoelectric, EMI, open traffic, sensing traffic opening, concrete, strength, stiffness, electrotechnical impedance, sensing, non-destructive testing (NDT) | | 18. Distribution Statement No restrictions. This document is available through the National Technical Information Service, Springfield, VA 22161. | |
| 19. Security Classif. (of this report) Unclassified | 20. Security Classif. (of this page) Unclassified | 21. No. of Pages 66 including appendices | 22. Price |

EXECUTIVE SUMMARY

Introduction

Developing a reliable in-situ testing method to determine the strength of concrete for traffic opening is a critical need for INDOT due to the fast-paced construction schedule that exposes concrete pavements to substantial loading conditions, even in its early ages. The current methods for determining traffic opening times are inefficient and expensive, which often causes construction delays or cost overruns. For instance, the conventionally used testing methods, compressive test and flexural test, are very time-consuming. Furthermore, the curing conditions of the tested specimens are quite different from field conditions on the job sites. To address this critical need, we developed an in-situ nondestructive testing (NDT) method that provides an accurate and efficient evaluation of concrete strength using the electromechanical impedance (EMI) method coupled with piezoelectric sensors (PZT).

In this project, the team developed an implementable EMI sensing method using a polymer-coated piezoelectric sensor. Thousands of samples with various mix designs were tested using EMI sensing technology and compressive strength testing methods (ASTM C39) in the laboratory. A data processing method and an EMI sensing index were developed to establish a regression model that correlated sensing results with the compressive strength of concrete. COMSOL Multiphysics was employed to investigate the fundamental mechanism of EMI sensing technology. The finite element model (FEM) indicated that the EMI spectra shifted with the stiffness growth of concrete, which agreed with the experimental results. The team also conducted several trial implementations on highway construction projects (I-70, I-74, and I-465) to monitor the real-time strength development of concrete. This data can be used by INDOT engineers to determine the optimal traffic opening time of concrete pavement projects after major renovations.

Findings

In this report, the feasibility of EMI sensing technology for monitoring the development of stiffness and the compressive strength of concrete was systematically investigated. The experiments were conducted on thousands of samples with various mix designs, which ranged from cement paste, mortar, and Portland cement concrete to being field-tested on the interstate highway. Computer modeling work was performed to elucidate the fundamental mechanisms of EMI sensing technology. The findings of this project are detailed as follows:

1. Findings related to cement paste experiments.
 - In the cement paste experiments, three different mixes were conducted using ordinary Portland cement (OPC), fly ash (FA), and silica fume (SF). More than 50 specimens were tested. The results suggested that the EMI data processed through the Root Mean Square Deviation (RMSD) statistical model had a high correlation with the compressive strength of cement paste samples from the 3rd to 28th day. The correlation coefficient (R^2) of the RMSD index was 0.9.
2. Findings related to numerically modeling.
 - The EMI sensing models constructed through the finite element method indicated that the EMI spectra, such as conductance and admittance signatures, shift with the increase of elastic modulus in concrete.
3. Findings related to cement mortar experiments.
 - Based on the simulation results, the wave propagation distance at low frequency was around 11 inches. However, the possible effective sensing range of the piezoelectric sensor was around 5.5 inches in diameter.
 - For the cement mortar part, different water-to-cement ratios, types of cement, and SCMs were evaluated to examine the reliability of the EMI method for the strength test. More than 600 cubic mortar specimens were fabricated and tested. The conductance spectrum obtained from EMI measurements indicated that the spectrum shifted rightward with time due to the stiffness growth of the sample during the hydration process.
 - The results indicated that the optimal frequency range lies between 100 k to 400 kHz, which shows a better correlation using the RMSD index. It was found that the R^2 values for compressive strength versus RMSD index were higher than 0.93 for all mortar samples with different water-to-cement ratios (W/C) and two types of cement (I and III), and R^2 values were above 0.91 for elastic modulus versus RMSD index.
 - To validate whether the various mix designs would affect the accuracy of the EMI sensing method, the results from concrete with different mix designs were processed using regression analysis. It is important to point out that the combined R^2 value of lumped data was 0.92, which implied that the EMI-RMSD index was independent of the W/C.
 - Three different SCMs were blended with mortar including Class C fly ash (FA), ground granulated blast furnace slag (GGBFS), and silica fume (SF). The SCMs were used to replace part of the cement with the replacing ratio of 15%, 25%, and 35%. The results of mortar blended with GGBFS with different contents showed that the R^2 of the slag samples were over 0.96, and R^2 values were higher than 0.98 for silica fume set. The lumped EMI sensing results of the different SCMs with various replacing ratios still exhibited a high correlation coefficient of 0.90. Due to the delayed setting time of fly ash mortar, the sensor cannot be surface bonded at the same hour (4th hour) with another SCMs sample. Thus, the embedded polymer-coated sensors were used to perform the EMI test. The regression results indicated the R^2 was higher than 0.88 for the fly ash samples.
4. Findings related to concrete experiments.
 - Ten concrete mixtures commonly used by INDOT were tested in this project. Over 300 cylindrical concrete specimens were fabricated and tested. The regression results indicated that the correlation coefficient between EMI sensing index and compressive strength of all mixes was higher than 0.90.
 - Also, the regression of different sizes of the sample had minimal impact on the accuracy of EMI sensing results, as all samples with various sizes obtained the correlation value of R^2 of 0.98 between EMI sensing and compressive testing.
 - A large scale concrete slab test was also conducted as a pilot study to evaluate the feasibility of using this method for monitoring real-time concrete strength in the construction field. Regression analysis was employed to

evaluate the correlation between the index and mechanical strength. The calculated correlation factor (R^2) was 0.97, which indicated that the sensing results have a high correlation with compressive strength. The linear function was built using the regression data to estimate real-time concrete strength on construction site.

5. Findings related to field implementations.

- Field tests were conducted in three interstates in Indiana, including interstate highway I-70, I-74, and I-465. Among the field tests, I-70 and I-465 were concrete patching jobs, and I-74 was a concrete paving job. Almost a hundred sensors were embedded in the concrete pavement to monitor the real-time strength development from 1 hour to 3 days. The polyester coated sensors used in this project performed well during the harsh jobsite construction process.
- The cylinder samples were prepared to perform the compressive strength test on days 1 and 3 for comparing with the EMI sensing results. The results indicated that the one-day compressive strength of concrete from the EMI sensing method was higher than the cylinder samples because the exothermic hydration reactions of mass concrete were higher than the cylinder sample.
- The third-day EMI sensing results were a bit lower than the mechanical test results because the water evaporation speed of field concrete pavement was higher than the cylinder samples. The water was able to retain the cylinder mold to enhance the degree of hydration.

Implementations

The ultimate goal of this project was to develop a reliable NDT method to monitor the compressive strength gain of concrete pavement in order to determine the optimal traffic opening time of concrete pavement jobs. The novel EMI technology was delivered to INDOT as one of the alternative methods for in-situ concrete strength monitoring.

- To protect the PZT sensors from heavy-duty field concrete work and maintain high sensitivity, polyester-coated sensors were utilized and embedded in concrete for strength monitoring.
- The EMI signature interpreting software was built for data processing. The results show that the RMSD index was the most efficient statistical index to monitor changes in the stiffness growth and compressive strength gain of concrete.
- The optimal frequency range for EMI spectrum calculation ranged from 100 kHz to 400 kHz with a resolution of 5 kHz.
- The EMI sensing system coupled with a portable impedance analyzer was used in this study, which is convenient for field implementation.

Limitations and Future Studies

The extensive experiments conducted in this project have proved that the piezoelectric sensor-based EMI sensing method is a promising technology to monitor the compressive strength gain and stiffness growth of concrete. Nevertheless, there are still several limitations that should be pointed out for future study.

- Although the sensors used in this study are commercially available and the bonding processes were followed using standard operation procedure, a slight variation between each sensor was observed during the study. The Purdue team is working on signal processing software to eliminate small variations and improve the consistency of this testing method.
- For mass concrete, the curing temperature can reach up to $\sim 160^\circ\text{F}$, which may affect the EMI sensing results. Proper temperature compensation for signal processing is needed to increase accuracy.
- The current PZT sensor is wired to the analyzer making it difficult to obtain the strength development of concrete pavement after traffic opens. Wireless sensors and wireless impedance analyzers coupled with Wi-Fi or Bluetooth communication systems must be developed for ease of operations.

CONTENTS

| | |
|--|----|
| 1. INTRODUCTION | 1 |
| 1.1 Background | 1 |
| 1.2 Objective | 1 |
| 1.3 Organization of the Report | 1 |
| 2. LITERATURE REVIEW OF EXISTING IN-PLACE STRENGTH TESTS. | 2 |
| 2.1 Introduction | 2 |
| 2.2 Mechanical Tests for Concrete Strength Estimation. | 2 |
| 2.3 Existing In-Place Testing Method for Concrete Strength Estimation | 2 |
| 3. PIEZOELECTRIC EMI METHOD USED IN THIS STUDY. | 5 |
| 3.1 Piezoelectric EMI Methods | 5 |
| 3.2 Testing Procedure. | 6 |
| 3.3 COMSOL Modeling for EMI Testing Method | 8 |
| 4. LABORATORY TESTING. | 11 |
| 4.1 Cement Paste | 12 |
| 4.2 Cement Mortar | 12 |
| 4.3 Testing Results of Concrete Samples Using EMI Sensing vs. Compressive Strength | 17 |
| 4.4 Concrete Slab Test | 18 |
| 5. FIELD TEST ON THREE INTERSTATES IN INDIANA. | 22 |
| 5.1 Objective | 22 |
| 5.2 I-70 Field Test | 22 |
| 5.3 I-74 Field Test | 23 |
| 5.4 I-465 Field Test | 25 |
| 6. FINAL CONCLUSIONS AND RECOMMENDATIONS. | 31 |
| REFERENCES | 32 |
| APPENDICES | |
| Appendix A. Additional Data. | 34 |
| Appendix B. Publication List | 34 |

LIST OF TABLES

| Table | Page |
|--|------|
| Table 3.1 Literature of applying EMI method for hydration monitoring of cementitious material | 6 |
| Table 4.1 Composition of cement paste | 12 |
| Table 4.2 Mixture design (lbs/cyd) | 19 |
| Table 5.1 Mix design of concrete pavement on I-74 (lbs/cubic yard) | 26 |
| Table 5.2 Mix design of concrete pavement on I-465 (lbs/cubic yard) | 29 |

LIST OF FIGURES

| Figure | Page |
|---|------|
| Figure 2.1 Schematic of the setup of the rebound hammer test | 3 |
| Figure 2.2 Setup of Windsor Probe test | 3 |
| Figure 2.3 Schematic of failure zone in concrete during a probe penetration test | 3 |
| Figure 2.4 Schematic of pull-off test and potential failure location | 4 |
| Figure 2.5 The flow chart for developing the maturity curve | 4 |
| Figure 2.6 Field application of maturity test | 4 |
| Figure 2.7 The special mold and support hardware to obtain cast-in-place concrete specimen | 5 |
| Figure 3.1 EMI test setup | 7 |
| Figure 3.2 Modeling EMI spectra of PZT patch | 8 |
| Figure 3.3 Model set-up for the coupled PZT patch with the host structure | 9 |
| Figure 3.4 Stress distribution of sensor vibrating at a frequency of 100 kHz | 9 |
| Figure 3.5 Modeling EMI spectra of the host structure with different stiffness | 10 |
| Figure 3.6 Model set-up for the coupled PZT patch with the large host structure | 10 |
| Figure 3.7 Iso-contour of the total displacement at frequency of 100 kHz | 10 |
| Figure 3.8 (a) Total displacement of each point of interest (b) Zoom-in total displacement of each point of interest | 11 |
| Figure 4.1 RMSD index versus the compressive strength of all the samples at different ages | 12 |
| Figure 4.2 CC index versus the compressive strength of all the samples at different ages | 13 |
| Figure 4.3 The correlation between the RMSD and CC index with the compressive strength of all the mixes | 13 |
| Figure 4.4 Conductance signature of representative sample at different age | 14 |
| Figure 4.5 The linear correlation fitting between compressive strength with EMI-RMSD index of W/C=0.46 sample | 14 |
| Figure 4.6 The linear correlation fitting between elastic modulus (E) with EMI-RMSD index of W/C=0.46 sample | 15 |
| Figure 4.7 The correlation value (R^2) of three proposed indices for all mixes | 15 |
| Figure 4.8 The correlation between compressive strength and EMI-RMSD mortar with a different water-to-cement ratio | 16 |
| Figure 4.9 The correlation between compressive strength and EMI-RMSD of all samples | 16 |
| Figure 4.10 Regression results of mortar samples with different SCMs using the surface-bonded sensor | 17 |
| Figure 4.11 The correlation between compressive strength and EMI-RMSD of SCMs samples | 18 |
| Figure 4.12 Correlation of EMI-RMSD with compressive strength using different size of cylinder | 19 |
| Figure 4.13 Deployment of sensors | 20 |
| Figure 4.14 Experiment setup of concrete slab test | 20 |
| Figure 4.15 Admittance spectrum of concrete slab at different age | 21 |
| Figure 4.16 RMSD-Admittance index vs. compressive strength at different age | 21 |
| Figure 5.1 (a) Patching hole and (b) deployment of PZT sensors | 22 |
| Figure 5.2 Sensor bonding procedure | 22 |
| Figure 5.3 Construction procedure of concrete patching job | 23 |
| Figure 5.4 Field EMI measurement | 23 |
| Figure 5.5 Representative EMI signature on I-70 | 24 |
| Figure 5.6 Predicted compressive strength using the EMI method (I-70) | 25 |
| Figure 5.7 Dimension of new concrete pavement | 26 |
| Figure 5.8 Field test on I-74 concrete paving | 27 |

| | |
|---|----|
| Figure 5.9 Admittance spectrum of I-74 concrete pavement | 28 |
| Figure 5.10 Predicted compressive strength using the EMI method (I-74) | 28 |
| Figure 5.11 Comparison of predicted compressive strength results and mechanical test results | 29 |
| Figure 5.12 Sensor bonding and deployment | 29 |
| Figure 5.13 Admittance spectrum of I-465 concrete patching work | 30 |
| Figure 5.14 Predicted compressive strength using the EMI method (I-465) | 30 |
| Figure 5.15 The one-day cylinder compressive strength versus EMI predicted the strength | 31 |

1. INTRODUCTION

1.1 Background

Concrete pavement is commonly used in highways, streets, industrial sites, parking lots, and airports. Owing to its high strength compared to asphalt pavement concrete pavement is able to carry and distribute the traffic loadings over a wide area, which can reduce the rutting caused by heavy traffic and weathering. Concrete is made from cement, sand, aggregate, supplementary cementitious materials (SCMs), water, and other additive materials. After the aforementioned material is blended with water, the cementitious material will react with water and go through the hydration process. The strength of concrete will develop gradually. Once the strength of concrete pavement has achieved a certain strength level to accommodate traffic loads, the road or bridges can be opened for public transportation.

To determine whether the strength of concrete pavement is strong enough to carry the traffic loads, two types of testing methods are commonly used including mechanical tests and in-place tests. The conventional mechanical tests, including compressive strength test (ASTM C39) and flexural strength test (ASTM C78—Third-Point Loading, C293—Center-Point Loading, AASHTO T97), are used to evaluate the mechanical properties of concrete through breaking the sample using hydraulic press. In the field, the specimens should be prepared following the curing procedures for sampling, as described in ASTM C31, and delivered for laboratory testing at the designated age. For the compressive test, cylindrical samples are prepared and the test result is the average of at least two specimens made by the same batch of concrete and conducted at the same age. However, the results of cylinder testing cannot truly reflect the field conditions, since the strength of concrete is often determined by the degree of compaction, the internal curing temperatures, and curing conditions. Flexural strength test is another mechanical test method that often used to measure the bending capacity of concrete beams or slabs. Typically, the beam specimen is made with dimension of $6 \times 6 \times 22$ inches. The flexural strength criteria of Portland cement concrete pavement (PCCP) in Indiana should pass 570 psi, according to INDOT Standard Specifications Division 500. Nevertheless, the result of flexural test is susceptible to sample preparation procedure and the lab conditions. Also, the size and weight of specimen make it inconvenient for handling and transportation.

The in-place concrete strength testing methods have also developed to replace the molded cylinder samples. According to American Concrete Institute (ACI) 228—Non Destructive Testing committee, several methods have developed to estimate the in-place concrete strength including rebound hammer (ASTM C805), penetration resistance (ASTM C803), pullout test (ASTM C900), pull-off test (ASTM C1583), ultrasonic pulse velocity method (ASTM C597), maturity method (ASTM C1074), cast-in-place cylinder (ASTM C873), and the combined methods (ACI Committee 228, 2019). Among these

methods, the maturity method is listed in Indiana Test Methods by INDOT (ITM 402) to determine the in-place flexural strength of PCCP for opening traffic. The fundamental theory of this method is to track the temperature change during the hydration of cement. Since the strength gain of concrete depends on both curing time and temperature, the maturity function which consists of time and temperature can reflect the strength gain of PCCP. However, it requires extensive calibrations of the maturity meter, developing a maturity curve and trial batch for each different mix design. This method can be cumbersome and costly for field implementation, particularly if the project uses specialty cement.

To address the above-mentioned challenges, this study proposes to develop an in-situ nondestructive testing (NDT) method that enables an accurate and efficient understanding of early age strength of concrete using electromechanical impedance (EMI) method coupled with piezoelectric sensors. EMI method is based on the electric impedance-frequency spectra variation of the piezoelectric sensor to measure dynamic coupling response between concrete and sensor with time, which can efficiently indicate the strength gain of concrete at its early age for determining the optimal traffic opening time. The detailed theory and engineering principle of EMI method is discussed in Section 3 of this report.

1.2 Objective

This study aims to develop an in-situ NDT testing method using the piezoelectric based sensors to determine the optimal traffic opening time via monitoring the concrete strength gain. Unlike conventional destructive testing conducted at lab and/or field, EMI sensing method monitors the variations in the electro-mechanical impedance of the concrete to determine the early properties of concrete, via the induced change in electrical impedance of a piezoelectric sensor. To evaluate the feasibility, the EMI sensing method was applied on cement paste, mortar, and concrete with different supplementary cementitious materials (SCMs), different type of cement, and water-to-cement ratio were conducted. Two approaches of sensor bonding were performed including surface bonded sensor on concrete and embedding the piezoelectric sensor in concrete pavement. As such, this project provides a reliable NDT method that enables monitoring real-time strength development of concrete and determine the optimal traffic opening time of concrete pavement construction.

1.3 Organization of the Report

This report consists of six chapters. This first chapter introduces the background and objective of this research. The second chapter reviews existing concrete strength testing methods including the destructive mechanical tests and in-place NDT testing methods. The third chapter explains the working principle of EMI sensing method and details of testing procedure of

this work. The fourth chapter reports the results of laboratory testing including cement paste, mortar, concrete, and concrete slab test. The fifth chapter presents the field implementations on interstate highways. The final part concludes the works and gives the recommendations of EMI method.

2. LITERATURE REVIEW OF EXISTING IN-PLACE STRENGTH TESTS

2.1 Introduction

The quality control and quality assurance of concrete are essential to ensure the safety of concrete pavement and concrete infrastructures. To examine the quality of concrete, several tests are performed, such as slump test, air-content test, compressive strength test or flexural test, etc. Among the tests, the strength testing result is one of the most critical parameters used by engineers to determine whether the concrete is mature enough to take the loads. In general, the testing methods for determining compressive strength, including destructive mechanical tests and in-place strength tests.

2.2 Mechanical Tests for Concrete Strength Estimation

The destructive mechanical testing methods are commonly conducted to estimate the strength of concrete. For the concrete pavement, either compressive strength tests or flexural strength tests are accepted by different DOTs in the US. The compressive strength test of the cylindrical concrete specimen (ASTM C39, AASHTO T22) are designed to evaluate the strength of the specimen under compression. The uniaxial load is applied to molded concrete cylinders until failure. The compressive strength of the sample is calculated by dividing the maximum applied force by the cross-sectional area of the cylinder. The sample preparation in the field should conform to ASTM C31 testing standard and delivered to the laboratory for testing at the required age. The compressive strength result is the average value of at least two specimens made by the same batch of concrete and conducted at the same age. Due to different temperature, moisture, and curing conditions between laboratory and field, the real compressive strength of concrete pavement in the field may not be truly reflected by the lab testing.

The flexural strength test of concrete (ASTM C78, ASTM C293, AASHTO T97) is used to determine the resistance capacity of the concrete beam under bending. Since the design of pavements is based on the theory of flexural strength, some DOT are using flexural test to evaluate the quality of concrete pavement. The beam specimen is typically made with dimensions of $6 \times 6 \times 22$ inches due to the size of aggregate and it should follow the standard per ASTM C31. Two configurations of loading including third-point loading and center-point loading are used to determine the Modulus of Rupture (MR) of concrete beam. The MR result of center-point loading is higher than the third-point loading up to 15% (American Concrete Pavement

Association, 2013). In Indiana, the flexural strength criteria of Portland cement concrete pavement (PCCP) is 570 psi, according to INDOT Specifications. However, if the flexural beam specimen is not well handled and cured in the proper manner the results of flexural concrete beam testing might be lower than the requirement. Moreover, the heavy beam sample is inconvenient for handling and transportation from worksite to laboratory. Thus, many state highway agencies are adopting the compressive strength test as the evaluating method for determining traffic opening time.

2.3 Existing In-Place Testing Method for Concrete Strength Estimation

Conventionally, the mechanical performance of newly cast concrete is evaluated by measuring the field-cured concrete sample via destructive testing, such as compressive test and flexural test. Although these samples are cast and cured in the field while the concrete structure or pavement is under construction, it is still challenging to have the same compacting condition, curing condition, and bleeding behavior for the relatively small size of concrete sample and the large concrete slab. Firstly, the volume of the concrete will affect its internal temperature, particularly at the early stages. The temperature of mass concrete can rise to 50°C or higher depending on the volume. For testing, the sample must be transported to the laboratory. The improper storage or handling of the samples during this period might affect their strength performance, which makes it impossible to reflect the in-situ concrete properties. Thus, the method to determine the in-situ strength evolution of concrete is essential to obtain the correct information on concrete properties. The most commonly used in-place testing methods for evaluating the in-situ concrete strength include rebound hammer test (ASTM C805), penetration resistance method (ASTM C803), pull-out test (ASTM C900), pull-off test (ASTM C1583), ultrasonic pulse velocity (UPV) (ASTM C597), maturity test (ASTM C1074), and cast-in-place cylinder (ASTM C873).

The rebound hammer test was invented by Swiss engineer Ernst Schmidt in the 1950s. The mechanism uses the plunger of the hammer to contact the surface of the concrete (Figure 2.1). Inside the rebound hammer, there's a spring-loaded mass, when the mass impacts the plunger with the defined impact energy, this rebound and the extension of the spring is converted to the "rebound number." The number, in fact, represents the hardness of the concrete and can be further correlated to the compressive strength. Rebound hammer is a relatively simple test which does not require complicated testing procedures. However, there are many factors that affect the results, such as the smoothness of the concrete surface, and orientation of the instrument and rebound distance, etc., therefore, the result is not reliable. In addition, the ranges of compressive strength to be evaluated are limited from 1,500 to 6,000 psi.

Penetration resistance test (Windsor probe) using a power cartridge to shoot the probe with a velocity of

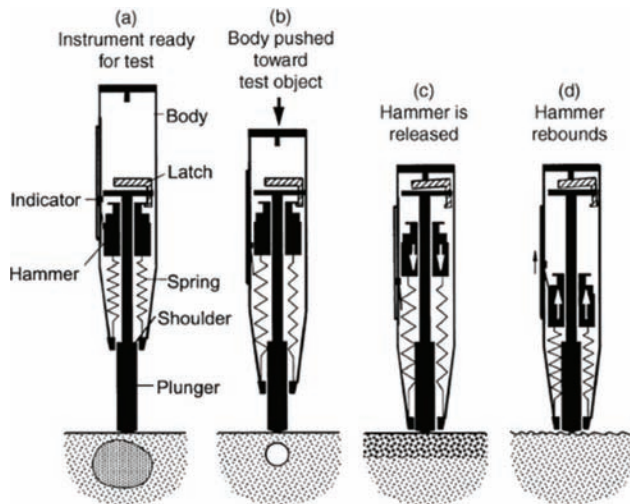


Figure 2.1 Schematic of the setup of the rebound hammer test (ACI Committee 228, 2003).



Figure 2.2 Setup of Windsor Probe test (Humboldt Construction Materials and Testing Equipment, n.d.)

183 m/s toward the concrete surface, and then measure the exposed length of the probe (Figure 2.2). The empirical correlations curves (or tables) associated with the exposed length of the probe with the strength of concrete provided by the manufacturer can be used to determine the concrete strength. Since the kinetic energy delivered by the Windsor Probe system is relatively low, the penetration depth can vary significantly depending on whether the probe encounters the coarse-aggregate region or not, as shown in Figure 2.3. Based on ASTM C803, the test is mainly recommended for the mortar fraction of the concrete sample. Also, this test is applicable only if the compressive strength of concrete is less than 4,000 psi.

The pull-out test is another widely-used technique for in-situ strength measurement. The underlying principle of the pull-out test is correlating the compression of concrete with the maximum pull-out force of the cast-in or fixed-in inserts in the hardened concrete.

To evaluate the bonding condition between new concrete and existed substrate, the pull-off test can be used according to ASTM C1583. The interfacial bonding strength between the two surfaces can be estimated using this method. The concrete surface that is to be tested should be cored to at least 0.5 in-depth. The metal disc is bonded on the testing surface with a

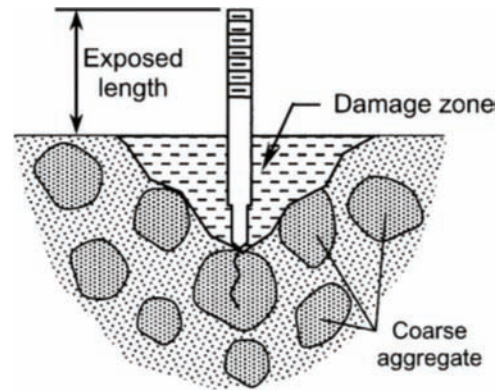


Figure 2.3 Schematic of failure zone in concrete during a probe penetration test (ACI Committee 228, 2003).

proper adhesive. After the preparation is done, the disc is pulled from the testing surface at a constant loading rate of 5 ± 2 psi until the disc is pulled-off. The failure modes and location in pull-off test can be classified into four types, including (1) failure in based concrete, (2) bond failure at new/old concrete interface, (3) failure in new concrete, and (4) disc bond failure as Figure 2.4 shown. The strength of pull-off test is averaging the failure strength with the same failure location. Nevertheless, these methods mentioned above will damage the concrete more or less, which must be repaired.

The ultrasonic pulse velocity (UPV) test is a popular testing method since being invented. The physical principle of the UPV method measures the change of velocity or the attenuation of the ultrasonic wave to evaluate the properties of cementitious materials. Zhang et al. (2009) investigated ultrasound to monitor the setting and hardening process of cementitious material made with various mineral admixtures (fly ash, slag, and silica fume). The result shows that the UPV can identify different hydration rates due to the change of mixtures and temperatures. As for the hydration of the cementitious materials during very early age, the mortar gradually transforms from a liquid stage, transition stage (partially solidified) to a solid stage. The ultrasonic wave reflection can be used to detect the microstructure of the mortar (Voigt, 2005). Nonetheless, the ultrasonic pulse velocity method requires that two transducers be placed on the opposite sides of the sample to get an accurate result. This would limit the feasibility of practical applications (Voigt, 2005). It's worth mentioning that the relationship between UPV results and compressive strength will vary with the different concrete mixes (e.g., different types of cement, aggregate, or supplementary material usage, etc.). Hence, empirical data is needed for practical applications.

The maturity test is another commonly used method to evaluate early age concrete hydration via monitoring the temperature difference of concrete. The premise of this method is that the concrete strength gain is attributed to the exothermal chemical reaction of cementitious materials (e.g., cement, supplementary materials) and water. Different complicated reactions are involved

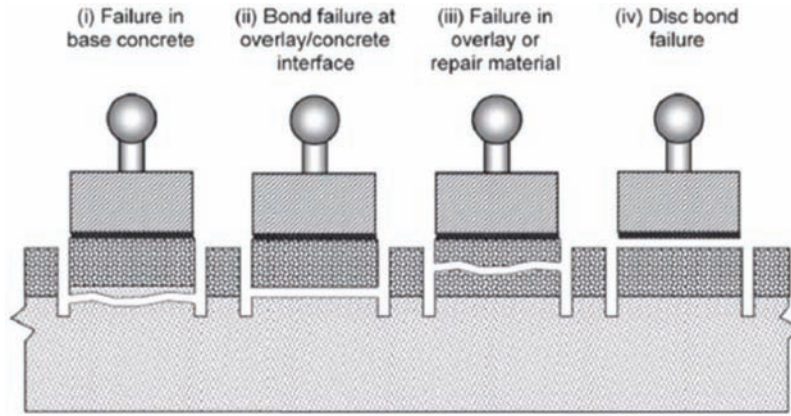


Figure 2.4 Schematic of pull-off test and potential failure location (ACI Committee 228, 2003).

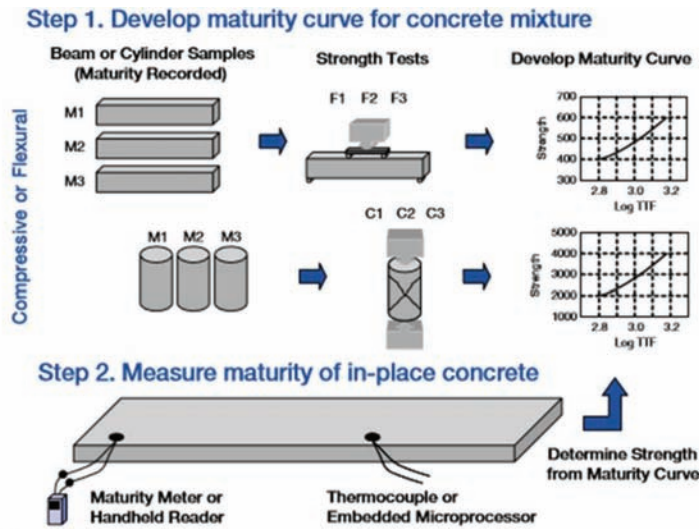


Figure 1. Schematic of maturity testing.

Figure 2.5 The flow chart for developing the maturity curve (American Concrete Pavement Association, 2015).

in this process, including hydration of cement, pozzolanic reaction, and secondary hydration. The interdependent chemical reactions were initiated as soon as the water was blended with the cementitious materials. The maturity method utilizes temperature history to correlate the strength gain of concrete. The standard ASTM C1074 provides an instruction of a procedure to evaluate concrete strength using the maturity method. As Figure 2.5 shows, before concrete construction begins, the maturity curve for concrete mixture should be developed using compressive test or flexural test results to correlate with maturity index. The maturity functions can be used to calculate the maturity index as Equation 2.1 and Equation 2.2 presented:

$$M(t) = \sum (T_a - T_0) \Delta t \quad (\text{Eq. 2.1})$$

$$t_e = \sum e^{-Q/(T_a - T_s)} \Delta t \quad (\text{Eq. 2.2})$$

where $M(t)$ is temperature-time factor at age t (deg-days or deg-h); Δt is a time interval (days or h); T_a is average



Figure 2.6 Field application of maturity test (Papworth Construction Testing Equipment, n.d.).

concrete temperature during time interval Δt ; T_0 is datum temperature; T_e is equivalent age at a specified temperature T_s (days or h); Q is activation energy divided by the gas constant (K); T_s is specified

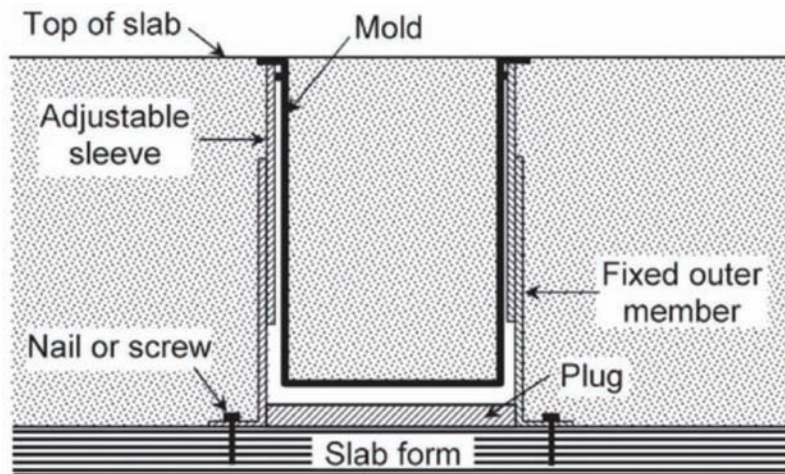


Figure 2.7 The special mold and support hardware to obtain cast-in-place concrete specimen (ACI Committee 228, 2003).

temperature (K). Both approaches are acceptable to quantify the combined effects of temperature and time in the temperature history.

After the strength-maturity curve is developed, this system can be used for the in-place concrete maturity measuring. Figure 2.6 shows the practical execution of the maturity test. A thermocouple is embedded in the concrete, and the temperature will be recorded using the data logger. The maturity test is relying on established strength-maturity curves in the laboratory for application. The laboratory results always have considerable variation compared with the results obtained from the in-situ field due to the influence of ambient temperature. Also, it needs to be calibrated each time the concrete mix change. Therefore, it is inconvenient for field implementations.

Cast-in-place cylinders are described in ASTM C873 to estimate the in-place concrete strength. This method can obtain the cylindrical concrete sample from newly-constructed concrete without core-drilling. The individual molds, as Figure 2.7 shown are designed to be placed in slab before concrete casting. The sleeve can be adjusted in accordance with the thickness of concrete. The cast-in-place concrete cylinder will experience a similar temperature history, consolidation, and curing condition with the main concrete structure. Spalvier et al. (2019) reported that the strength of cast-in-place concrete samples was higher than that of cored sample around 5% to 20%.

3. PIEZOELECTRIC EMI METHOD USED IN THIS STUDY

3.1 Piezoelectric EMI Methods

Piezoelectric materials based electromechanical impedance (EMI) technique has been proved feasible for structure health monitoring for metallic and non-metallic structures. It has also attracted some attention for both properties monitoring and damage detection of the concrete structure. Due to the direct and inverse piezoelectric effect, piezoelectric materials can act as

sensors, actuator, and transducer (Ghafari et al., 2018; Gu et al., 2006; Su et al., 2018). Among them, the piezo ceramic material—PZT (lead zirconate titanate)—has been widely used due to its outstanding piezoelectric properties such as high charge constant and sensitivity, fast response, long-term stability and low-cost (Park et al., 2003).

Shin et al. (2008) first used the EMI sensing technique for damage detection of concrete to material properties monitoring. They tracked the concrete strength gain at the age of 3 and 28 days. It was found that the EMI signature will shift from left to right as the time increases due to the hydration process change the mechanical properties of concrete. Tawie et al. (2010) has demonstrated the EMI technique for concrete strength monitoring on concrete with high water-to-cement ratio and has discovered that the EMI result showed an exponential increase in the frequency shift at the age from 3 to 28 days from their curve fitting result. Wang et al. (2011) designed the asphalt lacquer coated PZT sensor for the concrete strength monitoring. The testing age is from the first day until 28 days after the concrete in cast. They concluded that the post statistic treatment of real admittance could better reflect the compression gain of concrete than the imaginary admittance. Lu et al. (2012) proposed a PZT based sensor called “Smart Probe” to improve the efficiency of monitoring the concrete properties. The Smart Probe was made by using the aluminum beam with the PZT bonded on the surface and partially embedded into concrete for measurement. The experimental results exhibited that the resonance peak at the frequency range from 5 k to 30 kHz of sensor can efficiently monitor the strength gain of mortar. Ghafari et al. (2018) evaluated the compressive strength gain of cement paste with different supplementary cementitious materials (SCMs), including fly ash and silica fume. The results presented the feasibility of utilizing EMI-RMSD index on monitoring strength gain progress for the cementitious materials incorporated with SCMs at the age from 1 day to 28 days. Negi et al. (2018) discussed the efficiency of embedded orientation of PZT sensor in

concrete. They concluded that the inclined orientation (45°) is the least efficient compared with the horizontal and vertical placed (0° and 90°).

Up to now, using PZT based EMI method on concrete strength monitoring from 1 day to 28 days has been well studied. Nevertheless, there are very limited research conducted on understanding the EMI methods for in-situ monitoring of the very early age properties of cementitious materials. Tawie and Lee (2010) bonded the PZT sensor on the steel bar in the reinforced concrete (RC) to monitor the bonding properties between concrete and rebar at the age from 1 hour to 168 hours after casting. The frequency shift (%) of the conductance spectrum was accessed as the index to quantify the bonding condition. The results revealed that the frequency shift index would be affected by varying the w/c ratio and curing temperature. Kong et al. (2013) fabricated a sandwich structural PZT transducer (called smart aggregate) to characterize the concrete hydration at very early age (0–20 hours). The signal response from the sinusoid wave with a constant frequency of 90 kHz and 100 kHz can successfully differentiate the three-stages of concrete hydration. Providakis et al. (2013) proposed the reusable Teflon-based PZT transducer to monitor the early-age concrete hydration process. The sensor was bonded on the top of concrete sample and connected with the low-cost system-on-chip impedance spectrometer (AD5933), which has the potential for wireless sensing. The modified RMSD index decreased with the time elapsed after 9 and 12 hours after concrete casting. Narayanan et al. (2017) embedded the multi-layer protection PZT sensor into the cement mortar to track the impedance change of materials. Using EMI signature, they have analyzed several early age properties including setting time, Young’s modulus and isothermal calorimetry measurement. It has concluded that the magnitude changes in the impedance of PZT

and shift of frequency can be reflected as the changes of the stiffness of the cement mortar. Visalakshi et al. (2018) also bonded the PZT sensor on the rebar and embedded into concrete to monitor the concrete hydration. They proposed a hydration index (h) which comprise of stiffness concept extracted from the admittance signature to monitor the hydration of concrete. The hydration parameter increased as the sample aged, which means it can capture the evolution of hydration of concrete. Table 3.1 summarizes the current literature of hydration related monitoring of cementitious materials via using EMI technique.

Previous research has shown the potential of using the PZT based EMI method on monitoring the hydration or strength development of cementitious materials. However, the methodology of each work is different such as size of PZT, configuration of sensor, tested materials, data processing method, and curing condition of concrete. In this project, the team aims to develop an accurate and reliable PZT based EMI testing method to monitor the strength of concrete pavement for opening to traffic. The laboratory validation experiments are started from simple cement paste, mortar to concrete. The standard operating procedure of EMI technique is established.

3.2 Testing Procedure

3.2.1 Principles of piezoelectric sensor based EMI method

An EMI signature is dependent on a direct and inverse piezoelectric effect of a piezoelectric material. During an EMI test, the impedance analyzer discharges a sinusoidal AC voltage (500 mV) to excite a bonded PZT patch with a high-frequency range between 5 k and 1,000 kHz. The analyzer then records the response

TABLE 3.1
Literature of applying EMI method for hydration monitoring of cementitious material

| Reference | Materials | Dimension/Configuration of PZT | Sample (Testing) Age |
|-------------------------|------------------------|--|---|
| Shin et al., 2008, | Concrete | 10 × 10 × 0.2 mm/surface bonded | 3, 5, 7, 14, 28 days |
| Tawie et al., 2010 | Concrete | 10 × 10 × 0.5 mm/surface bonded | 3, 7, 14, 28 days |
| Tawie et al., 2010 | Concrete | 10 × 10 × 0.3 mm/embedded–bonded on steel bar | 1, 3, 6, 9, 12, 24, 72, 168 hrs |
| Annamdas et al., 2010 | Concrete | 10 × 10 × 0.2 mm/embedded–epoxy wrapped | 2, 5, 8, 15, 26, 31 days |
| Wang et al., 2011 | Concrete | 8 × 8 × 0.3 mm/embedded–asphalt lacquer coated | 1, 2, 3, 4, 7, 14, 21, 28 days |
| Kim et al., 2013 | High strength concrete | 20 × 20 × 0.5 mm/surface bonded | 3, 5, 7, 14, 21, 28 days |
| Kong et al., 2013 | Concrete | 15 × 15 × 0.3 mm/embedded–sandwich with two marble blocks | 0–20 hrs |
| Providakis et al., 2013 | Concrete | 10 × 10 × 0.2 mm/ partially embedded–teflon-based enclosure | 3, 6, 9, 12, 15, 18, 21, 24 hrs–28 days |
| Wang et al., 2014 | Concrete | 8 × 8 × 0.3 mm/embedded–asphalt lacquer coated | 1, 2, 3, 4, 7, 14, 21, 28 days |
| Narayanan et al., 2017 | Mortar | 20 × 20 × 1 mm/embedded–thermosetting epoxy coated | 1, 8, 16 hrs; 2, 5, 12, 16, 20, 22, 25, 28 days |
| Lu et al., 2017 | Concrete | 10 × 10 × 0.3 mm/partially embedded– surfaced bonded on the aluminum plate | 1, 2, 3, 7, 14, 28 days |
| Ghafari et al., 2018 | Cement paste (SCMs) | 10 × 10 × 0.2 mm/surface bonded | 1, 3, 7, 14, 28 days |
| Negi et al., 2018 | RC | 10 × 10 × 0.3 mm/embedded–bonded on cement block | 3, 7, 14, 21, 25, 28 days |
| Visalakshi et al., 2018 | Concrete | 10 × 10 × 0.3 mm/embedded–bonded on steel bar | 1–12 hrs, 1–28 days |

of the PZT's electromechanical dynamic impedance. The mechanical impedance of the host structure (Z_s) and that of PZT sensor (Z_a) can induce an electrical impedance of PZT, which is the reciprocal of admittance (Y). The admittance response is governed by the PZT's theoretical admittance model shown below (Su, Han, Amran, Nantung et al., 2019):

$$Y = G + Bj = 4w \frac{l^2}{h} \left[\varepsilon_{33} - \frac{2d_{31}^2 Y^E}{(1-\nu)} + \frac{2d_{31}^2 Y^E}{(1-\nu)} \left(\frac{Z_a}{Z_a + Z_s} \right) \frac{\tan kl}{kl} \right] \quad (\text{Eq. 3.1})$$

Where the admittance is a function of conductance (G), susceptance (B) with its imaginary unit (j), PZT sensor dimension (w , l , and h —width, length, and height), electrical permittivity (ε_{33}), piezoelectric coefficient (d_{31}), Young's Modulus (Y^E), Poisson's ratio (ν), and wavenumber (k). Except for Y , G , Z_a , and Z_s , all variables are a material property.

3.2.2 EMI test conducted in this study

In the EMI test, two different configurations of the sensors were used including surface bonded sensor and embedded sensor. For the surface bonded configuration, the host sample is surface mounted by a PZT patch with a fast-set epoxy (5 minutes set, cured in 1 hour) as the binding agent. On the other hand, the embedded sensor is located in the center of mold or the designated location before the casting of cementitious materials. The wires of PZT sensors were attached to an impedance analyzer, which is linked to a computer equipped with a data acquisition software (Figure 3.1). Two types of impedance analyzers were utilized, as Figure 3.1 (a) and (b) show. Figure 3.1 (a) illustrates the EMI set up using an impedance analyzer (1260 Solartron) with a computer equipped with the data acquisition software. The sensor was connected with impedance analyzer using kelvin clip wires. Figure 3.1 (b) is the portable

sensing system using the impedance analyzer (AIM-4300) with laptop. The alligator clip wires are used to connect the sensor with the device.

3.2.3 Data processing

For each sample, the conductance signature is further quantified by referencing the baseline signature via the three different statistical models, including root mean square deviation (RMSD), correlation coefficient deviation (CCD), and mean absolute percentage deviation (MAPD). The equations are shown below:

$$RMSD(\%) = \sqrt{\frac{\sum_{i=1}^N (G_i - G_{bl})^2}{\sum_{i=1}^N (G_{bl})^2}} \quad (\text{Eq. 3.2})$$

$$CCD(\%) = 100 - \left\{ \frac{1}{N \sigma_{G_i} \sigma_{G_{bl}}} \sum_{i=1}^N [(G_i - \bar{G}_i) \cdot (G_{bl} - \bar{G}_{bl})] \right\} \quad (\text{Eq. 3.3})$$

$$MAPD(\%) = \frac{1}{N} \sum_{i=1}^N \left| \frac{(G_i - G_{bl})}{G_{bl}} \right| \quad (\text{Eq. 3.4})$$

Where G_i is the spectrum of different curing age, G_{bl} is the baseline spectra obtained at the designated age, N signify the number of data points in the EMI spectra, σ and \bar{G} stand for the standard deviation and the mean, respectively.

3.2.4 Compressive test

While the EMI test runs, conventional compressive tests are conducted on three identical specimens of each mix according to the ASTM C109 for the cubic sample and ASTM C39 for cylindrical samples. The samples are demolded after the initial setting time with dexterity for very early age testing. The test is performed by positioning the sample in a uniaxial load frame. At each

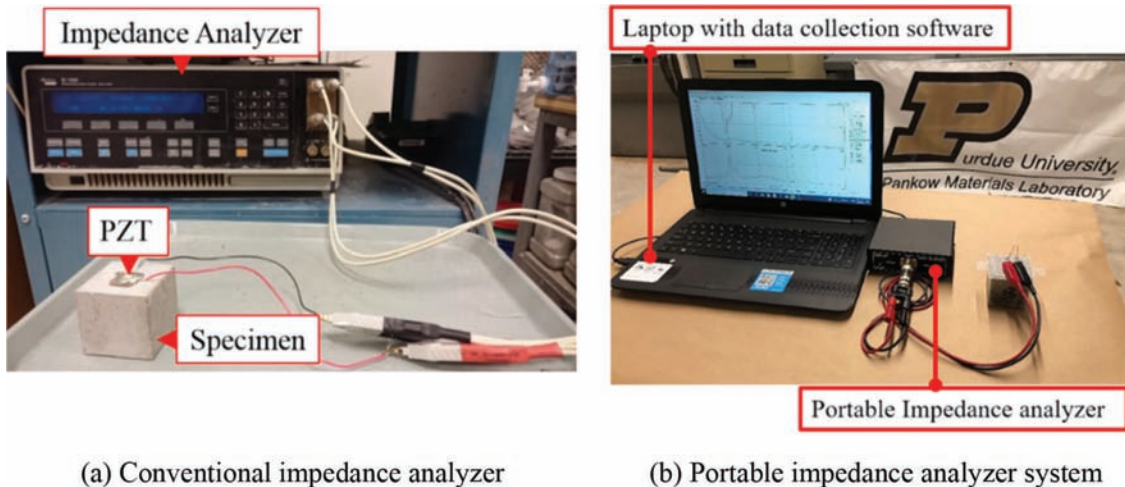


Figure 3.1 EMI test setup.

curing age of interest, the peak stresses of the three specimens are recorded and averaged. EMI tests and compressive tests are conducted simultaneously at the curing age. The first conducted EMI measurement serves as the baseline for the EMI signature of the subsequent test. In this method, every change in the signature of a sample will be referenced to the baseline signature using the three statistical indices. This is also a way of quantifying the signature change as the sample aged. At each curing age of interest, the signature change from the EMI technique is compared to the data of the compressive test via regression correlation analysis.

3.3 COMSOL Modeling for EMI Testing Method

3.3.1 COMSOL modeling overview

COMSOL Multiphysics was used in this study to investigate the mechanism of EMI sensing technology. COMSOL Multiphysics is a finite element method (FEM) based software for simulation designs, devices, and processes in all fields for engineering, manufacturing, and scientific research. In this work, the piezoelectric device module from Micro-electromechanical systems (MEMS) was utilized to simulate the PZT sensor vibrating with the concrete host structure at different frequencies. Both free and coupled behavior of the PZT patch was numerically analyzed.

3.3.2 Numerical analysis of the free PZT patch

The free PZT patch model was established according to the real dimension of the patch (length = 10 mm, width = 10 mm, thickness = 0.2 mm). The material properties were first provided by the PZT vendor (PI ceramics) and then slightly calibrated according to the real experiment result. One of the 10 mm square faces of the free PZT was applied a terminal voltage of 500 mV, and the opposite face was grounded. The admittance obtained from the recommended frequency range from 100 kHz to 400 kHz was then calculated.

Figure 3.2 shows the modeling result of PZT patch. The modeling result has a good agreement with the experiment result. The stress distribution when PZT vibration at different frequencies can be found in Figure A.1. The deformation mainly happens in the two main directions (x and y) due to the size effect.

3.3.3 Numerical analysis of coupled PZT patch

The PZT-host structure interaction was further analyzed. A numerical model of the PZT patch either surface bonded or embedded in the host structure was established. Figure 3.3 shows the model set-up for both surface bonded sensors and embedded sensors. In order to save the computational cost, one-quarter of the structure was calculated by adopting the symmetric boundary shown in Figure 3.3. The width, length, and thickness of the host structure are all fixed at 50 mm. The stiffness of the host structure was first set up to 10 GPa.

Figure 3.4 (a) and (b) show the stress distribution of the surface bonding sensor and embedded sensor vibrating with the host structure under frequency of 100 kHz. The stress distribution figure at different frequency can be found in Figure A.2 and Figure A.3. It can be observed that the host structure starts vibrating when the sensor is excited by the voltage. The bulk properties of the host structure influence the sensor's vibrating and the EMI spectra of the PZT sensor.

Then, the modeling of the host structure with different stiffness was performed. Figure 3.5 is the modeling admittance EMI spectra. The increasing stiffness emulates the hardening behavior of early age concrete as it aged. The admittance has a downward shift as concrete aged, which proved the feasibility of using the piezoelectric sensor to evaluate the mechanical properties of the concrete host structure.

3.3.4 EMI sensing range estimation

The EMI response of the PZT sensor coupled with larger host structure was future numerically analyzed.

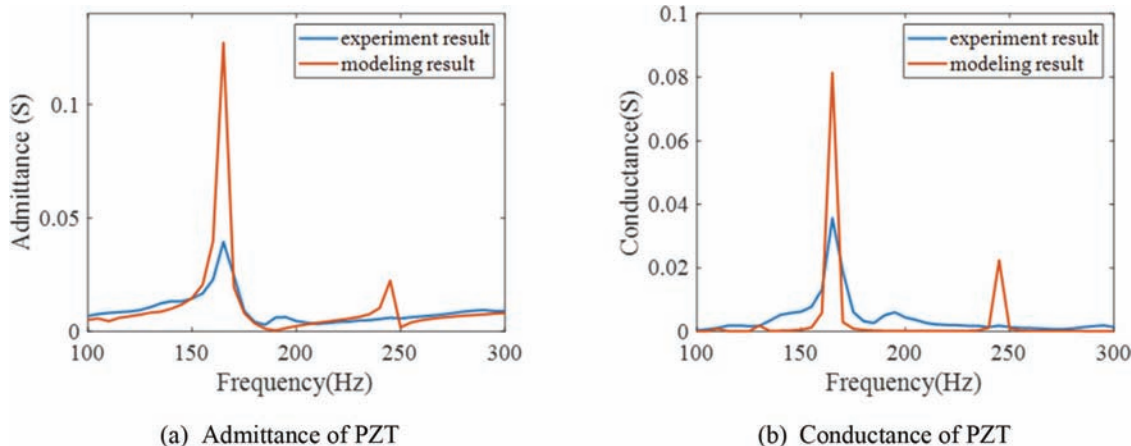


Figure 3.2 Modeling EMI spectra of PZT patch.

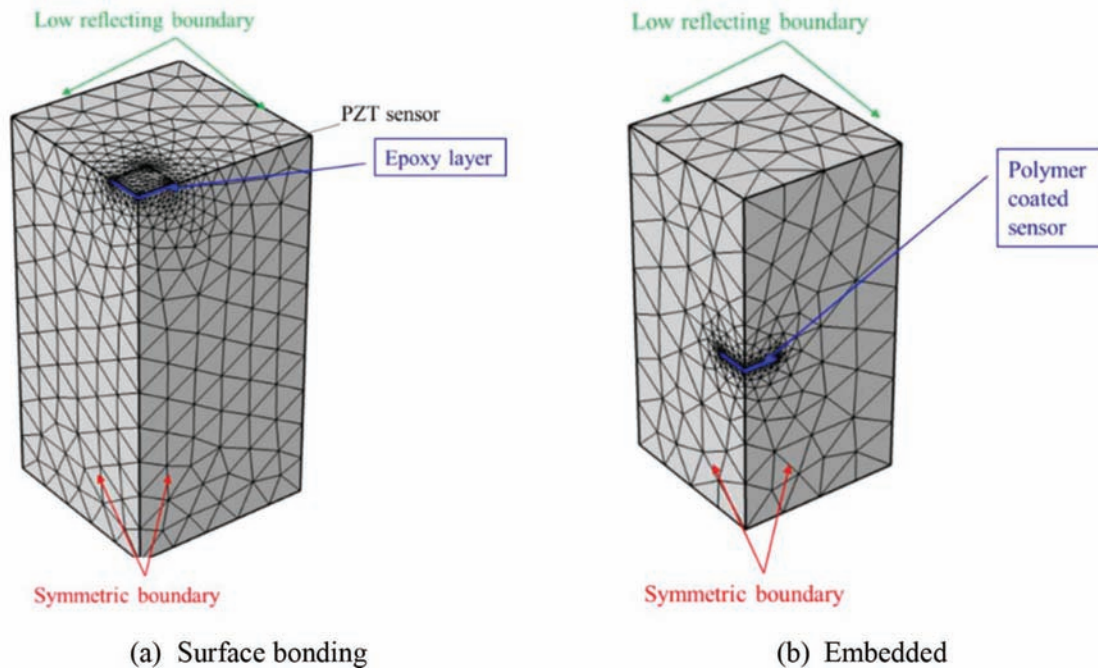


Figure 3.3 Model set-up for the coupled PZT patch with the host structure.

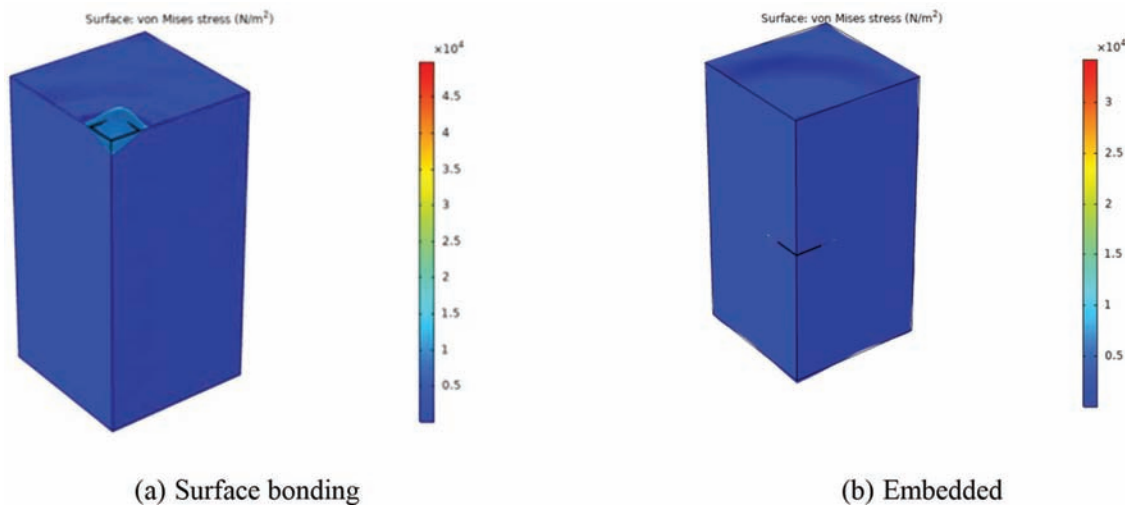


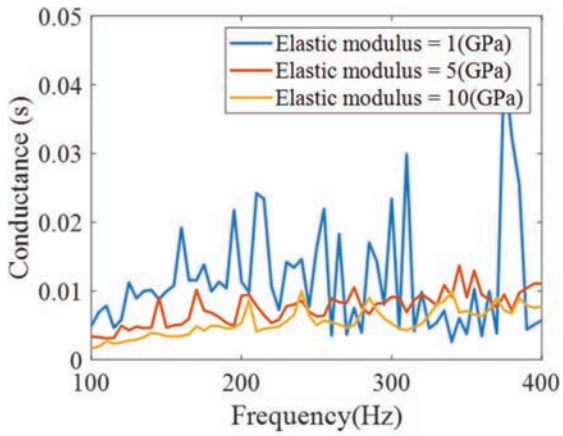
Figure 3.4 Stress distribution of sensor vibrating at a frequency of 100 kHz.

To emulate the sensor’s behavior in the mass concrete, a PZT sensor was embedded in the concrete beam. The length, width, and thickness of the concrete beam is 6 inches, 6 inches, and 22 inches. Figure 3.6 is the model setup. To save the computational cost and enhance the efficiency, one fourth of the whole model was calculated. The simulation calculated the PZT sensor’s vibrating from 100 kHz to 600 kHz. The total displacement of each point of interest was compared to estimate the effective sensing range.

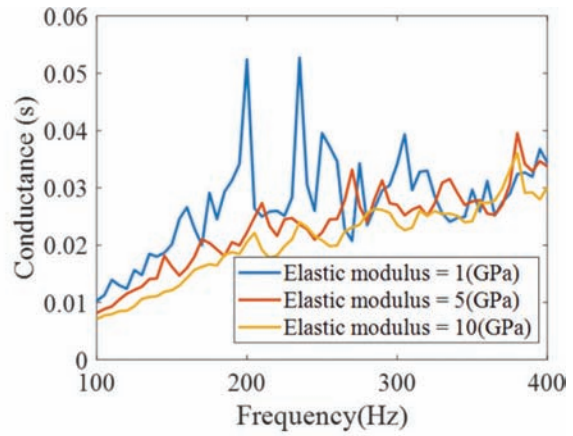
Figure 3.7 shows the substrate’s iso-contour of the total displacement at different frequency. As the frequency increased, the range of iso-contour decreased. Figure 3.8 (a) quantitatively analyzed the total

displacement of each point of interest. As Figure 3.8 (b) shows, higher frequency can cause larger displacement in the range which is relatively close to the sensor. A clear attenuation was also observed in the range which is relatively distant to the sensor. The simulation concluded that the sensing range strongly depend on the frequency range. As for the frequency range recommended by this work (100 kHz to 400 kHz) the estimated sensing range is within a diameter of 5.5 inches. However, the wave propagation distance at low frequency (below 200 kHz) is around 11 inches.

In closing, COMSOL modeling was first validated by the free PZT sensor. The coupled PZT sensor EMI response was then calculated. This has indicated that the



(a) Modeling EMI spectra of surface bonded PZT



(b) Modeling EMI spectra of embedded PZT

Figure 3.5 Modeling EMI spectra of the host structure with different stiffness.

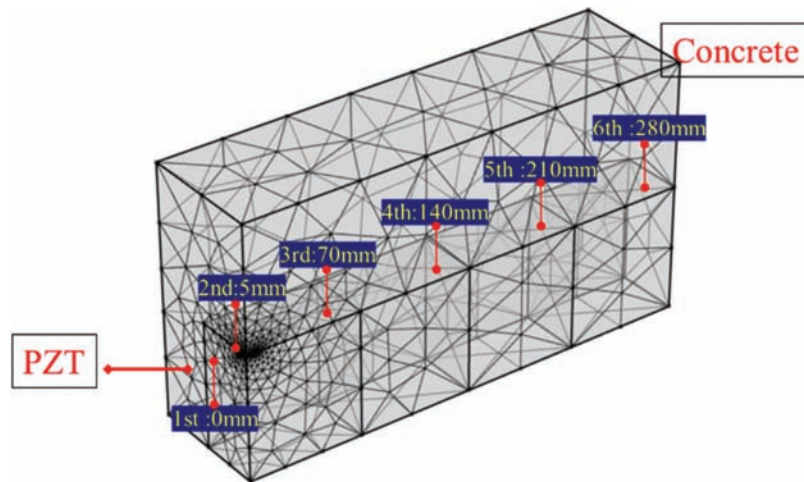


Figure 3.6 Model set-up for the coupled PZT patch with the large host structure.

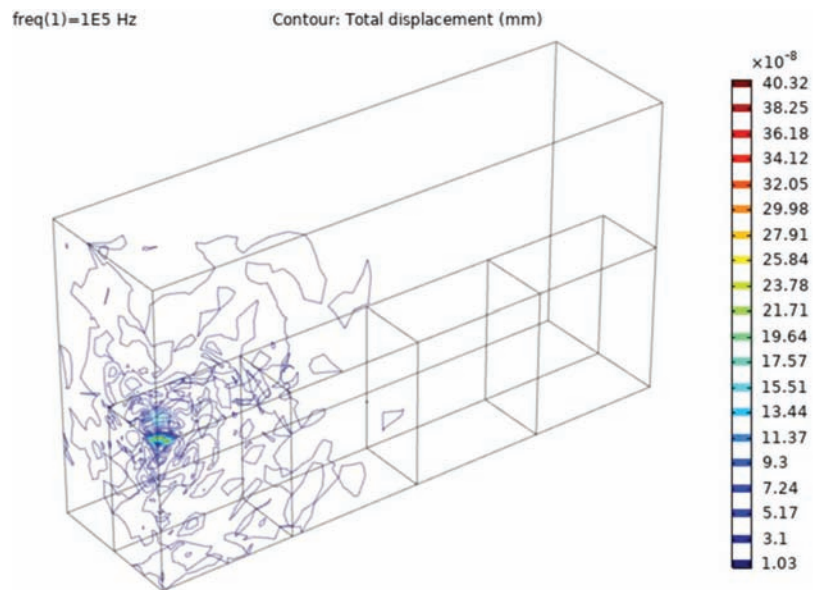
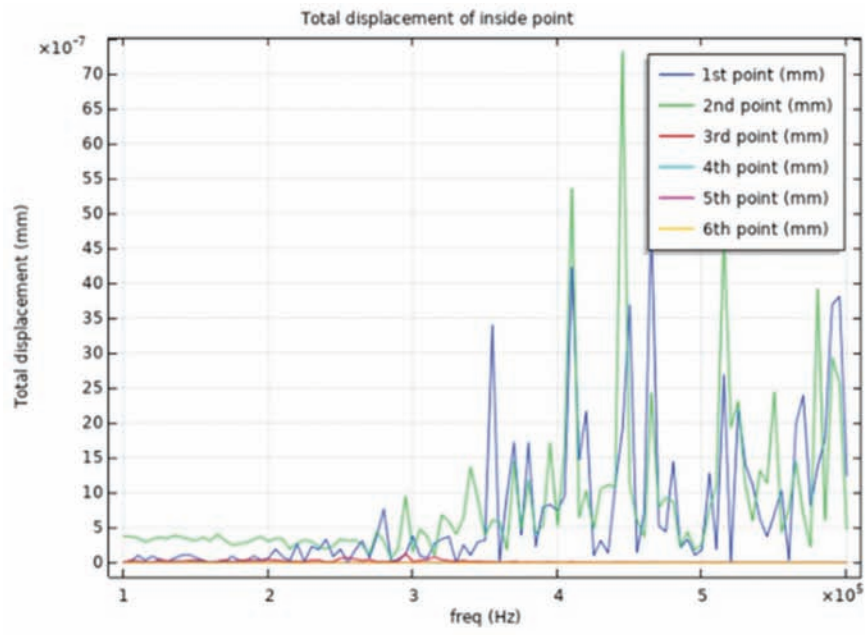
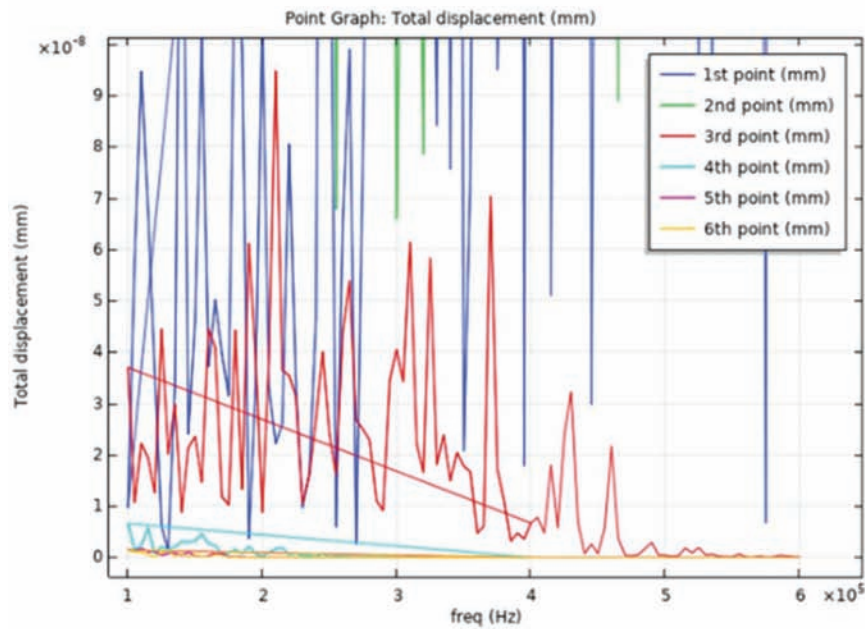


Figure 3.7 Iso-contour of the total displacement at frequency of 100 kHz.



(a)



(b)

Figure 3.8 (a) Total displacement of each point of interest and (b) zoom-in total displacement of each point of interest.

EMI signals from coupled PZT sensor has the ability to estimate the strength of the host structure. In addition, the simulation result has provided the estimated sensing. However, the result still needs to be validated by proper experimental method.

4. LABORATORY TESTING

To develop the EMI technology on concrete strength monitoring and verify the feasibility, we started from

the basic cement paste and gradually moved to cement mortar and concrete. More than a thousand specimens were conducted systematically with various mixes of design in the laboratory. The EMI signatures are measured with compressive test conducted simultaneously at the age of interest to validate the EMI sensing result. Due to the conditions of laboratory scaled cubic/cylindrical samples are different from the large-scaled mass concrete, the large concrete slab was also conducted in this study.

4.1 Cement Paste

4.1.1 Objective

Cement paste consists of cement and water, which is the basic binder of concrete. The hydration of cement paste is well investigated; thus, starting from cement paste is a reasonable first step for developing the new sensing technology.

4.1.2 Experiment and results

In this project, a series of cement paste experiments were performed including the SCMs (supplementary cementitious materials) blended cement paste. Three different mixes were conducted using ordinary Portland cement (OPC), fly ash (FA), and silica fume (SF). The composition of cement paste is shown in Table 4.1. For the SCMs paste, OPC was replaced by FA and SF at a dosage level of 10% by mass of binder. The water to binder ratio was kept constant for all the mixes at 0.30. The 2" cubic specimens were prepared for test.

The EMI test started at the 1st day as a baseline, and the signals are taken from at the 3rd, 7th, 14th, and 28th day. The compressive test of cubic specimens was conducted from the 3rd to 28th day at the same time.

TABLE 4.1
Composition of cement paste

| Mix | OPC | FA | SF | W/B ¹ |
|------------------|-----|-----|-----|------------------|
| REF ² | 1 | 0 | 0 | 0.3 |
| FA-paste | 1 | 0.1 | 0 | 0.3 |
| SF-paste | 1 | 0 | 0.1 | 0.3 |

¹Water-to-binder ratio.

²OPC paste as reference (REF).

The RMSD and CCD statistical models were used to determine the relationship between the index and the compressive strength. Figure 4.1 and Figure 4.2 plots the RMSD index and CC index versus compressive test results at different ages, respectively. As can be seen, the RMSD and CC index of each mix tends to increase as the compressive strength increase with time. However, the CC index shows relatively more significant deviation than RMSD index for fitting the real compressive strength results.

The regression analysis was performed to evaluate the linear fitting of each index versus compressive strength. The correlation coefficient (R^2) is used to determine the regression results of each index as Figure 4.3 shows. The R^2 of the RMSD index is 0.9 which performed better fitting than the CC index of 0.54.

4.2 Cement Mortar

4.2.1 Objective

The cement paste experiments have provided the feasibility of EMI sensing technology to monitor the compressive strength gain with time. However, the cement paste is relatively a simple system. Thus, mortars consist of binder (cementitious materials), sand, and water are being investigated in this part. More than 600 cubic mortar specimens with different water-to-cement ratio, types of cement, and SCMs were conducted to examine the EMI method in different mixture design.

4.2.2 Experiment—Mortar with different water-to-cement ratio and types of cement

4.2.2.1 Experiment design and materials. Type I (ordinary) and type III (high early strength) Portland cement are both used as the binder of 2" cubic

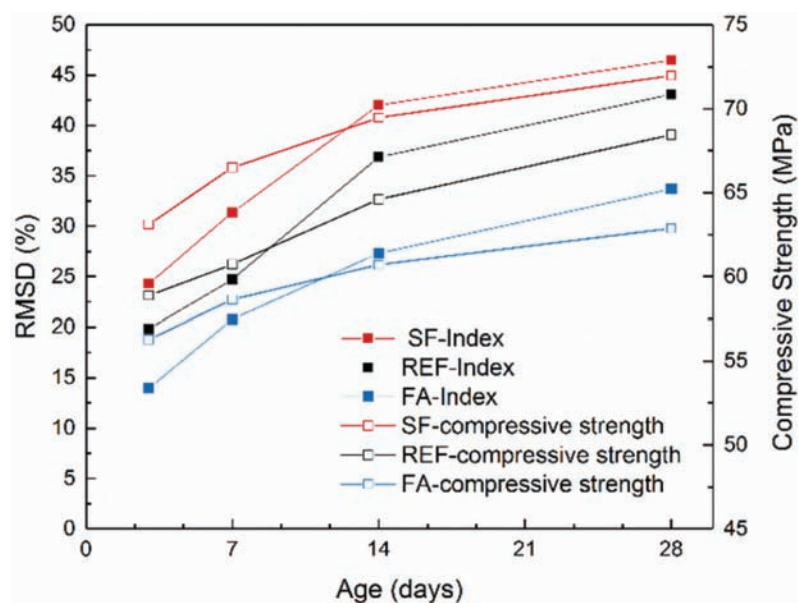


Figure 4.1 RMSD index versus the compressive strength of all the samples at different ages (Ghafari et al., 2018).

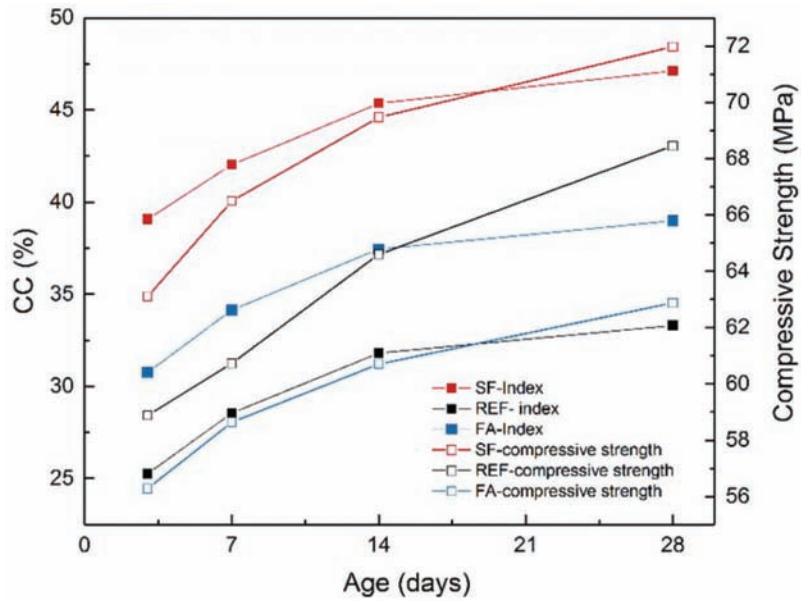


Figure 4.2 CC index versus the compressive strength of all the samples at a different age (Ghafari et al., 2018).

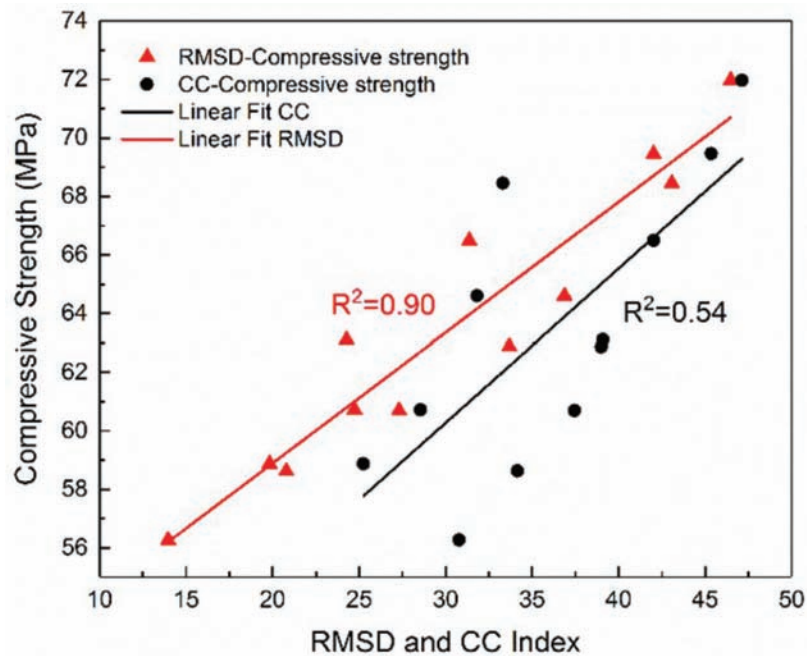


Figure 4.3 The correlation between the RMSD and CC index with the compressive strength of all the mixes (Ghafari et al., 2018).

specimens. The W/C ratio range varied from 0.38 to 0.46 with an increment of 0.02. Mortar is prepared by adding fine graded Ottawa test sand according to the ASTM C150 and ASTM C778 standards. The cement-to-sand ratio of all mixes is kept at 1:3. All 10 sets of the mix in this study are tested at a very early age (4th to 8th hour after blended water with cement) and early age (1, 3, 7 days). In order to minimize the variables, the EMI test and mechanical test are performed at the exact same time during each age. The samples are stored in

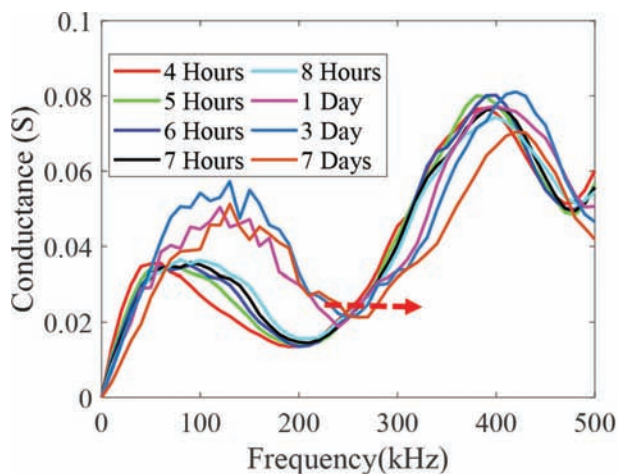
standard moisture curing room at the temperature of $23 \pm 2^\circ\text{C}$ until the test age.

The EMI signals of all 10 mixes are measured at each age of interest. The impedance signal extracts from the analyzer including the real part and the imaginary part. Among two parts, the reciprocal of the real part, in terms of conductance, is the most used data to be analyzed due to the explicit changes with the change of the sample conditions, i.e., age, humidity, component of sample (Wang & Zhu, 2011).

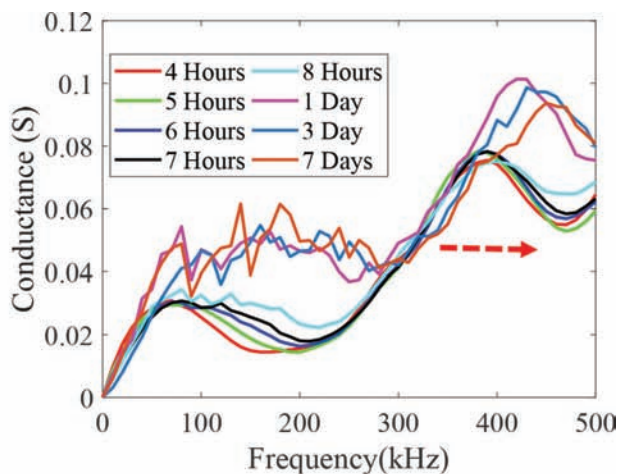
4.2.2.2 Results. Figure 4.4 shows the representative plot of conductance versus frequency of w/c=0.46 samples with type I and type III cement, respectively. As can be seen that the conductance spectrum shifts from left to right with the age increase. The shifting trend of type I mortar is more evident than that of type III mortar. A rightward shift can also be observed from the result. The reason contributed to the shift of spectrum is the development of the stiffness due to the hydration of cement-based material along with age. During the hydration process, the water will either be consumed for the formation of hydration products such as alite (C_3S), belites (C_2S), and aluminate (C_3A), etc. or evaporated. The stiffness of the sample will increase during this period. The rightward shift of spectrum is reflecting the growth of stiffness.

A previous study (Su, Han, Amran, Nantung et al., 2019) suggested that the frequency range lies between

100 k to 400 kHz shows a better correlation. Thus, the data in this study are processed at the frequency range of 100 k to 400 kHz. Figure 4.5 displays the correlation result between RMSD index of the representative sample (W/C=0.46) with corresponding compressive strength at each age. It has been found that the R^2 value is higher than 0.93 for all samples as Table A.2 shows. Moreover, the R^2 values of compression for type I sample are higher than 0.98, especially the value of the samples with W/C of 0.46, 0.44, and 0.42 are more significant than 0.99. The elastic modulus is also recorded and correlated with the RMSD index as Figure 4.6 presented. Based on Hooke's law, compressive strength is linear with elastic modulus; thus, it's not hard to understand that if compressive strength of the samples has high correlation with RMSD index, elastic modulus will behave in the same way. As Figure 4.6 reveals, the R^2 values for the elastic modulus of W/C=0.46 samples

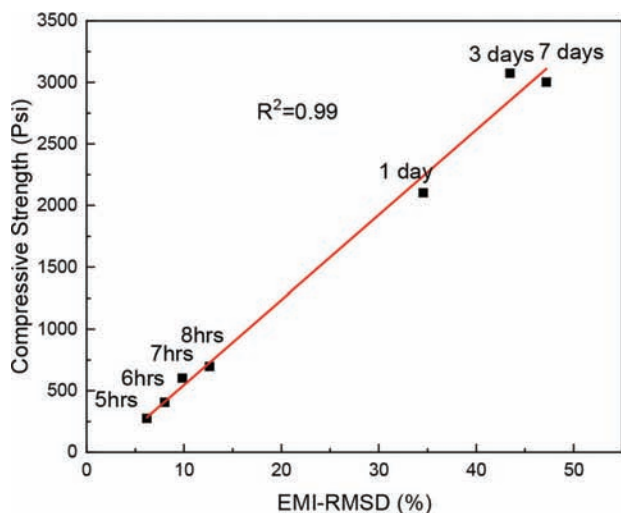


(a) Type I cement mortar, w/c=0.46

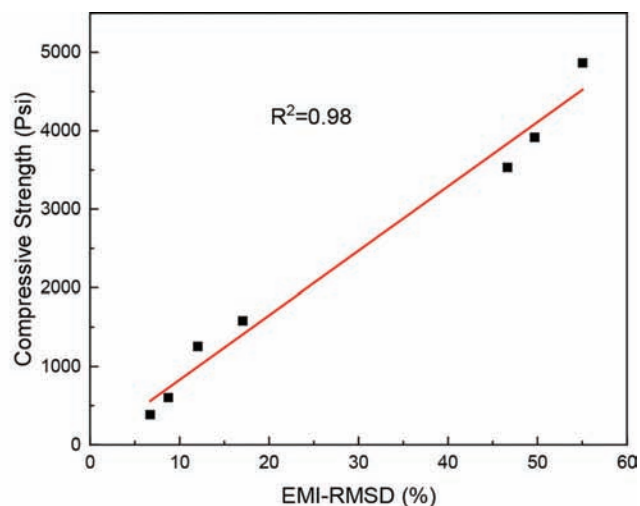


(b) Type III cement mortar, w/c=0.46

Figure 4.4 Conductance signature of representative sample at different age.



(a) Type I cement mortar, W/C=0.46



(b) Type III cement mortar, W/C=0.46

Figure 4.5 The linear correlation fitting between compressive strength with EMI-RMSD index of W/C=0.46 sample.

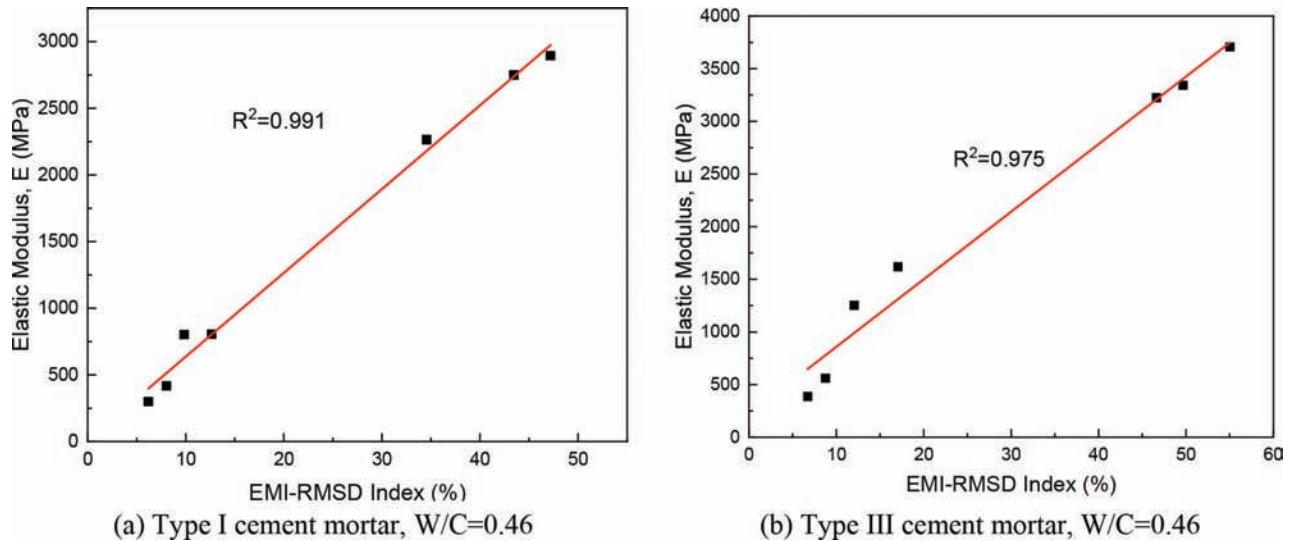


Figure 4.6 The linear correlation fitting between elastic modulus (E) with EMI-RMSD index of W/C=0.46 sample.

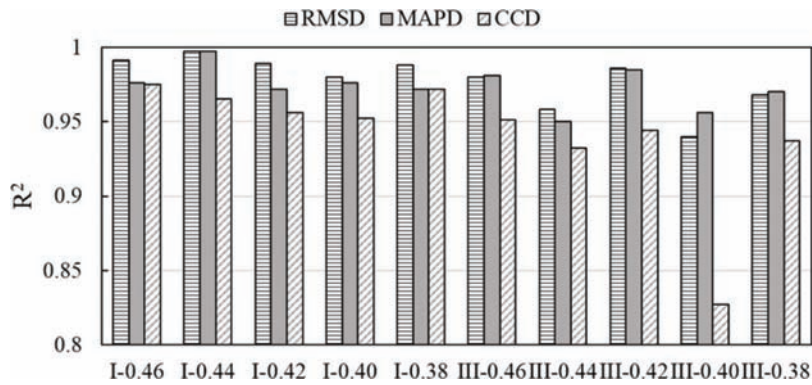


Figure 4.7 The correlation value (R^2) of three proposed indices for all mixes.

are above 0.97. This signifies that the EMI-RMSD can be used to evaluate the mechanical properties of cementitious materials with high accuracy.

The other statistical models, including correlation coefficient deviation (CCD) (Ghafari et al., 2018; Tawie & Lee, 2010; Wang et al., 2014) and mean absolute percentage deviation (MAPD) (Lu et al., 2012; Narayanan et al., 2017; Tawie et al., 2010; Wang & Zhu, 2011) are also proposed as a valid index on strength gain monitoring of concrete. In this research, MAPD and CCD indexes are also used. As Figure 4.7 shows, the RMSD index has a higher R^2 than that of the others. The MAPD index also shows acceptable accuracy with the R^2 for all mixes higher than 0.95. The CCD index is relatively lower compared with others. As can be seen in the figure that the R^2 value is lower than 0.85 for CCD index of type III-0.40 sample.

For the statistical comparison, the data of type I mortar and type III mortar are further lumped as Figure 4.8 (a) and (b) show, respectively. The R^2 of lumped type I data is 0.94, and it's 0.93 for type III data, both exhibit the satisfying correlation, which indicates that the EMI-RMSD index might be independent of the W/C. The 90% confidence band and 90%

prediction band are further calculated and plot on the figures. Most of the data points of the two figures are in the 90% prediction band.

To validate whether the various mix designs would affect the correlation, the data from every different mix design is put together for the regression analysis. As can be seen in Figure 4.9, the R^2 drops to 0.92, and the prediction band is broader than that of Figure 4.8 (a) and (b). This can be attributed to the slight differences between each sensor and the bonding process. Although the sensors used in this study are fabricated, and bonding followed the same standard operation procedure, a slight variation is unavoidable. Lu's team at Purdue is working on signal processing software to eliminate this small variation and improve the consistency of this testing method.

4.2.3 Experiment—Mortar with different SCMs

4.2.3.1 Experiment design and materials. In this part, three different SCMs were blended with mortar including Class C fly ash (FA), ground granulated blast furnace slag (GGBFS), and silica fume (SF). Fly ash is provided by the local cement supplier in Indiana. Grade

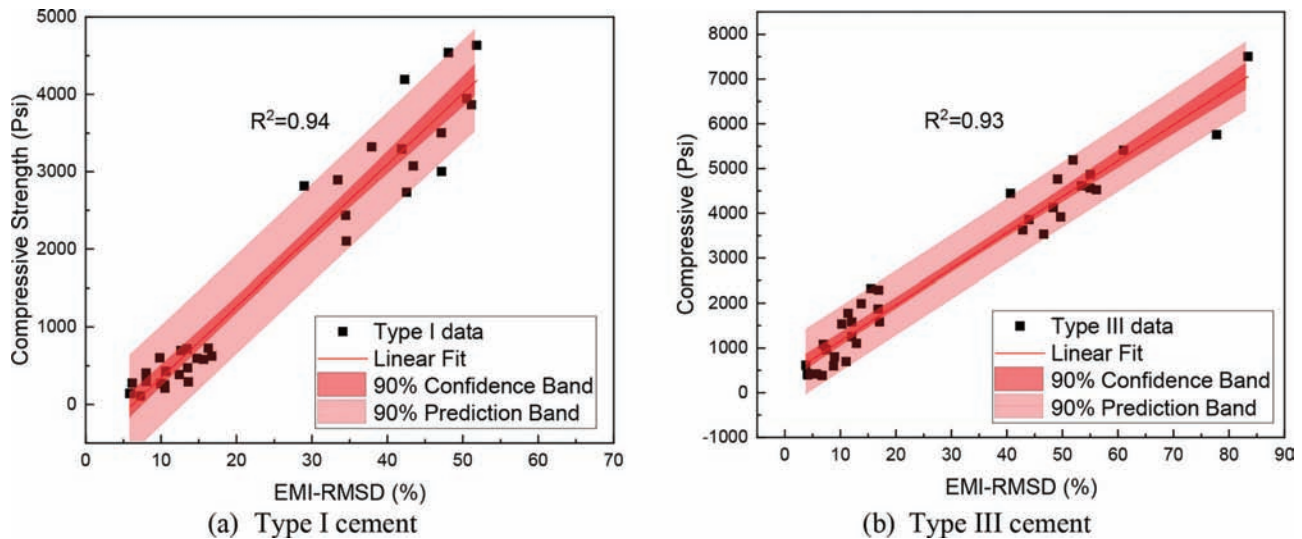


Figure 4.8 The correlation between compressive strength and EMI-RMSD mortar with a different water-to-cement ratio.

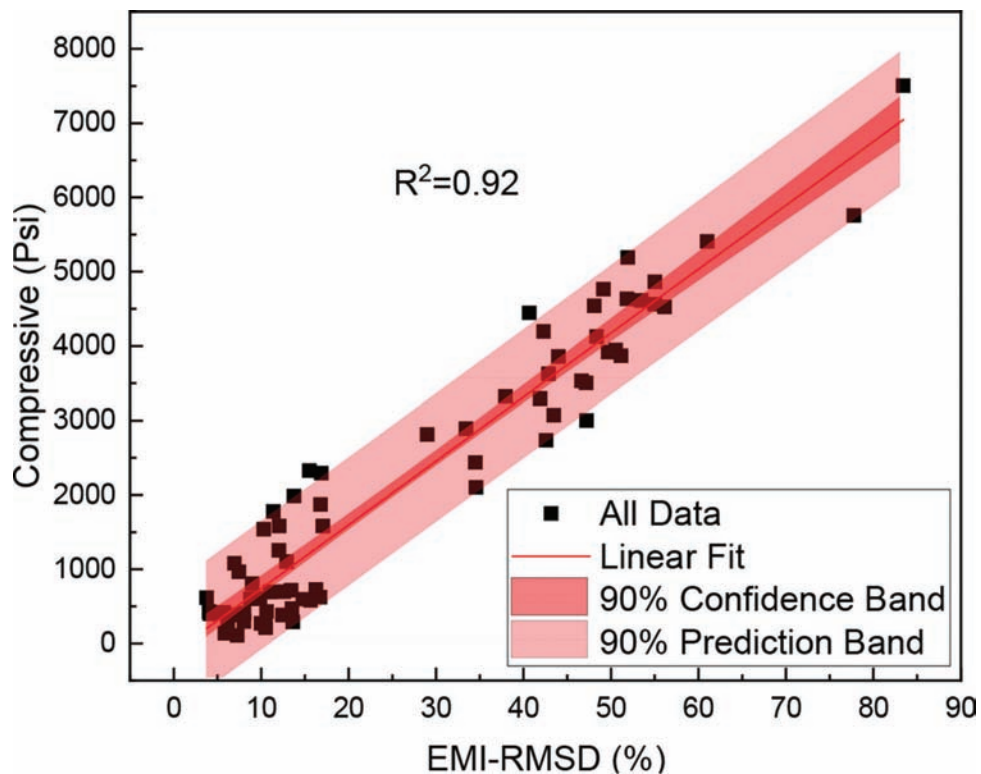


Figure 4.9 The correlation between compressive strength and EMI-RMSD of all samples.

100 GGBFS is supplied by Skyway Cement Company, and silica fume is supplied by GCP Applied Technologies. The type I OPC is used to mix with fine graded Ottawa test sand and different SCMs, as Table A.3 lists. The SCMs were used to replace part of cement with the replacing ratio of 15%, 25%, and 35%. The water-to-binder (cement and SCMs) ratio and the cement-to-sand ratio of all mixes are kept at 0.45 and 1:3, respectively. Slag sets, SF sets, and FA-15 mixes are tested at a very early age (4th to 8th hour after blended water with

cement) and early age (1, 3, 7 days), and the surface bonded sensors were used in those samples. However, the fly ash has the retarding effect which results in the longer setting time. The sensor cannot be surface bonded in the 3rd hour due to the lack of cohesion. Thus, the polymer-coated sensors were used to be embedded in the FA set specimens. The EMI test and mechanical tests are performed at the exact same time during each age. The samples are stored in standard moisture curing room at the temperature of $23 \pm 2^\circ\text{C}$ until the test age.

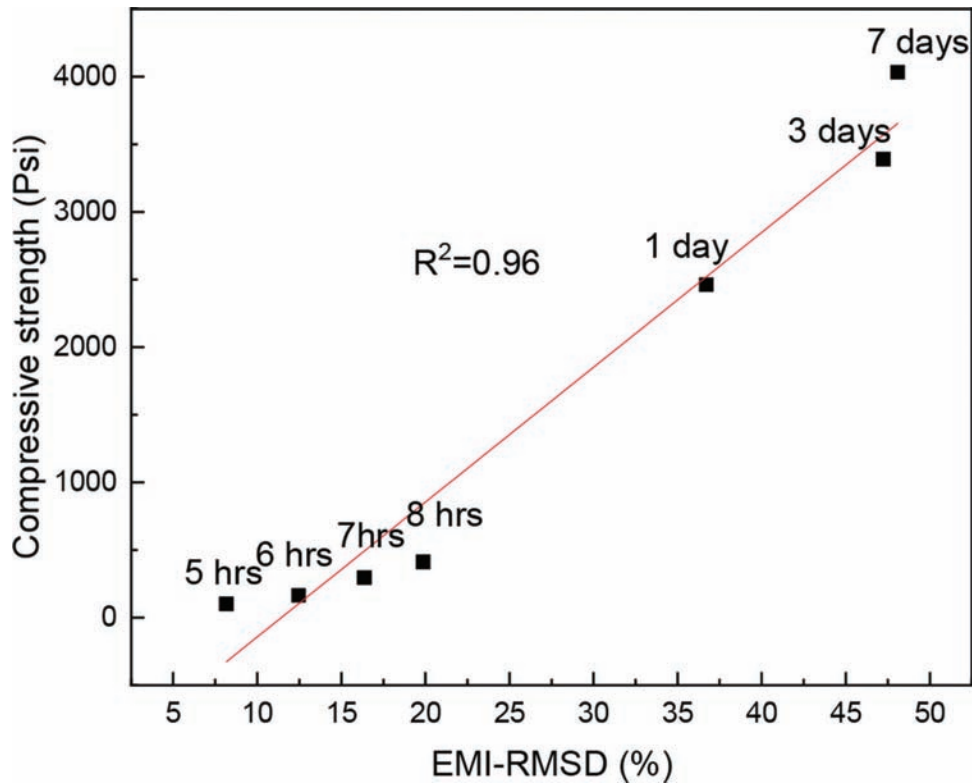


Figure 4.10 Regression results of mortar samples with different SCMs using the surface-bonded sensor.

4.2.3.2 Results. Figure 4.10 shows the representative regression results (slag 15) of EMI RMSD index with compressive strength. The other regression figures with different SCMs mortar can be found in Figure A.7. The EMI measurement was monitored from 4th hour to 8th hour with 1-hour interval for very early age, and early age of 1st, 3rd, and 7th day. The 4th hour EMI data was used as baseline to calculate the RMSD index. ACI 228 (2003) suggested that the test points for regression of sensing-strength relationship should be at least six points to reduce the uncertainty and less than nine-point for economics. In this project, the points we tested were over six points, which are satisfied to obtain the reliable regression results. Figure A.7 exhibits the results of mortar blended with GGBFS with different contents. The R^2 of the slag samples are over 0.96. The regression results of silica fume set are displayed in Figure A.7 which shows excellent linear regression of R^2 higher than 0.98. Owing to the retarding effect of the fly ash which results in the delay of setting time. The sensor cannot be surface bonded at the same hour with another sample. Thus, the relatively high-volume fly ash mixes such as 25% and 35% are not preferable for surface bonding sensor. Figure A.7 (e) shows FA-15 sample's regression of 0.91.

Figure 4.11 shows the correlation results of lumped SCMs data. It can be seen that the lumped EMI sensing results of the different SCMs with various contents still exhibits a high correlation coefficient of 0.90. This

indicates that the EMI sensing index is independent from mixes design, and it is independent from mixes with different SCMs with various contents.

Due to the delay setting time of fly ash mortar, the sensors cannot be surface bonded at the same hour (4th hour) with another SCMs sample. Thus, the embedded polymer-coated sensors were used to perform the EMI test. The testing age included a very early age (4th to 12th hour with 2-hour interval) and early age (1, 3, and 7 days). The regression results displayed in Figure A.8 present the acceptable R^2 of higher than 0.88.

4.3 Testing Results of Concrete Samples Using EMI Sensing vs. Compressive Strength

4.3.1 Objective

The previous chapters have proven that the EMI sensing technology can be applied in cement paste and mortar. Moreover, the regression results indicated that the EMI method is mix independent. In other words, the EMI method does not need to be calibrated for each mix with different water-to-cement ratio, type of cement, or SCMs. Yet, the concrete system is more complicated than mortar and paste due to the involvement of different sizes of aggregate and admixtures. Thus, over 300 cylindrical concrete specimens with ten

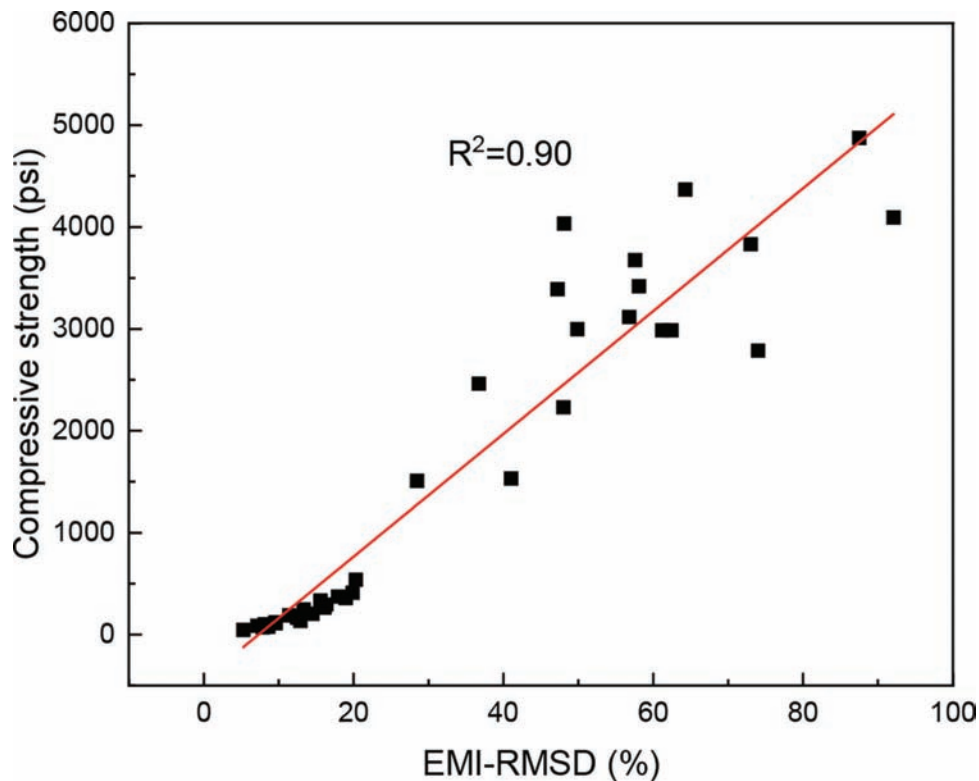


Figure 4.11 The correlation between compressive strength and EMI-RMSD of SCMs samples.

INDOT suggested concrete mixtures were conducted in this study to investigate the feasibility of EMI method for concrete strength monitoring.

4.3.2 Experiment design and materials

Ten mixtures suggested by INDOT engineers (Table A.4) that were used for experimentation. The mixture design includes different types of cement (type I and type III), various content of cement and SCMs, and the amount of aggregates. The 3" × 6" concrete cylinders were prepared using Portland cement (type I & III), Class F fly ash, grade 100 GGBFS, INDOT #23 sand (fine aggregate), INDOT #8 stone (coarse aggregate), air-entrainer, and water reducer. The water-to-cement (W/C) is fixed at 0.42 as typical INDOT concrete pavement. All ten sets of the mix in this study are tested at a very early age (4th to 12th after blended water with cement) and early age (1, 3, and 7 days). EMI test and cylinder compressive tests are performed at the exact same time during each age. The samples are stored in a standard moisture curing room at the temperature of 23 ± 2°C until the test age.

4.3.3 Results

Various INDOT suggested concrete mixes were tested including different types of cement, cement content, SCMs, and volume of aggregates. Figure A.10

exhibits all ten concrete mixes' regression results using EMI RMSD index with cylindrical compressive strength. Table A.5 summarizes the R^2 value of each concrete mix. It can be seen that the correlation coefficient of all mixes is higher than 0.90 which further proves the feasibility of EMI sensing technology for concrete strength monitoring.

It's important to understand whether the EMI sensing results are affected by the sample size. An EMI measurement was conducted with cylinder sample sizes of 2" × 4", 3" × 6", and 4" × 8". A 564 Type I PCCP mix was used for preparing the specimens. The compressive strength results were performed using 3" × 6" cylinders. The testing age was 4th to 8th hour, 1 day and 3 days. Figure 4.12 shows that the regression of different sizes of samples have very little impact on the accuracy of EMI sensing results, as all samples with various sizes obtained the correlation value of R^2 of 0.98. The maturity test and flexural test are also conducted for reference shown in Appendix in Figure A.9 and Table A.6.

4.4 Concrete Slab Test

4.4.1 Objective

The concrete slab test served as a pilot study to evaluate the feasibility of this method for the in-situ

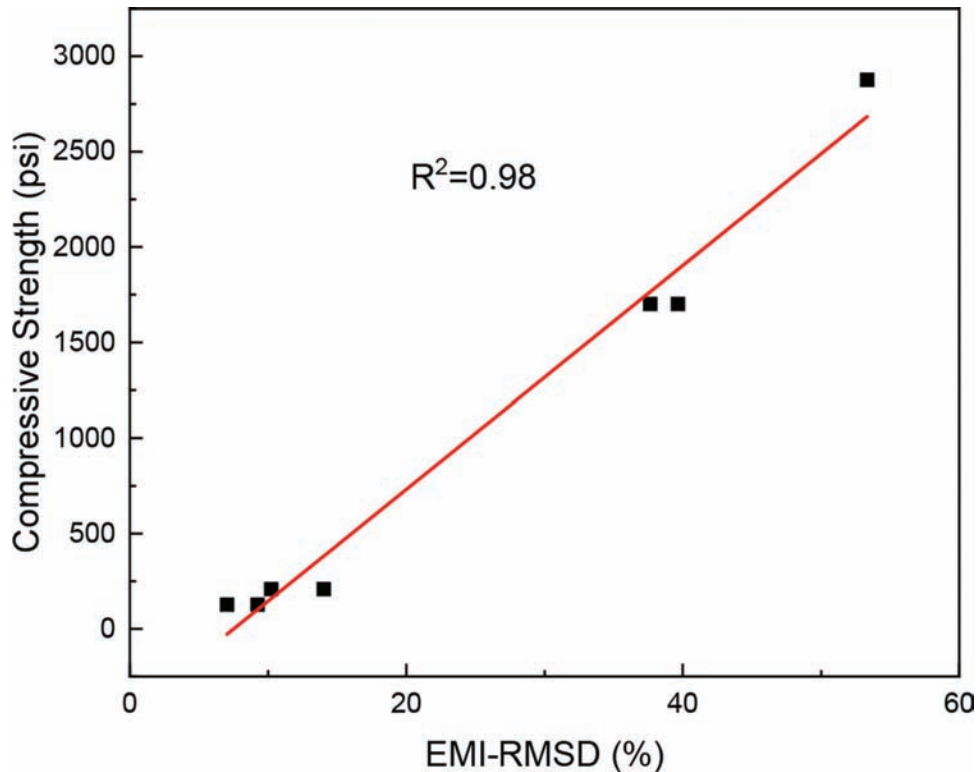


Figure 4.12 Correlation of EMI-RMSD with compressive strength using different size of cylinder.

concrete test in construction in the field. Due to the conditions such as the internal temperature of mass concrete is different from the small sample, the testing procedure and data analysis method are adjusted to adapt to the practical condition. Also, the predictive model is built using a statistical method. The experimental details for the slab test are discussed in the following section.

4.4.2 Experiment design

Table 4.2 shows the mixture of the concrete slab that in two feet square by one-foot-depth. The concrete pavement mix used complies with the specification of the INDOT. The concrete consists of type I OPC, INDOT #23 fine aggregate (passed 3/8" sieve), and INDOT #8 coarse aggregate (passed 1" sieve). The chemical additives, such as water reducer and air entraining agent, were also utilized. The water-to-cement ratio is 0.42.

A wood frame was constructed before concrete casting, and the embedded piezoelectric sensors were located strategically to capture the properties of the entire slab. Later, the concrete was poured into the wood mold layer by layer. Thirty, 3" × 6" cylinder samples using the same mix design were prepared per ASTM C39 at the same time to test the compressive strength of the concrete at each age of interest. The slab and cylinder samples were applied with white curing compound on

TABLE 4.2
Mixture design (lbs/cyd)

| Cement | Fine Aggregate | Coarse Aggregate | W/C ¹ |
|--------|----------------|------------------|------------------|
| 564 | 1344 | 1800 | 0.42 |

¹W/C: water-to-cement ratio.

top to retain the water and covered with plastic sheets. All samples were stored in a laboratory-controlled environment next to the concrete slab at the temperature of $23 \pm 2^\circ\text{C}$ until the testing age.

Four, $10 \times 10 \times 0.2 \text{ mm}^3$ PZT sensors with polymer coating were prepared. Four sensors were embedded at 6" in depth and 8" from the wood frame. Another four sensors were surface bonded on the top of the slab at the 3rd hour after casting. Three thermocouples were inserted in concrete slab to monitor the internal temperature with time. The deployment of sensors is shown in Figure 4.13.

Figure 4.14 shows the experimental setup for the slab test. The first EMI measurement was performed on the 4th hour after casting and continually conducted every hours until the 12th hour. The signals of the 1st to 7th day were also collected. The measurement of each age was repeated three times to ensure consistency.

The conventional compressive test was also performed by using three, 3" × 6" cylinder specimens from

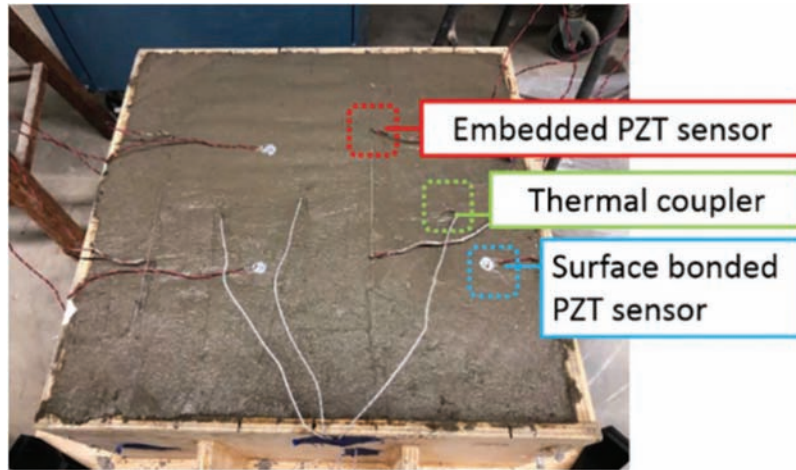


Figure 4.13 Deployment of sensors.

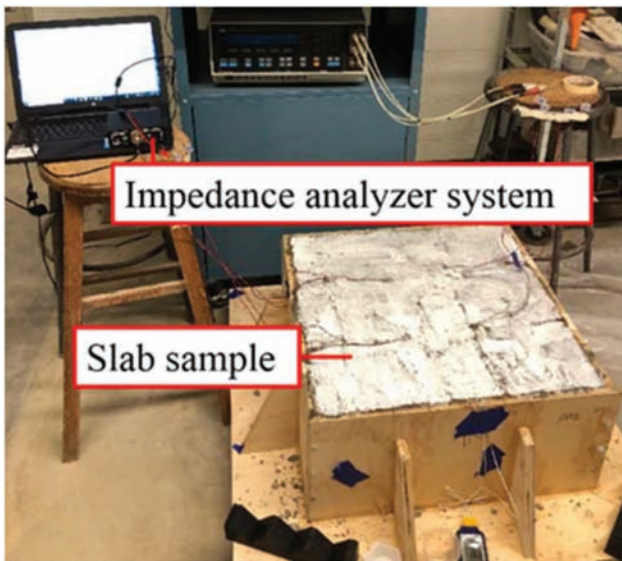


Figure 4.14 Experiment setup of concrete slab test.

the same batch of concrete used in the slab testing at each age of interest. EMI tests and compressive test were conducted simultaneously at 6th to 12th hour, 1st to 7th day. The compressive strength will be used to assess the correlation of the statistical index for strength gain process monitoring.

4.4.3 Concrete slab test results

For the concrete slab test, the PZT sensors were embedded in the concrete to monitor how the properties change. In previous research, the conductance (real part of electromechanical admittance) has shown a close relationship between the mechanical properties of the cementitious materials (Narayanan et al., 2017; Su, Han, Amran, Nantung, et al., 2019). However, those studies were conducted using the small sample, which

the heat released from the hydration process didn't significantly affect the sensing results. In practical concrete construction, the exothermic hydration reactions of mass concrete cannot be neglected. The study shows that the susceptance slope would be affected by temperature (Grisso & Inman, 2010). To consider the practical situation, the admittance signatures, which consist of conductance (structure information) and susceptance (temperature effect) have been utilized. Figure 4.15 shows the admittance magnitude (reciprocal of impedance) spectrum of the concrete slab obtained from the analyzer. As can be seen, the admittance signal of the embedded sensor tends to decrease with the increase of age. The difference of the signal at different ages can be distinguished owing to the growth of stiffness during the hydration process (Su, Han, Amran, Nantung et al., 2019).

The admittance signals were post-processed using cumulative RMSD method. The RMSD value between each adjacent measurement was calculated using the Equation 4.1 and cumulated. For example, the 6th-hour RMSD value is calculating the difference between 4th hour (the adjacent measurement) and 6th hour, and so forth. Then, each value is cumulated.

$$RMSD(i)\% = \sqrt{\frac{\sum_{i=1}^N (G_{i+1} - G_i)^2}{\sum_{i=1}^N (G_i)^2}} \quad (\text{Eq. 4.1})$$

The frequency range for data processing is suggested from previous research to set from 100 kHz to 400 kHz (Su, Han, Amran, Nantung et al., 2019). The RMSD results of four embedded sensors were averaged. Figure 4.16 plots the cumulated RMSD of admittance index verse compressive strength at each age of interest. The regression analysis is employed to evaluate the correlation between the index and mechanical strength. The calculated correlation factor (R2) is 0.97, which indicates the sensing results have a direct correlation with compressive strength. The linear function was

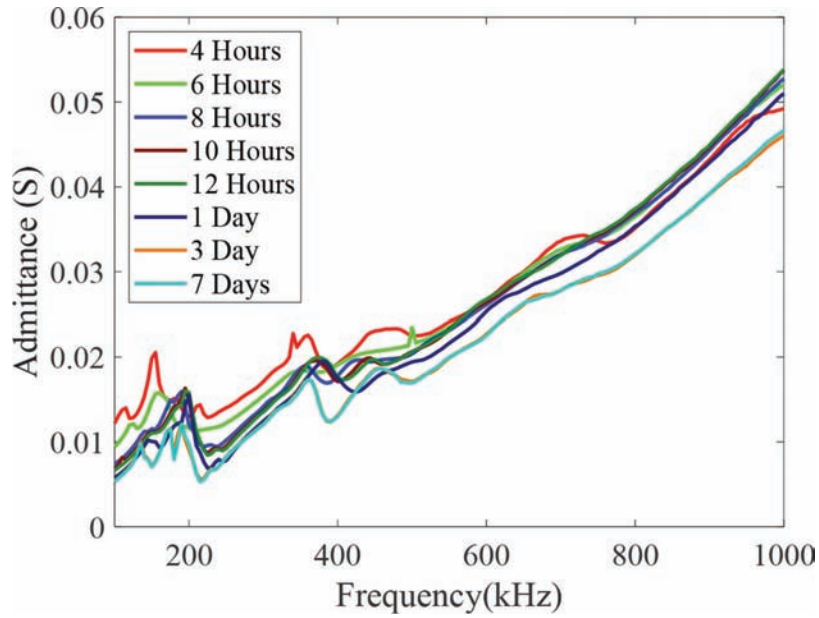


Figure 4.15 Admittance spectrum of concrete slab at different age.

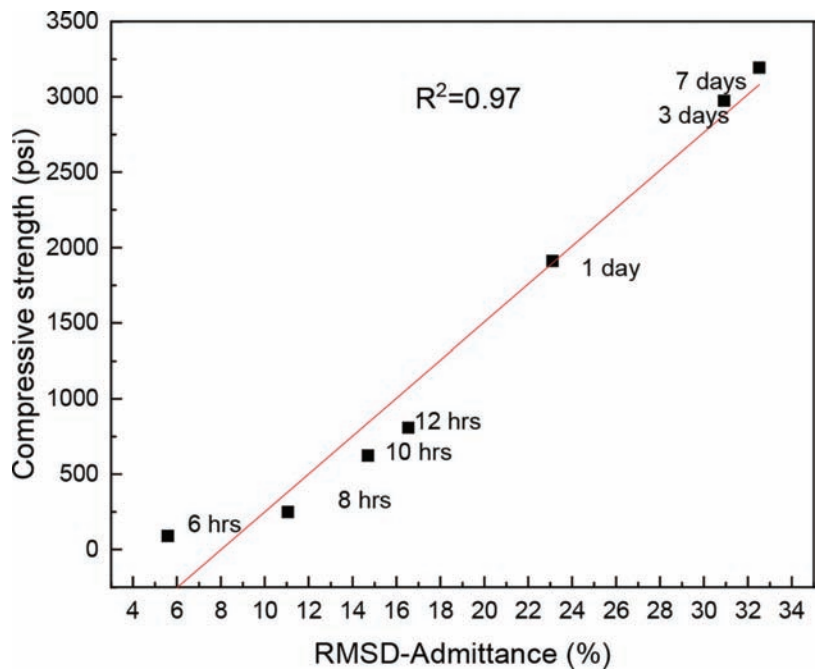


Figure 4.16 RMSD-Admittance index vs. compressive strength at different age.

calculated through the regression analysis as Equation 4.2. The calculated unknown is 125.7 and -1007.7, which was used in the following regression function for estimating field testing results.

$$125.7 \times \text{RMSD-Admittance} - 1007.7 = \text{Predicted Compressive Strength (psi)} \quad (\text{Eq. 4.2})$$

5. FIELD TEST ON THREE INTERSTATES IN INDIANA

5.1 Objective

The field test is essential to verify the practicability of the developed EMI sensing technology in real construction. In this project, the team coordinated with INDOT field engineers and contractors (Milestone Contractors, L.P., IMI Irving Materials Inc, and E&B Paving, Inc.) for several field tests on interstate highway I-70, I-74, and I-465. Among the field tests, I-70 and I-465 constructions were for concrete patching, and I-74 was for the concrete paving. Almost a hundred sensors were employed for the EMI sensing in concrete pavement. The EMI measurements were performed on the sites from the 1st hour after concrete casting to the 8th hours and 1st day and 3rd day, depending on the work schedule at the job site. The cylindrical specimens were prepared for the compressive strength test compared with the EMI predictive sensing results developed by the previous concrete slab test.

5.2 I-70 Field test

5.2.1 Experimental works

The very first field test was conducted on interstate highway I-70 west (Plainfield) in Indiana. The location is shown in Figure A.11. The job was executed during the night time for concrete patching work. The patching

works started from the preparation of the 6' × 12' hole with 1' depth as Figure 5.1 shows. The dowel bars were drilled into the adjacent slabs at a 1' spacing. The PZT sensors were bonded onto the second dowel bar with the 2' from the edge of pavement as shows. Figure 5.1 shows the deployment of six PZT sensors in three different holes (A, B, and C); two sensors were bonded on the opposite side of each hole.

Figure 5.2 shows the sensor bonding procedure (a) and the closer view of the bonded sensor on the dowel bar (b). The sensors were firmly tied onto the bar with a plastic cable tie to prevent the movement or shifts during the concrete pour. The wires were extended outside the hole and temporarily fixed on the surface of adjacent pavement.

After the sensors were manually installed in the holes, the concrete workers started to pour concrete. The field condition of the concrete casting is shown in Figure 5.3 (a) to (d). The concrete was delivered by the ready-mixed concrete mixer from plant to site and poured into the patch hole. The workers later vibrated the concrete and compacted it. Then, the concrete was screeded using the roller tool. The following work was finishing. The curing compound was sprayed on the top on concrete at the 3rd hour and covered with the wet burlap and plastic sheet at the fifth hour to maintain the humidity and temperature of concrete.

The EMI sensing system consists of laptop, portable impedance analyzer, and power supply system. Figure 5.4 shows the field EMI measuring condition,



Figure 5.1 (a) Patching hole and (b) deployment of PZT sensors.

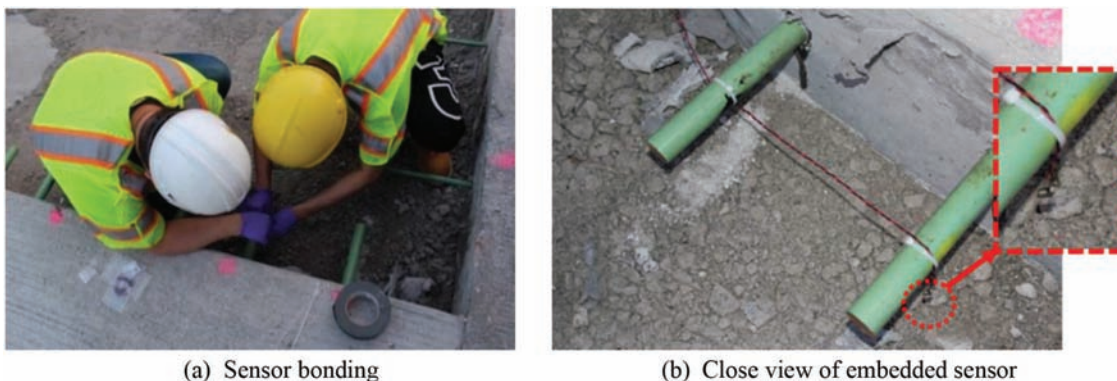


Figure 5.2 Sensor bonding procedure.



(a) Casting and vibrating



(b) Roller screeding



(c) Finishing



(d) Tined finish

Figure 5.3 Construction procedure of concrete patching job.



Figure 5.4 Field EMI measurement.

one person controlled the software in laptop, and other people connected the sensor to the impedance analyzer. The EMI signal of each sensor was measured three times to obtain a stable signal. The measurements were conducted from the 1st hour after the concrete pour until the eighth hour. Due to the weather condition and working schedule, we were not able to collect the 1st day (24th hour) data. Three, 3" × 6" cylinder specimens were molded and cured in the field. The compressive test was conducted on the first day to compare with the sensing results.

5.2.2 Results

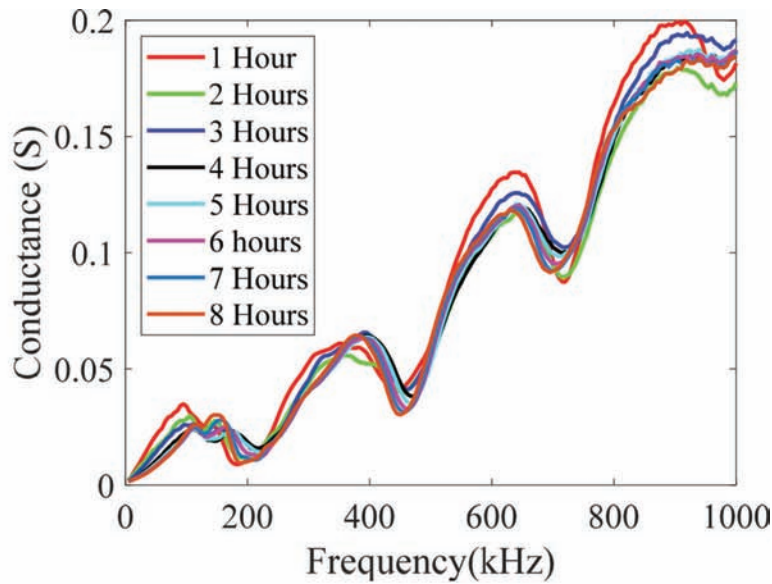
Since the field condition was critical, one out of six sensors were broken. The very first field test on I-70 gave us the idea to improve the durability of the sensor and the bonding method for the next field test. Figure 5.5 (a) and (b) exhibit the conductance signal and admittance signal versus frequency at a different age, respectively. Both the conductance signal and admittance signal were similar to the laboratory experiments. The conductance and admittance signals shift rightward with time due to the stiffness growth of concrete. These results indicated that the coated sensors are robust and durable for field implementations.

Figure 5.6 shows the predicted compressive strength using the statistical model developed by the concrete slab. The predicted compressive strength of patched concrete reached 2,203 psi at 8th hour after the concrete pour. However, due to the weather conditions, the job site was opened to traffic, thus, we were not able to obtain the one-day EMI data. Yet, the field cured cylinder sample shows the compressive strength at 5,570 psi.

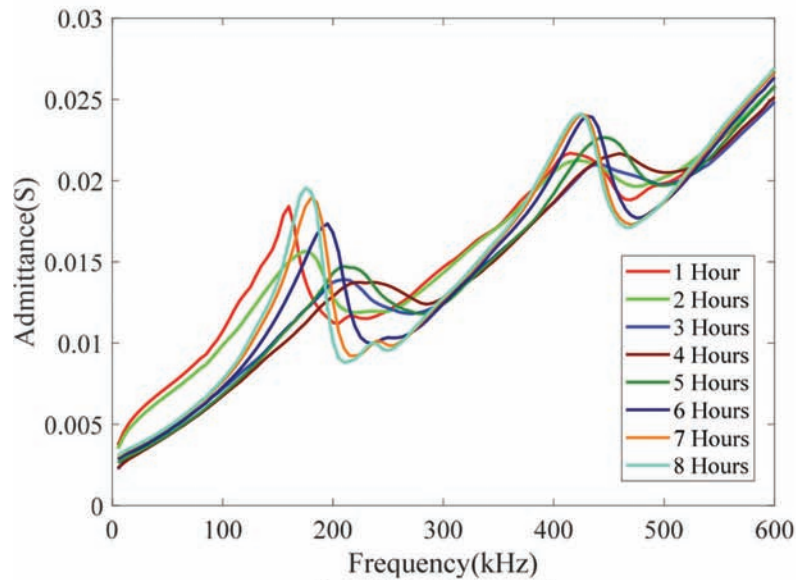
5.3 I-74 Field Test

5.3.1 Experimental works

The second field test was conducted on interstate highway I-74 for a concrete paving job at Batesville,



(a) Conductance data



(b) Admittance data

Figure 5.5 Representative EMI signature on I-70.

Indiana. The location is shown in Figure A.12. The new concrete pavement on this site was paved during the daytime. The workers can pave 1 to 1.5 miles of concrete per day.

The subbase and subgrade layers were well compacted first, before the concrete pavement was poured on top. Figure 5.7 (a) and (b) show the dimension and scope of the new concrete pavement. The connecting dowel bar basket was placed on the subgrade every 15 feet the traveling length direction. Each rod spaced 1' and away from ground for 0.5'. The concrete paving machine can pave the concrete to a width of 23' and depth of 14". The mix design of the concrete is presented in Table 5.1. The water-to-cement ratio of the

concrete was 0.415, and the air content was 5.9%. The density of fresh concrete was $2,312 \text{ kg/m}^3$, and the slump was 1.5 inches. All the data above was provided by the contractor.

The field experiment procedure is displayed in Figure 5.8 (a) to (f). The sensors were firmly tied on the second dowel bar every 15'. The plastic tube was used to protect the wire from fracture or damage during the paving as Figure 5.8 (a). The concrete was delivered via the line-up trucks from the plant to the site. The truck dumped the concrete in the concrete paver; then, the concrete pavement was cast through the machine as (c) shown. After the paving, the thermocouples were inserted in the middle of the concrete pavement (7" in

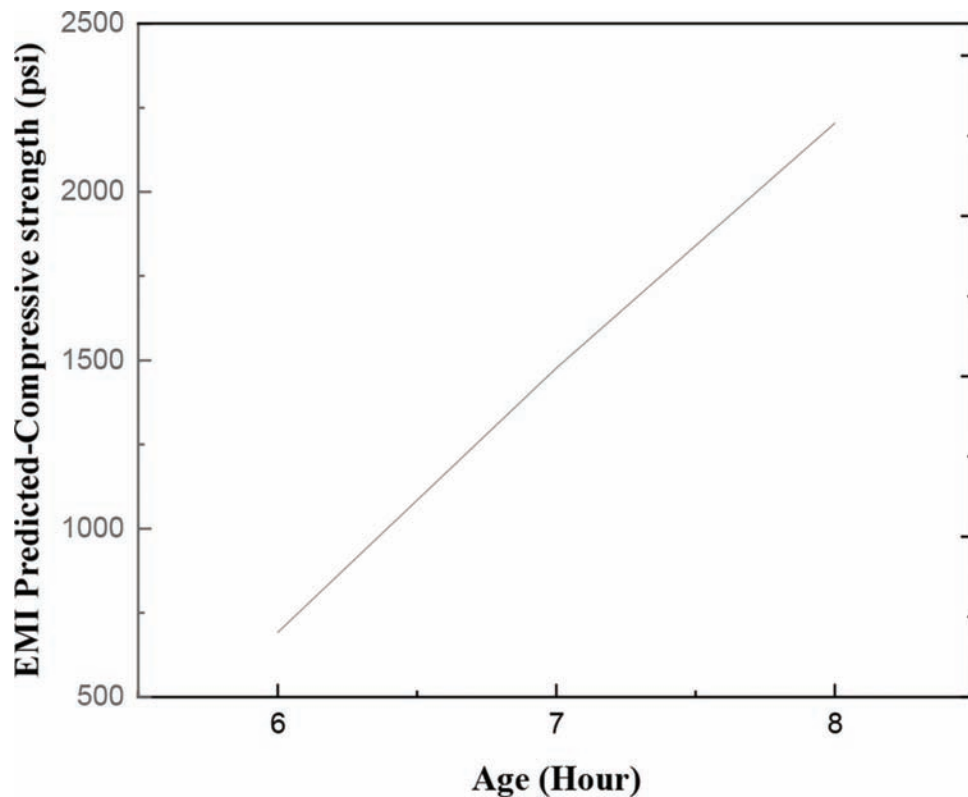


Figure 5.6 Predicted compressive strength using the EMI method (I-70).

depth) from the profile section. In this experiment, we also investigated the feasibility of surface-bonded sensors; thus, the sensors were surface bonded on the side of pavement at the 4th hour after pouring as (e) shown. The EMI measurements were conducted from the first hour after concrete pour began until the 8th hour, 1st day and 3rd day. Six, 3" × 6" cylinder specimens were molded and cured in the field. The compressive test was conducted on the first and third days to compare with the sensing results.

5.3.2 Results

The configuration of the sensors for EMI test in this field experiment was included an embedded sensor and surface-bonded sensor. The admittance spectra are shown in Figure 5.9 (a) and (b). It can be observed that the spectrum shifted rightward with time due to the concrete stiffness growth.

The predicted compressive strength in I-74 is shown in Figure 5.10. Figure 5.11 shows the comparison of predicted compressive strength results and mechanical test results. The predicted compressive strength reached 2,372 psi and 3,457 psi on the 1st and 3rd day, respectively, on the June 11, 2019 field works. The strengths obtained via mechanical cylinder test are 2,223 psi for 1 day and 3,793 psi for 3 days. The results indicated that the one-day compressive strength of concrete from the EMI sensing method are higher than the cylinder samples due to the exothermic hydration reactions of mass concrete is higher. Nevertheless, the third-day

EMI sensing results are a bit lower than mechanical test results. The reason might be due to the water evaporation speed of field concrete pavement was higher than the cylinder samples. The water was able to be retained in the cylinder mold to enhance the degree of hydration. More tests need to be conducted to verify the observations and assumption of the field tests.

For the second visit, the EMI predicted compressive strength on the I-74 site is 2,604 psi and 3,455 psi, correspondingly. The predictive strengths of two field tests for the first day and third-day samples are similar. However, the cylinder results of the second site visit are 1,694 psi (1 day) and 2,628 psi (3 days) with high variation, which are lesser than the first site visit and the predictive results. This might be due to the compacting condition and handling of cylinder that affect the results.

5.4 I-465 Field Test

5.4.1 Experimental works

The third field test was conducted on interstate highway I-465 for concrete patching job at Indianapolis, Indiana. The location is shown in Figure A.13. The patching work on this site was performed during the daytime.

Based on the previous experience, the sensors were improved to add a plastic reinforcement to ensure the position of each embedded sensor were similar.

TABLE 5.1
 Mix design of concrete pavement on I-74 (lbs/cubic yard)

| Cement | Sand | AP 8 Stone | QA 3 Stone | Fly Ash | Water | AEA | WRDA 82 | W/C |
|--------|------|------------|------------|---------|-------|------------|----------|-------|
| 350 | 1390 | 1270 | 514 | 150 | 24.6 | 6.5 oz/lyd | 4 oz/CWT | 0.415 |



(a) Connecting steel rods



(b) The width of the pavement

Figure 5.7 Dimension of new concrete pavement.

The sensor (PZT) was tied away from the tip of dowel bar for 2" as Figure 5.12 (a) shows. The deployment of sensors is displayed in Figure 5.12 (b). The sensors were bonded on the first bar, and two sensors were fixed on the opposite side of the hole. The mix design of concrete is presented in Table 5.2. The water-to-cement ratio of

concrete is 0.398, and the air content is 6.5% and the slump is 3.5 inches. All the data above are provided by the contractor.

The field test procedure is exhibited in Figure A.14 (a) to (d), including the sensor bonding, concrete casting, curing compound spraying, and EMI measuring. The EMI measurements were conducted from the 1st hour after concrete pavement until the 8th hour and the 1st day. Three, 3" × 6" cylinder specimens were molded and cured in the field. The compressive test was conducted on the 1st day to compare with the sensing results.

5.4.2 Results

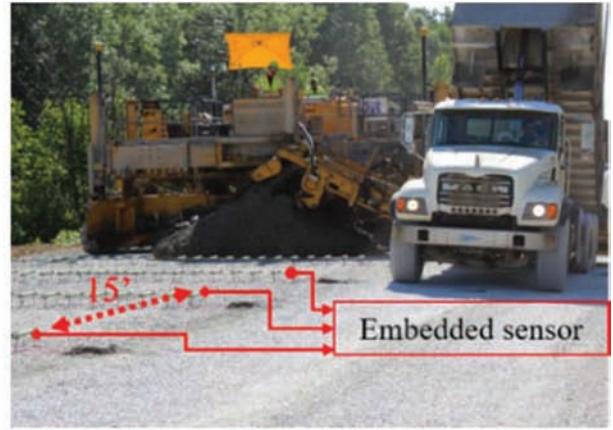
The team has visited I-465 to conduct the field test three times. Figure 5.13 shows the representative admittance spectrum of patched concrete. The clear shifting trend of admittance with time can be observed as previous experiments did.

The I-465 concrete patching works were conducted during the weekend. The traffic should be open on the following Monday. Thus, the experiment was only performed one day. Figure 5.14 (a) to (c) displays the predicted compressive strength of all three I-465 field tests. The strength growth can be observed as the concrete aged. The predicted compressive strength reached 1,637 psi, 1,453 psi, and 1,573 psi for three visits, separately. The mechanical cylinder test results for these three field tests are 1,656 psi, 1,322 psi, and 1,583 psi. The predicted strengths are quite close to the cylinder test.

Figure 5.15 collected on the one-day test to compare the cylinder compressive strength versus EMI predicted strength. For the concrete paving works (I-74), the predicted strength values are higher than the cylinder strength. Similar to the other sites phenomenon might be due to the exothermic hydration reactions of mass concrete, which is higher than the cylinder sample; thus, the sensing results reflected the high strength on the first day. On the other hand, the concrete patching works present quite similar results between compressive strength and EMI prediction values.



(a) Bonding the sensor



(b) Deployment of sensors



(c) Machine paving



(d) Insert the thermocouple

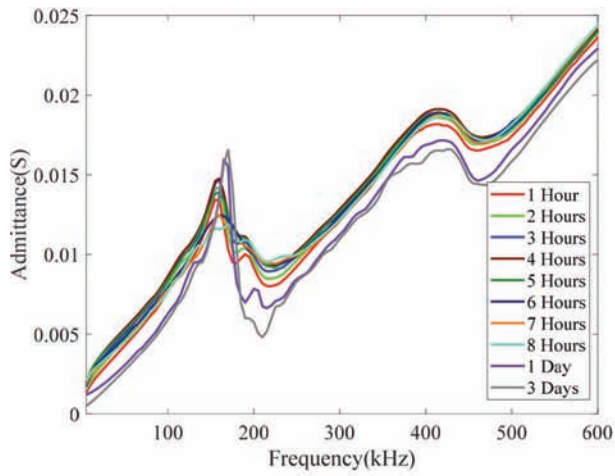


(e) Surface bonded sensor

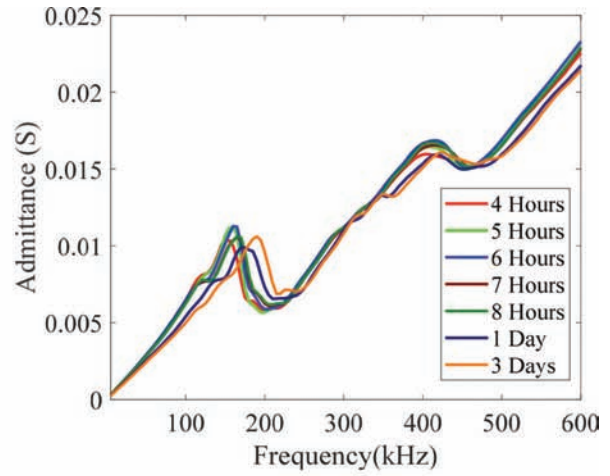


(f) EMI measurement

Figure 5.8 Field test on I-74 concrete paving.

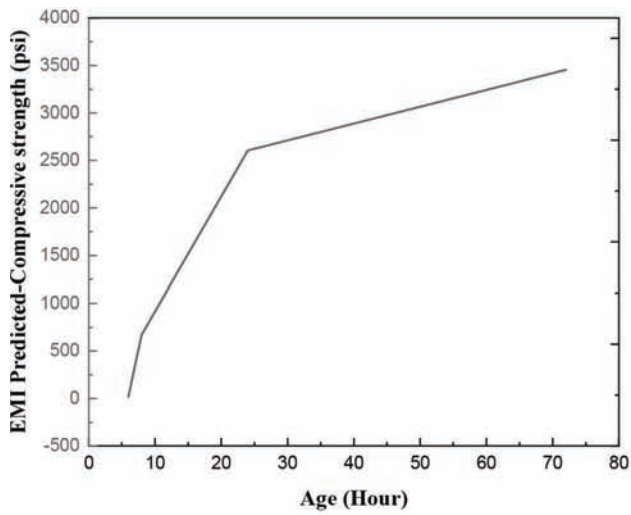


(a) Embedded sensor

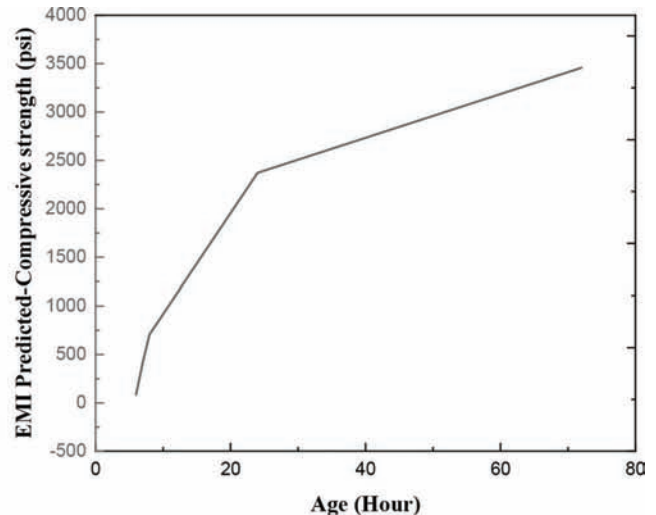


(b) Surface bonded sensor

Figure 5.9 Admittance spectrum of I-74 concrete pavement.



(a) I-74 (06/11/2019)



(b) I-74 (08/03/2019)

Figure 5.10 Predicted compressive strength using the EMI method (I-74).

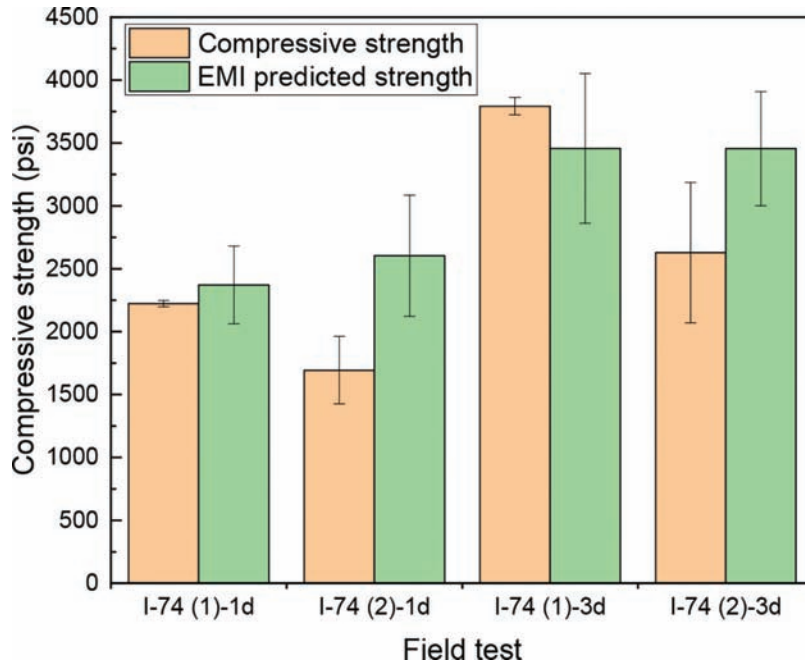
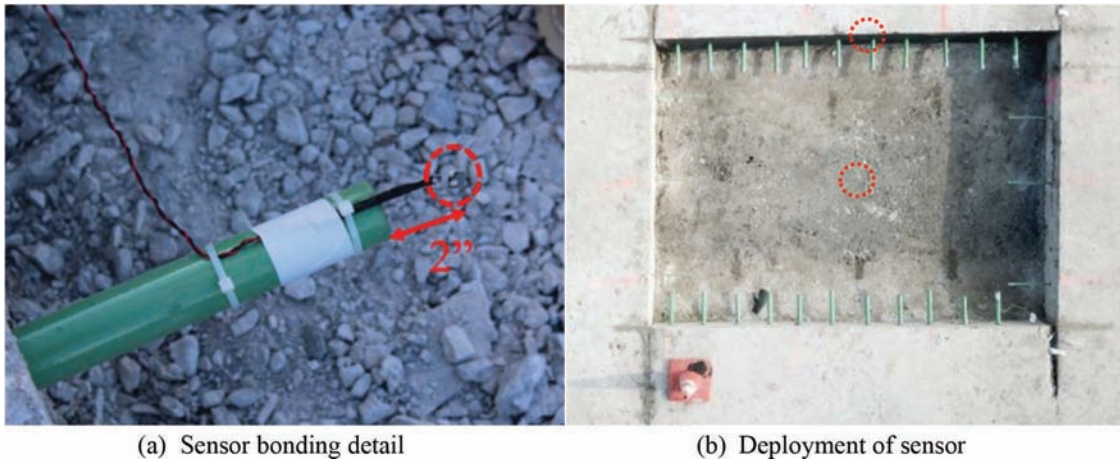


Figure 5.11 Comparison of predicted compressive strength results and mechanical test results.



(a) Sensor bonding detail

(b) Deployment of sensor

Figure 5.12 Sensor bonding and deployment.

TABLE 5.2
Mix design of concrete pavement on I-465 (lbs/cubic yard)

| Cement | Sand | AP 8 Stone | Water | Daratard | Darex2 | W/C |
|--------|------|------------|-------|----------|------------|-------|
| 752 | 1115 | 1650 | 299.5 | 3 oz/yd | 1.8 oz/CWT | 0.398 |

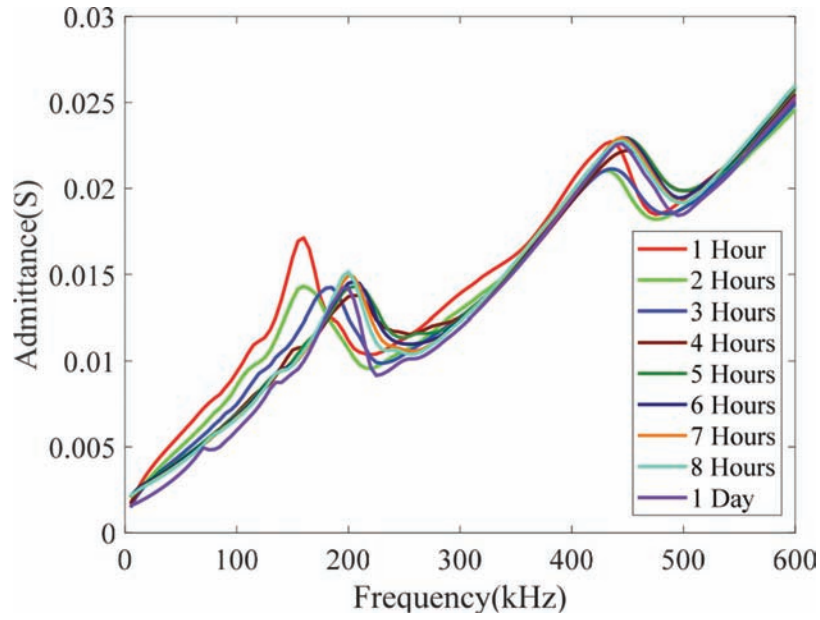
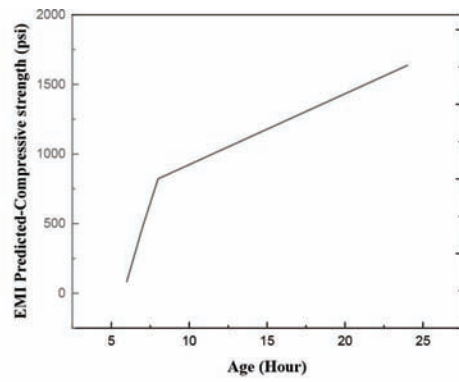
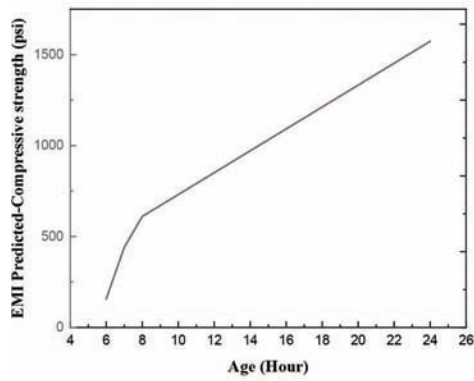


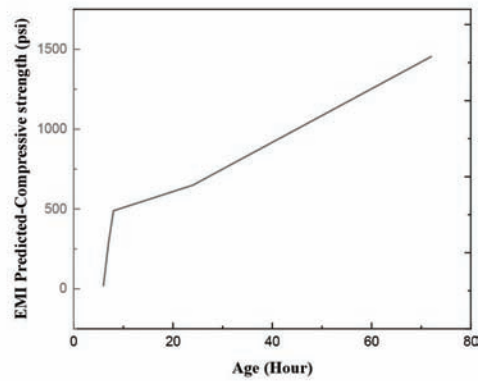
Figure 5.13 Admittance spectrum of I-465 concrete patching work.



(a) I-465 (07/20/2019)



(b) I-465 (09/07/2019)



(c) I-465 (08/11/2019)

Figure 5.14 Predicted compressive strength using the EMI method (I-465).

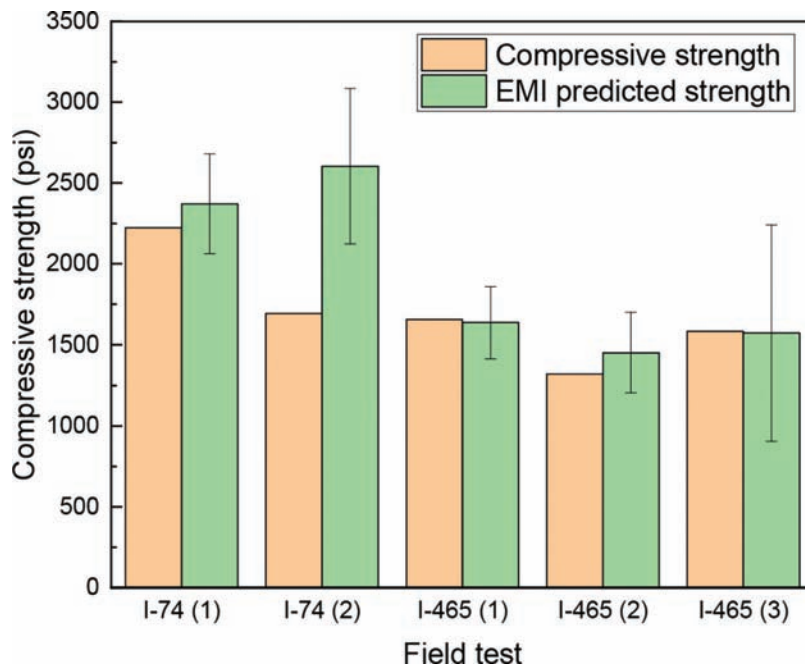


Figure 5.15 The one-day cylinder compressive strength versus EMI predicted the strength.

6. FINAL CONCLUSIONS AND RECOMMENDATIONS

This work has developed an in-situ monitoring method to evaluate concrete compressive strength using the piezoelectric sensor coupled with the EMI technique to determine the optimal traffic opening time. Two configurations of PZT sensor have been investigated, and different polymer coating methods were also developed to prevent sensor corrosion and brittle failure in the field. We have also developed associated hardware and software to ensure the field implementations in highway pavement project.

The feasibility of using this method for compressive strength gain monitoring is approved by combined experimental and simulation work. Experimentally, we have systematically applied the EMI sensing methods and compressive strength testing (ASTM C109 for the cubic samples, ASTM C39 for cylindrical samples) simultaneously on cement paste, mortar with various water/cement ratio, ten different INDOT concrete mixes, and large concrete slab test. Three different statistic models were applied for data processing. The regression analysis is also employed to evaluate the correlation between conventional compressive test versus the proposed EMI sensing results. More than a thousand specimens were fabricated and tested, including 2" cubic and 3" by 6" cylindrical samples. The multi-physics COMSOL modeling works were also conducted to understand the fundamental mechanisms of sensing work and guide the experimental works. Field implementations were also conducted on both concrete paving and

patching jobs, including I-70, I-74, and I-465. The key summary is listed as follows:

- The experiments started from the cement paste. Three different mixes were conducted using ordinary Portland cement (OPC), fly ash (FA), and silica fume (SF). The results indicated that the EMI data processed through RMSD statistical matrix presented a high correlation ($R^2 = 0.9$) with compressive strength of samples from 3rd to 28th day.
- The COMSOL modeling indicated that the PZT sensor's EMI response is sensitive to the stiffness of the host structure. The admittance and conductance of the sensor's EMI signals can serve as a good indicator as concrete aged. Besides, the possible sensing range of each PZT patch has also been provided. The effective sensing range of one single PZT patch is within the diameter of 5.5 inches. Further validation experiment needs to be conducted to verify this result.
- In the mortar experiments, over 600 specimens were conducted. For all samples with different water-to-cement ratio (W/C) and two types of cement (I and III), the R^2 values for compressive strength versus RMSD index are higher than 0.93 and R^2 are above 0.91 for elastic modulus. The different SCMs with various contents exhibit a high correlation coefficient of 0.90 for the lumped EMI sensing results. It was observed that the EMI sensing results are independent of the water-to-cement ratio, cement type, and various SCMs content. Among the investigated statistical model, the RMSD is the best index, which is highly correlated with compressive strength.
- The regression results of the ten sets of INDOT suggested concrete mixtures indicated that the correlation coefficient between the EMI sensing index and the compressive strength of all mixes is higher than 0.90. For the

concrete slab test, the R^2 is 0.97 for monitoring strength development. The linear function was built through the data regression of concrete slab to evaluate the in-situ concrete strength.

- In the component of EMI signals, the pilot study shows that the conductance performance satisfied correlation with compressive strength on laboratory samples. However, the mass concrete often releases a large amount of heat due to the exothermic hydration reactions of mass concrete. The admittance signature is preferable for monitoring the stiffness growth of the real-world mass concrete. The cumulated RMSD methods and the developed prediction function can be employed to predict the in-situ compressive strength. The prediction results are acceptable.

The research team has also conducted trial implementations on construction projects. Almost a hundred sensors were embedded into the concrete pavement on interstate highways (I-70, I-74, and I-465) to monitor the real-time strength development of concrete from 1 hour to 3 days. To compare the mechanical result versus the predicted strength via EMI sensing, the compressive strength tests were conducted on cylinder samples on days 1 and 3. The results indicated that for one-day strength testing, the in-situ concrete strength measured by EMI results is higher than that of small cylinder specimens. This can be explained due to the higher hydration rate of mass concrete than that of cylinder samples. However, the 3rd-day results exhibit that EMI sensing results are a bit lower than compressive test because the water evaporation speed of field concrete pavement was higher than the cylinder samples. The sensing results may better reflect the real curing condition of concrete pavement; however, the final approval needs to be done by conducting in-place compressive testing along with EMI sensing.

In conclusion, this study has proved the feasibility of using EMI sensing to determine the real-time compressive strength of the concrete pavement. The piezoelectric material-based EMI sensing method shows a great promise for monitoring the in-situ strength and stiffness development of concrete. To verify our data and field implementation results a large lab test needs to be conducted to compare the EMI sensing results on concrete pavement with in-place cast cylinder samples. The advanced algorithm, such as machine learning-based methods may be applied to incorporate the factors aforementioned. In the meanwhile, more data should be collected to enhance the accuracy and verify the repeatability of this method.

REFERENCES

- ACI Committee 228. (2003). *In-place methods to estimate concrete strength* (ACI 228.1R-03). American Concrete Institute. http://dl.mycivil.ir/dozanani/ACI/ACI%20228.1R-03%20In-Place%20Methods%20to%20Estimate%20Concrete%20Strength_MyCivil.ir.pdf
- ACI Committee 228. (2019). *Report on methods for estimating in-place concrete strength* (ACI 228.1R-19). American Concrete Institute.
- American Concrete Pavement Association. (2013). *What are the strength tests that can be performed on concrete specimens, and how do they relate to one another? Flexural tests* [Webpage]. http://1204075.sites.myregisteredsite.com/Concrete_Pavement/Technical/FATQ/Construction/Strength_Tests.asp
- American Concrete Pavement Association. (2015, June 18). *Maturity testing* [Webpage]. http://wikipave.org/index.php?title=Maturity_Testing
- Annamdas, V. G. M., & Rizzo, P. (2010, March 31). Monitoring concrete by means of embedded sensors and electromechanical impedance technique. In *SPIE Smart Structures and Materials + Nondestructive Evaluation and Health Monitoring Proceedings*, 7647, 8. <https://doi.org/10.1117/12.847687>
- Ghafari, E., Yuan, Y., Wu, C., Nantung, T., & Lu, N. (2018, May 20). Evaluation the compressive strength of the cement paste blended with supplementary cementitious materials using a piezoelectric-based sensor. *Construction and Building Materials*, 171, 504–510. <https://doi.org/10.1016/j.conbuildmat.2018.03.165>
- Grisso, B. L., & Inman, D. J. (2010 June). Temperature corrected sensor diagnostics for impedance-based SHM. *Journal Sound and Vibration*, 329(12), 2323–2336. <https://doi.org/10.1016/j.jsv.2009.04.007>
- Gu, H., Song, G., Dhonde, H., Mo, Y. L., & Yan, S. (2006, November 2). Concrete early-age strength monitoring using embedded piezoelectric transducers. *Smart Materials and Structures*, 15(6), 1837–1845. <https://doi.org/10.1088/0964-1726/15/6/038>
- Humboldt Construction Materials and Testing Equipment. (n.d.). *Windsor HP probe system* [Photograph]. <https://www.humboldtmg.com/windsor-hp-probe-system-2.html>
- Kim, J.-W., Lee, C., Park, S., & Koh, K.-T. (2013 August). Real-time strength development monitoring for concrete structures using wired and wireless electro-mechanical impedance techniques. *KSCE Journal of Civil Engineering*, 17(6), 1432–1436. <https://doi.org/10.1007/s12205-013-0390-1>
- Kong, Q., Hou, S., Ji, Q., Mo, Y. L., & Song, G. (2013 July). Very early age concrete hydration characterization monitoring using piezoceramic based smart aggregates. *Smart Materials and Structures*, 22(8), 085025. <https://doi.org/10.1088/0964-1726/22/8/085025>
- Lu, X., Lim, Y. Y., & Soh, C. K. (2012). A novel electro-mechanical impedance-based model for strength development monitoring of cementitious materials. *Structural Health Monitoring*, 17(4), 902–918. <https://doi.org/10.1177/1475921717725028>
- Narayanan, A., & Kocherla, A., & Subramaniam, K. V. L. (2017 November). Embedded PZT sensor for monitoring mechanical impedance of hydrating cementitious materials. *Journal of Nondestructive Evaluation*, 36(64). <https://doi.org/10.1007/s10921-017-0442-4>
- Negi, P., Chakraborty, T., Kaur, N., & Bhalla, S. (2018 April). Investigations on effectiveness of embedded PZT patches at varying orientations for monitoring concrete hydration using EMI technique. *Construction and Building Materials*, 169, 489–498. <https://doi.org/10.1016/j.conbuildmat.2018.03.006>
- Papworth Construction Testing Equipment. (n.d.). *IntelliRock III concrete maturity loggers* [Photograph]. <http://www.pcte.com.au/intellirock-wireless-and-intellirock-live>
- Park, G., Sohn, H., Farrar, C. R., & Inman, D. J. (2003). Overview of piezoelectric impedance-based health monitor-

- ing and path forward. *Shock and Vibration Digest*, 35(6), 13. http://ssslab.kaist.ac.kr/article/pdf/2003_Overview.pdf
- Providakis, C. P., Liarakos, E. V., & Kampionakis, E. (2013 April). Nondestructive wireless monitoring of early-age concrete strength gain using an innovative electromechanical impedance sensing system. *Smart Materials Research*, 2013(5–6), 932568. <https://doi.org/10.1155/2013/932568>
- Shin, S. W., Qureshi, A. R., Lee, J.-Y., & Yun, C.-B. (2008, July 18). Piezoelectric sensor based nondestructive active monitoring of strength gain in concrete. *Smart Material Structure*, 17(5). <https://doi.org/10.1088/0964-1726/17/5/055002>
- Soh, C. K., & Bhalla, S. (2005, June 29). Calibration of piezo-impedance transducers for strength prediction and damage assessment of concrete. *Smart Materials and Structures*, 14(4), 671–684. <https://doi.org/10.1088/0964-1726/14/4/026>
- Spalvier, A., Bittner, J. A., Hall, K., & Popovics, J. S. (2019 May). Comparison of core and in-place compressive strengths for early-age concrete. *ACI Materials Journal*, 116(3), 63–72. <https://doi.org/10.14359/51715584>
- Su, Y.-F., Han, G., Amran, A., Graham S. T., & Lu, N. L. (2019). *Investigating polymer coated piezo-ceramic sensor for the very early strength monitoring of cementitious materials* [Conference presentation]. SPIE Smart Structures + Nondestructive Evaluation, Denver, CO. <https://www.spiedigitallibrary.org/conference-proceedings-of-spie/10970/1097022/Investigating-polymer-coated-piezo-ceramic-sensor-for-the-very-early/10.1117/12.2513977.full?webSyncID=7a49dab6-a0cb-ad05-9329-ad883c9d902b&sessionGUID=c9993ced-268b-ead4-9a28-531ab0d3a6b0>
- Su, Y.-F., Han, G., Amran, A., Nantung, T. E., & Lu, N. (2019, November 20). Instantaneous monitoring the early age properties of cementitious materials using PZT-based electromechanical impedance (EMI) technique. *Construction and Building Materials*, 225, 340–347. <https://doi.org/10.1016/j.conbuildmat.2019.07.164>
- Su, Y.-F., Kotian, R. R., & Lu, N. (2018, November 15). Energy harvesting potential of bendable concrete using polymer based piezoelectric generator. *Composites Part B: Engineering*, 153, 124–129. <https://doi.org/10.1016/j.compositesb.2018.07.018>
- Tawie, R., & Lee, H. K. (2010 September). Monitoring the strength development in concrete by EMI sensing technique. *Construction and Building Materials*, 24(9), 1746–1753. <https://doi.org/10.1016/j.conbuildmat.2010.02.014>
- Tawie, R., & Lee, H. K. (2010 December). Piezoelectric-based non-destructive monitoring of hydration of reinforced concrete as an indicator of bond development at the steel-concrete interface, 40(12), 1697–1703. <https://doi.org/10.1016/j.cemconres.2010.08.011>
- Visalakshi, T., Bhalla, S., & Gupta, A. (2018, January 15). Monitoring early hydration of reinforced concrete structures using structural parameters identified by piezo sensors via electromechanical impedance technique. *Mechanical Systems and Signal Processing*, 99, 129–141. <https://doi.org/10.1016/j.ymsp.2017.05.042>
- Voigt, T., Ye, G., Sun, Z., Shah, S., & Breugel, K. (2005 May). Early age microstructure of Portland cement mortar investigated by ultrasonic shear waves and numerical simulation. *Cement and Concrete Research*, 35(5), 858–866. <https://doi.org/10.1016/j.cemconres.2004.09.004>
- Wang, D. S., Song, H., & Zhu, H. (2014). Embedded 3D electromechanical impedance model for strength monitoring of concrete using a PZT transducer. *Smart Materials and Structures*, 23(11). <https://doi.org/10.1088/0964-1726/23/11/115019>
- Wang, D., & Zhu, H. (2011). Monitoring of the strength gain of concrete using embedded PZT impedance transducer. *Construction and Building Materials*, 25(9), 3703–3708. <https://doi.org/10.1016/j.conbuildmat.2011.04.020>
- Zhang, Y., Zhang, W., She, W., Ma, L., & Zhu, W. (2009, October 25). *Ultrasound monitoring of setting and hardening process of ultra-high performance cementitious materials*, 47, 177–184.

APPENDICES

Appendix A. Additional Data

Appendix B. Publication List

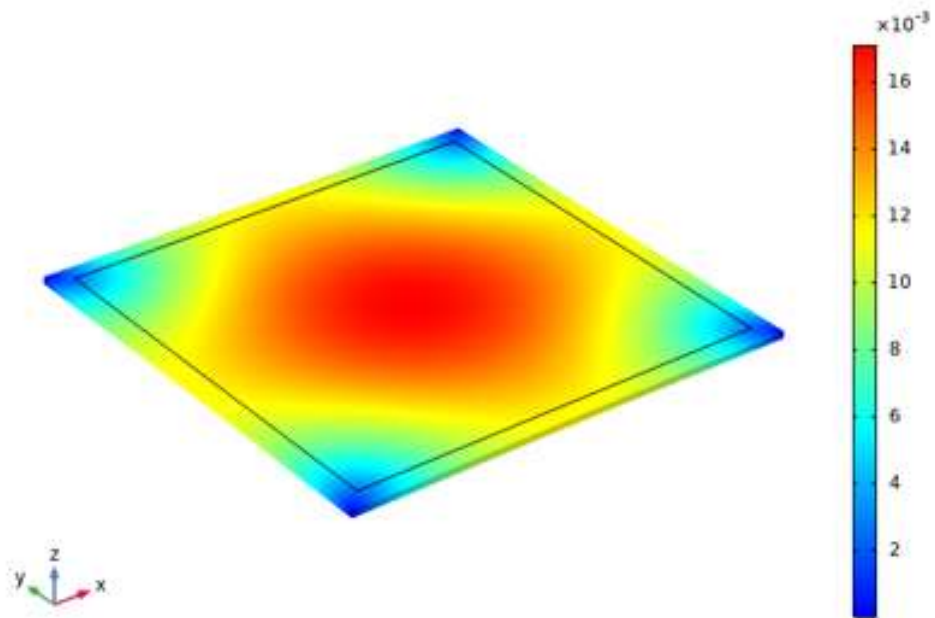
APPENDIX A. ADDITIONAL DATA

Table A.1 Material data of PZT sensor

| | Notation (Unit) | PIC 151 |
|--|--|--------------------|
| Physical and Dielectric Properties | | |
| Density | P (g/cm ³) | 7.8 |
| Curie temperature | T_c (°C) | 250 |
| Relative permittivity (in the polarization direction) | $\epsilon_{33}^T/\epsilon_0$ | 2400 |
| (perpendicular to polarity) | $\epsilon_{11}^T/\epsilon_0$ | 1980 |
| Dielectric loss factor | $\tan\delta$ (10 ⁻³) | 20 |
| Electromechanical Properties | | |
| Coupling factor | k_p | 0.62 |
| | k_t | 0.53 |
| | k_{31} | 0.38 |
| | k_{33} | 0.69 |
| Piezoelectric charge coefficient | d_{31} (10 ⁻¹² C/N) | -210 |
| | d_{33} (10 ⁻¹² C/N) | 500 |
| Piezoelectric voltage coefficient | g_{31} (10 ⁻³ Vm/N) | -11.5 |
| | g_{33} (10 ⁻³ Vm/N) | 22 |
| Acousto-Mechanical Properties | | |
| Frequency coefficients | N_p (Hz · m) | 1950 |
| | N_1 (Hz · m) | 1500 |
| | N_3 (Hz · m) | 1750 |
| | N_t (Hz · m) | 1950 |
| Elastic compliance coefficient | S_{11}^E (10 ⁻¹² m ² /N) | 15.0 |
| | S_{33}^E (10 ⁻¹² m ² /N) | 19.0 |
| Elastic stiffness coefficient | C_{33}^D (10 ¹⁰ N/m ²) | 10.0 |
| Mechanical quality factor | Q_m | 100 |
| Temperature Stability | | |
| Temperature coefficient of ϵ_{33} (in the range -20°C to +125 °C) | $TK \epsilon_{33}$ (10 ⁻³ /K) | 6 |

freq(1)=100 kHz

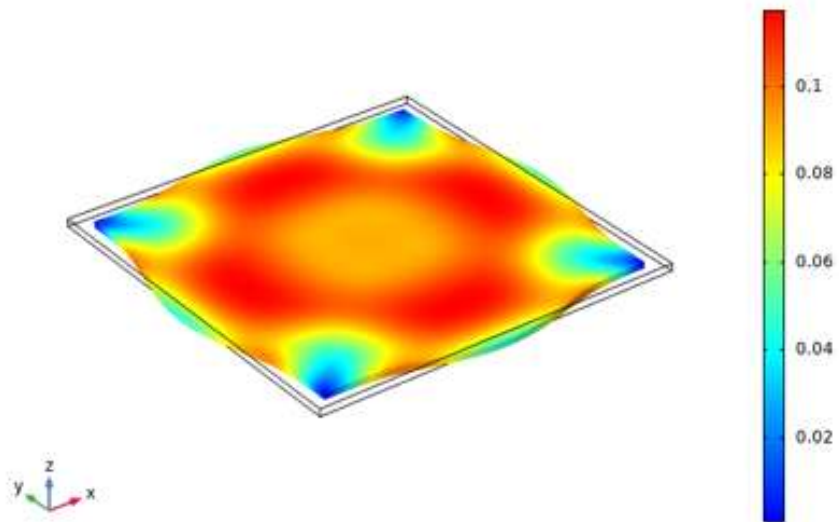
Surface: von Mises stress (MPa)



(a) Frequency=100 kHz

freq(31)=250 kHz

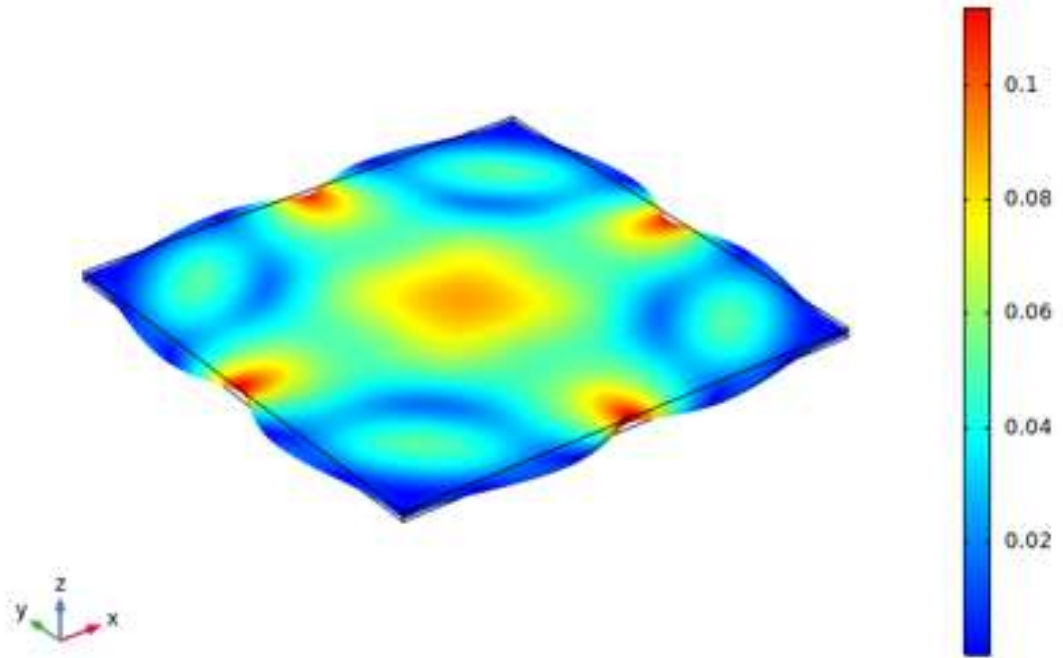
Surface: von Mises stress (MPa)



(b) Frequency=250 kHz

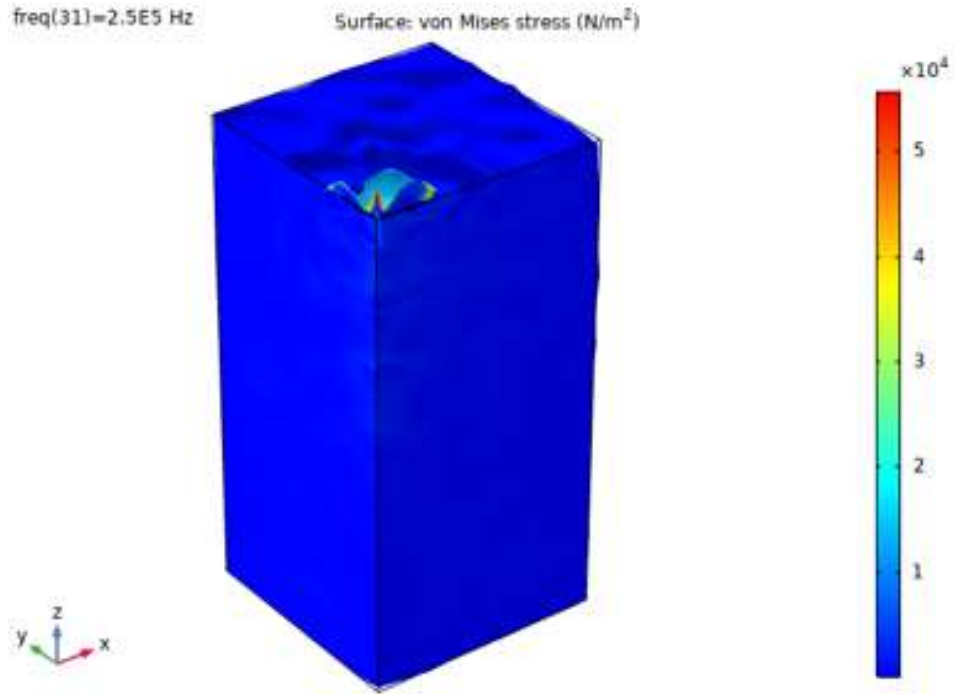
freq(61)=400 kHz

Surface: von Mises stress (MPa)

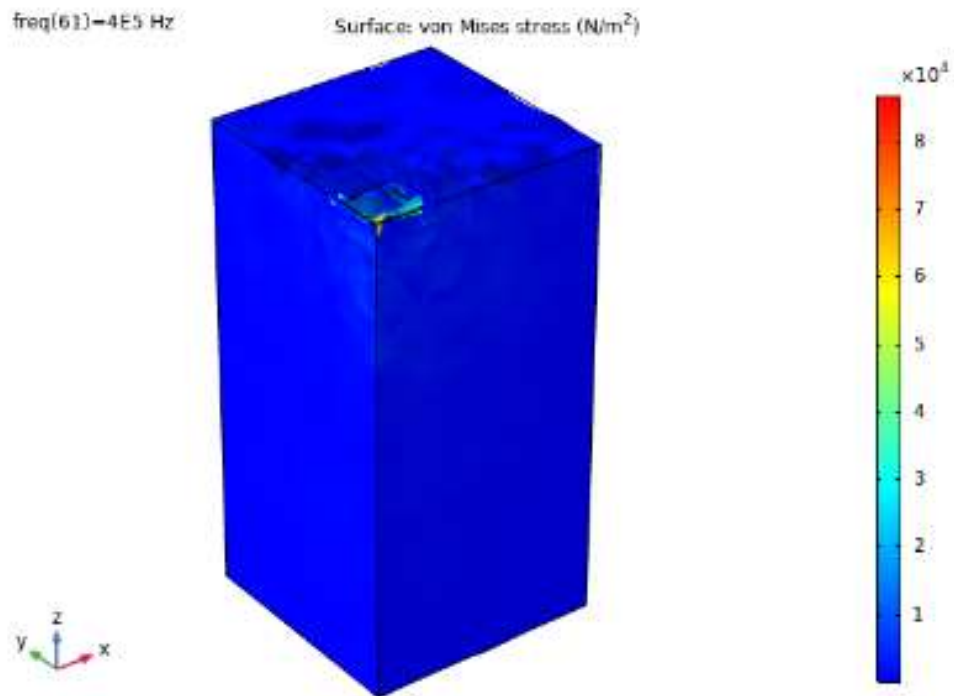


(c) Frequency=400 kHz

Figure A.1 Stress distribution of free PZT vibrating at a different frequency.

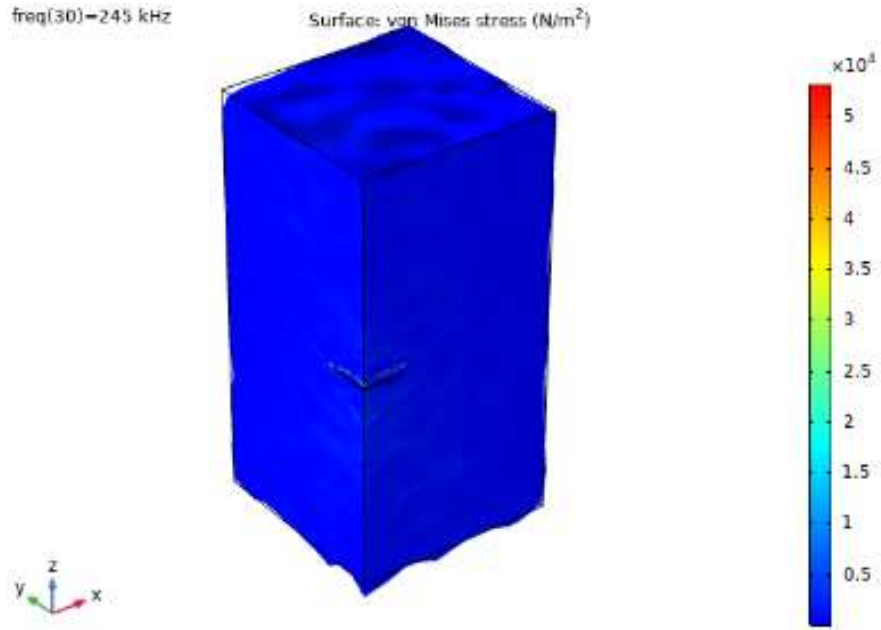


(a) Frequency=250 kHz

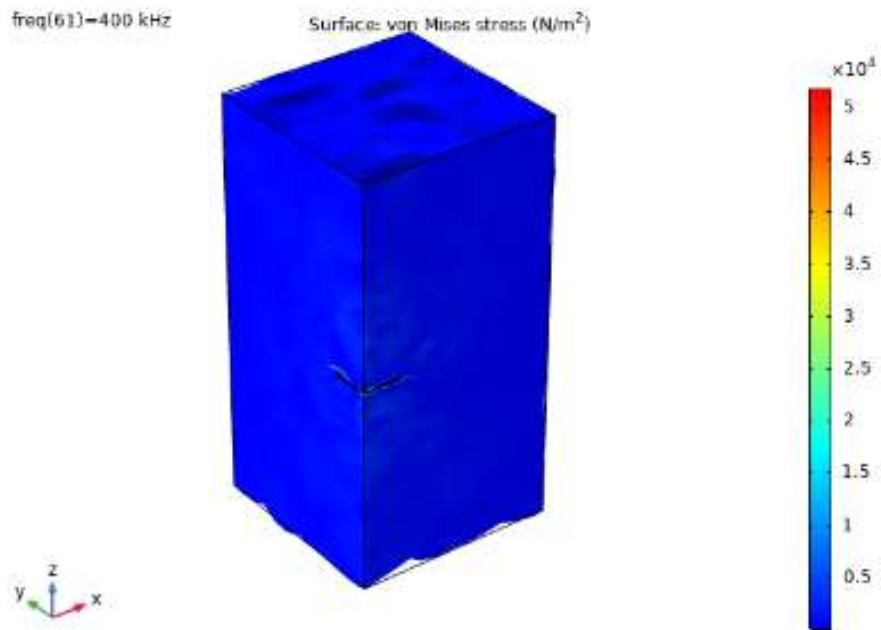


(b) Frequency=400 kHz

Figure A.2 Stress distribution of surface bonding sensor vibrating at different frequency.

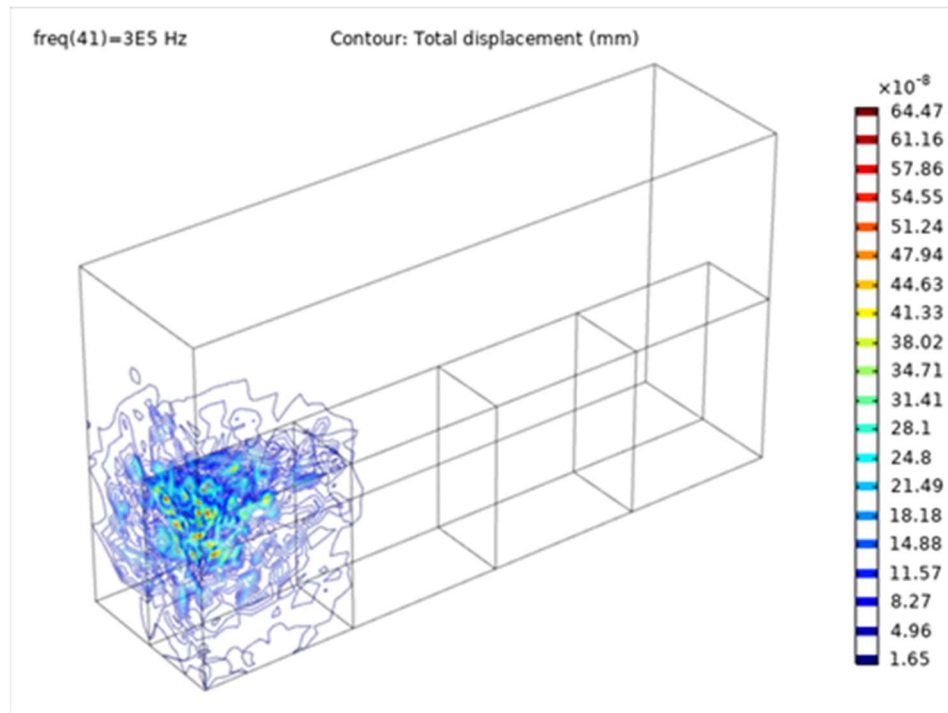


(a) Frequency=250 kHz

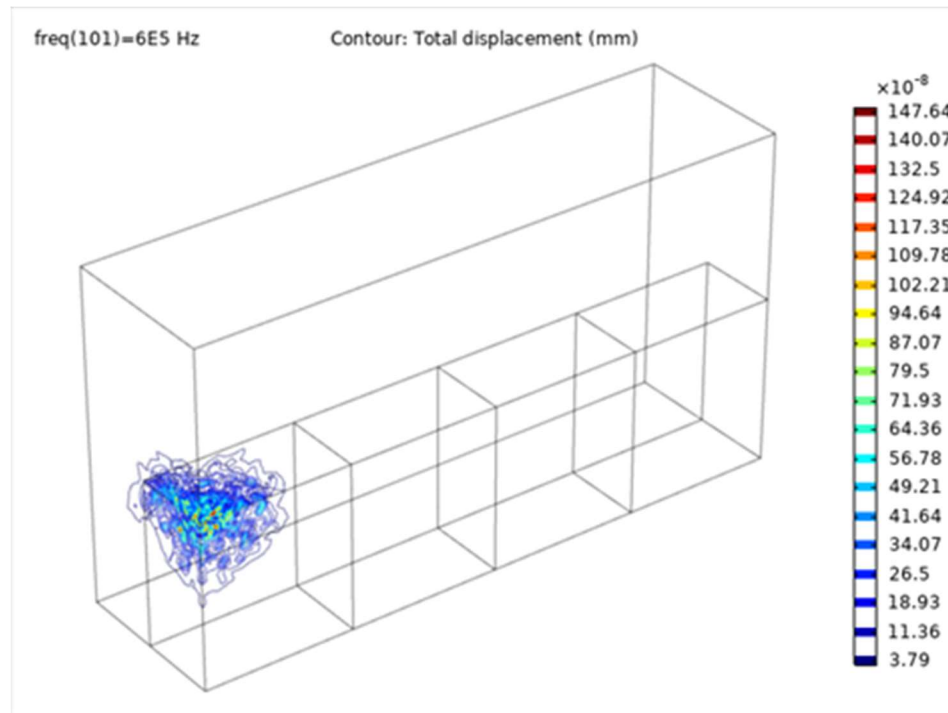


(b) Frequency=400 kHz

Figure A.3 Stress distribution of embedded sensor vibrating at different frequency.



(a) Frequency = 300 kHz

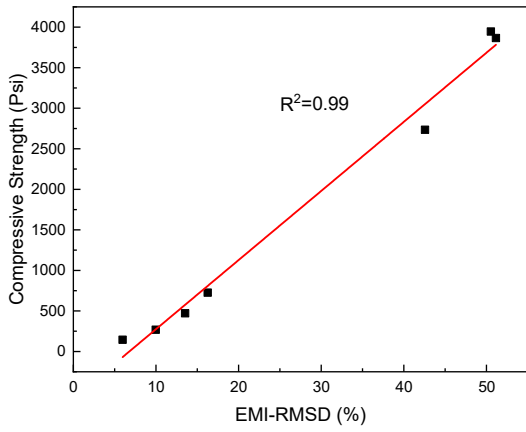


(b) Frequency = 600 kHz

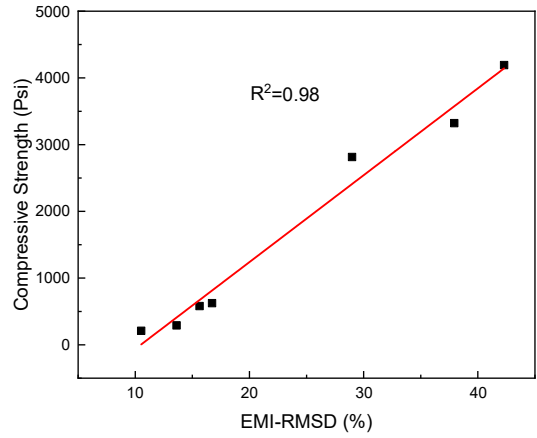
Figure A.4 Iso-contour of the total displacement at different frequency.

Table A.2 Regression result of compressive test versus EMI-RMSD index

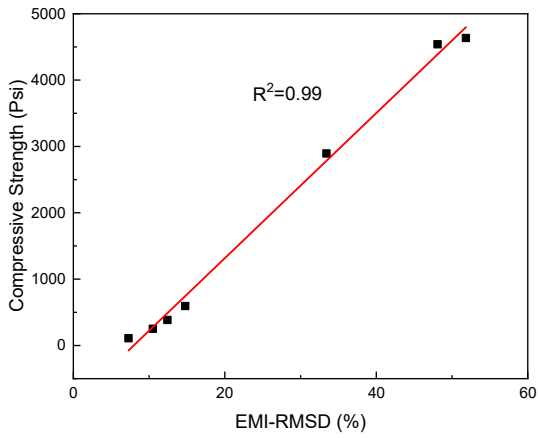
| Mixes | R² (Compression vs. RMSD index) | R² (Elastic Modulus vs. RMSD index) |
|--------------------|---|---|
| Type I, W/C=0.46 | 0.99 | 0.99 |
| Type I, W/C=0.44 | 0.99 | 0.98 |
| Type I, W/C=0.42 | 0.99 | 0.99 |
| Type I, W/C=0.40 | 0.98 | 0.99 |
| Type I, W/C=0.38 | 0.99 | 0.99 |
| Type III, W/C=0.46 | 0.98 | 0.98 |
| Type III, W/C=0.44 | 0.95 | 0.94 |
| Type III, W/C=0.42 | 0.98 | 0.94 |
| Type III, W/C=0.40 | 0.93 | 0.95 |
| Type III, W/C=0.38 | 0.96 | 0.91 |



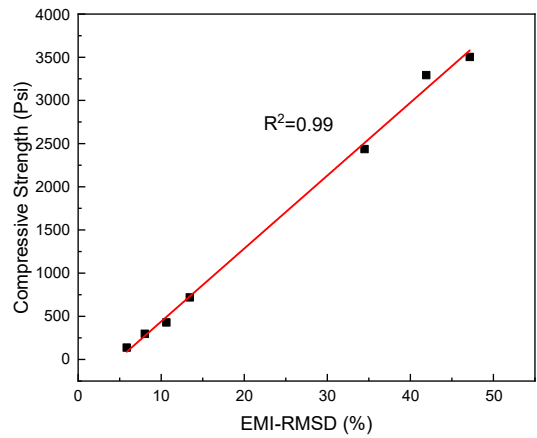
(a) W/C=0.38



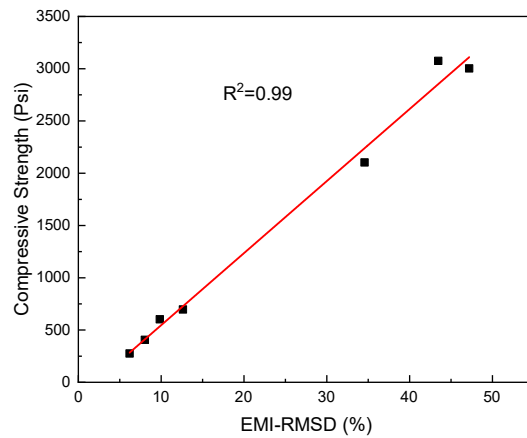
(b) W/C=0.4



(c) W/C=0.42

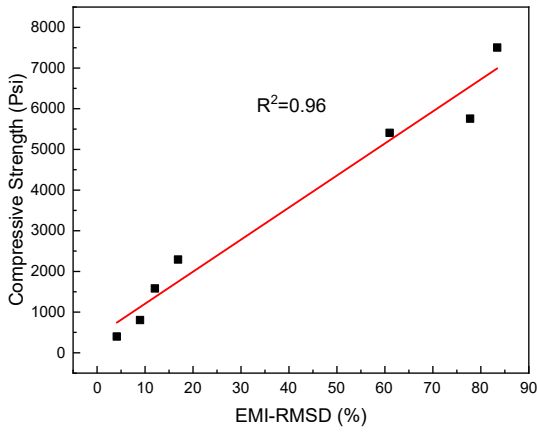


(d) W/C=0.44

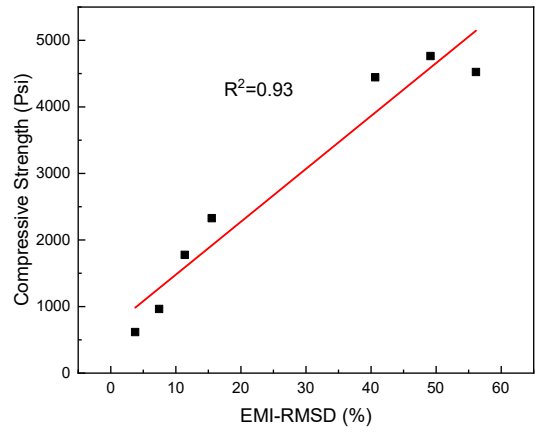


W/C=0.46

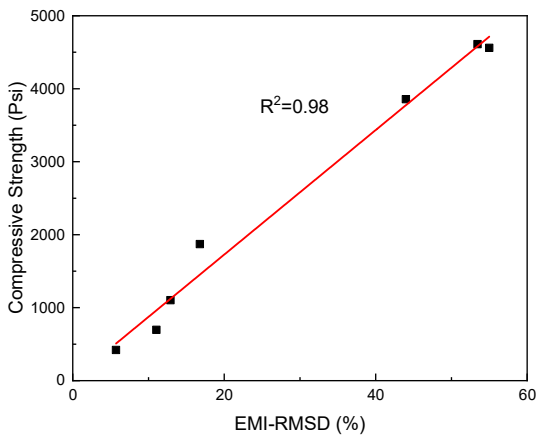
Figure A.5 Type I cement mortar.



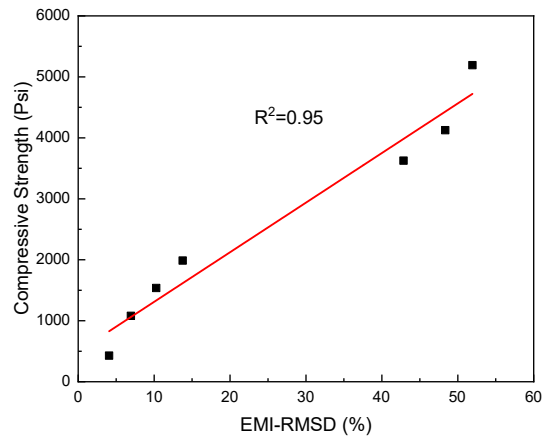
(a) W/C=0.38



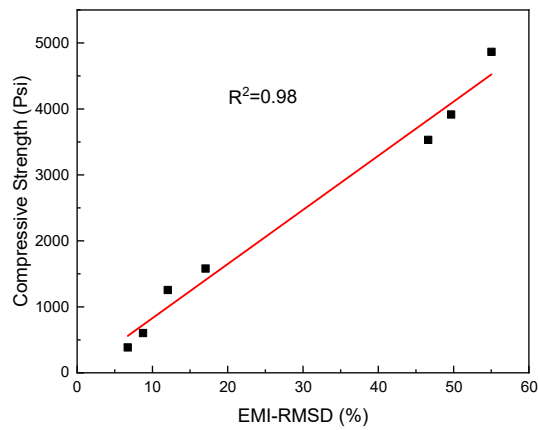
(b) W/C=0.4



(c) W/C=0.42



(d) W/C=0.44

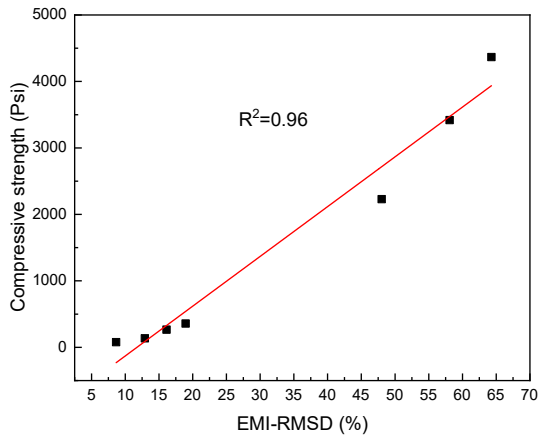


W/C=0.46

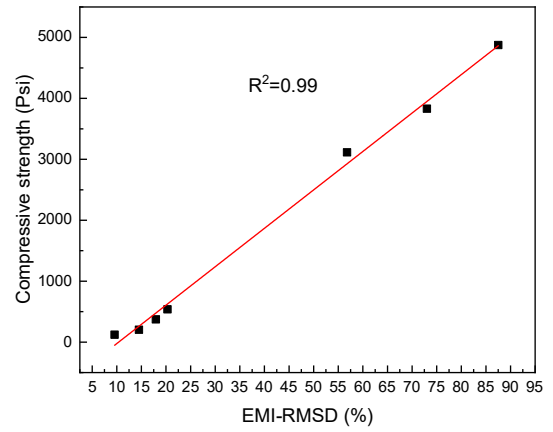
Figure A.6 Type III Cement mortar.

Table A.3 Mixture of the mortar

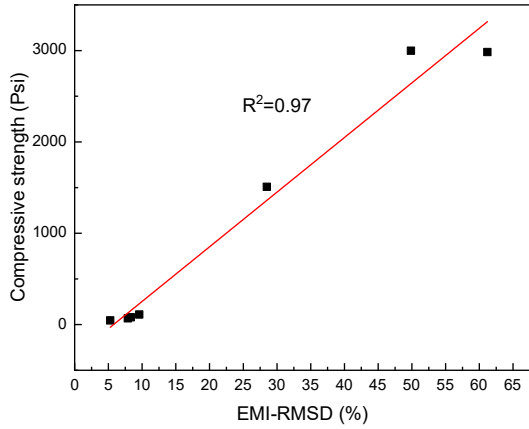
| Mix | Cement (lbs/cyd) | Fly Ash (lbs/cyd) | Silica Fume (lbs/cyd) | Slag (lbs/cyd) | Sand (lbs/cyd) | Water (lbs/cyd) | SCMs Replace (%) |
|----------------|-----------------------------|------------------------------|----------------------------------|---------------------------|---------------------------|----------------------------|-----------------------------|
| Slag-15 | 752.9 | 0.0 | 0.0 | 132.9 | 2657.4 | 397.1 | 15 |
| Slag-25 | 701.3 | 0.0 | 0.0 | 233.8 | 2805.2 | 419.4 | 25 |
| Slag-35 | 607.8 | 0.0 | 0.0 | 327.3 | 2805.2 | 419.6 | 35 |
| SF-15 | 752.9 | 0.0 | 0.0 | 132.9 | 2657.4 | 397.1 | 15 |
| SF-25 | 663.6 | 0.0 | 0.0 | 221.2 | 2654.2 | 396.8 | 25 |
| SF-35 | 574.4 | 0.0 | 0.0 | 309.3 | 2651.0 | 396.5 | 35 |
| FA-15 | 883.7 | 132.6 | 0.0 | 0.0 | 2651.0 | 369.7 | 15 |
| FA-25 | 660.3 | 220.1 | 0.0 | 0.0 | 2641.2 | 396.2 | 25 |
| FA-35 | 570.5 | 307.2 | 0.0 | 0.0 | 2633.0 | 394.9 | 35 |



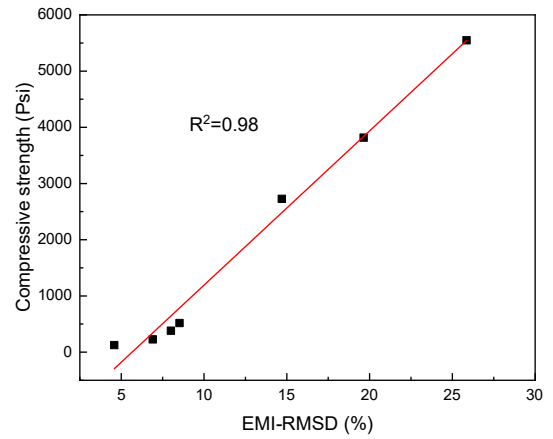
(a) Slag-25



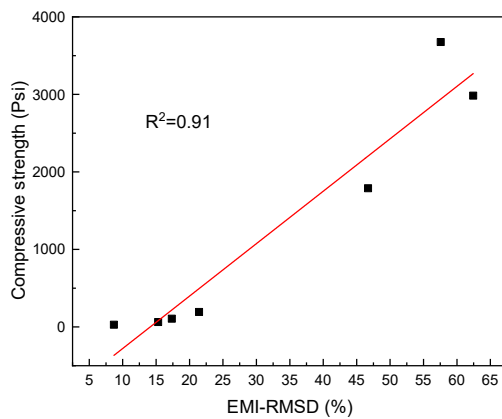
(b) SF-15



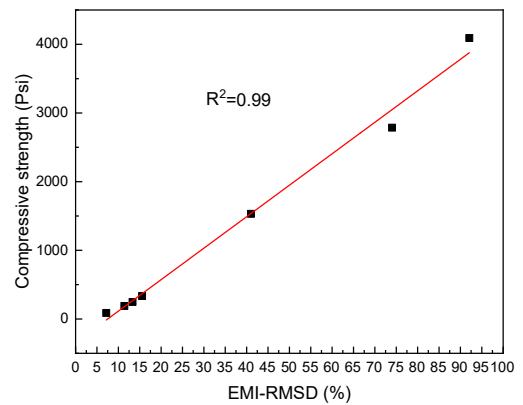
(e) Slag-35



(c) SF-25

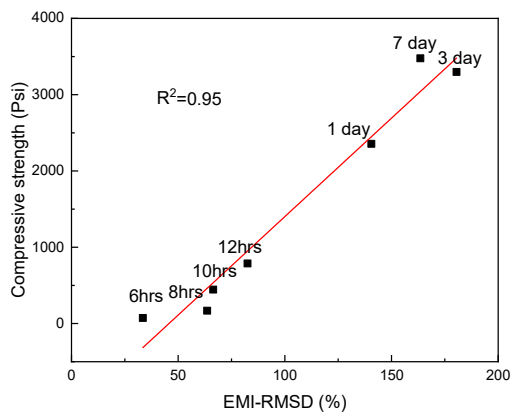


(g) FA-15

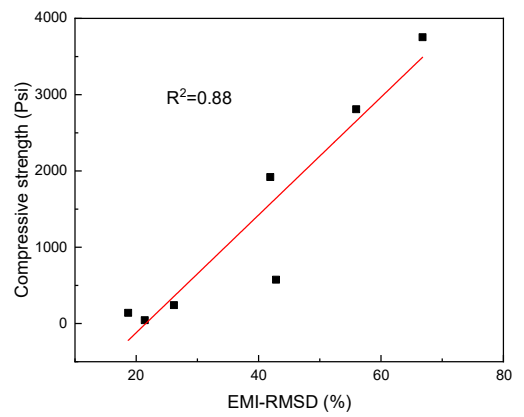


(f) SF-35

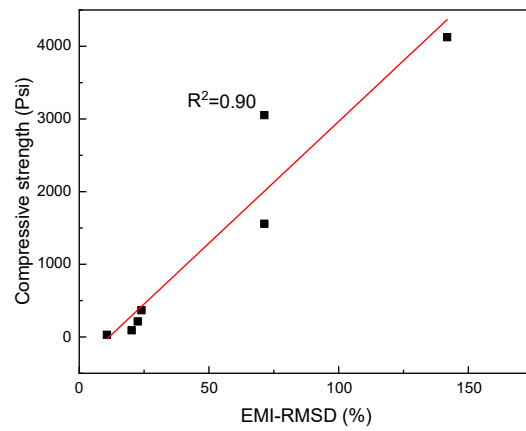
Figure A.7 Regression results of mortar samples with different SCMs using the surface-bonded sensor.



(a) FA-15



(b) FA-25



(c) FA-35

Figure A.8 Regression results of FA mortar with different replacing ratio using the embedded sensor.

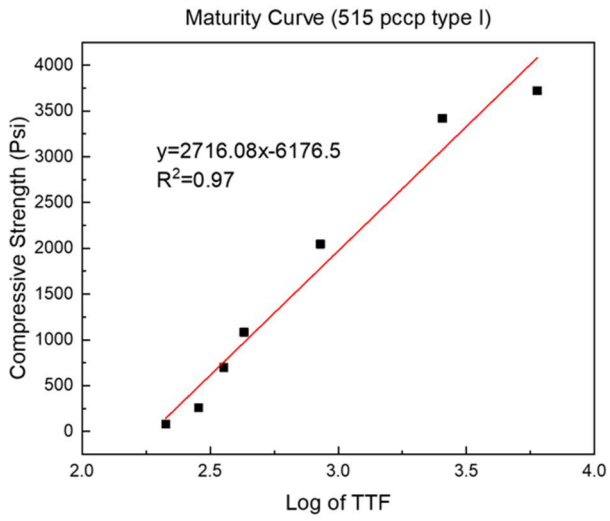
Table A.4 Mixture design (lbs/cyds)

| Cementitious | | Aggregates | | | | | |
|-------------------------------|------------|------------|--------------|--------------|----------------|-----------------------------|-------------------|
| Cement (Type)- SCMs | Fly Ash | Slag | W/B Ratio | Fine Agg. | Coarse Agg. | CA/FA ¹ ratio | SCMs Replaced (%) |
| 515 (I) | — | — | 0.42 | 1459 | 1773 | 1.22 | 0.0 |
| 515 (III) | — | — | 0.42 | 1459 | 1773 | 1.22 | 0.0 |
| 564 (I) | — | — | 0.42 | 1344 | 1800 | 1.34 | 0.0 |
| 564 (III) | — | — | 0.42 | 1344 | 1800 | 1.34 | 0.0 |
| 564 (I)+10%CA ² | — | — | 0.42 | 1344 | 1980 | 1.47 | 0.0 |
| 564 (I)-10%CA ² | — | — | 0.42 | 1344 | 1620 | 1.21 | 0.0 |
| 440 (I) - FA | 70 | — | 0.42 | 1455 | 1769 | 1.22 | 14 |
| 350 (I) - SLAG | — | 200 | 0.42 | 1310 | 1840 | 1.40 | 36 |
| 480 (I) - FA | 120 | — | 0.42 | 1277 | 1687 | 1.32 | 20 |
| 480 (I) - SLAG | — | 120 | 0.42 | 1277 | 1687 | 1.32 | 20 |

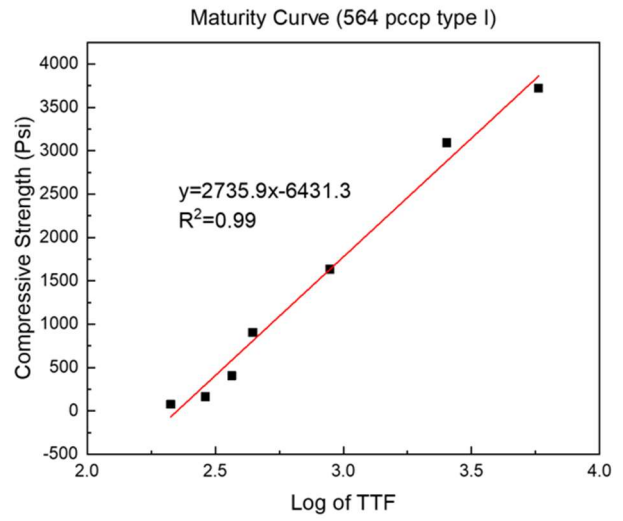
Notes:

¹ CA/FA is the ratio of coarse aggregate to fine aggregate.

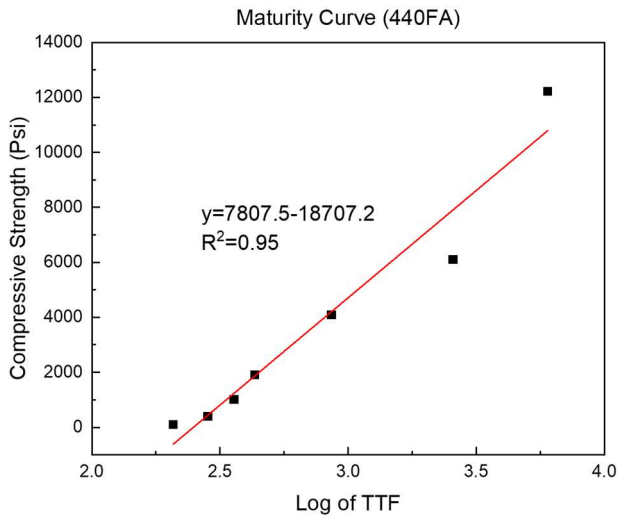
² ±10CA means 10% more or less coarse aggregate compared with 564 (I) mix.



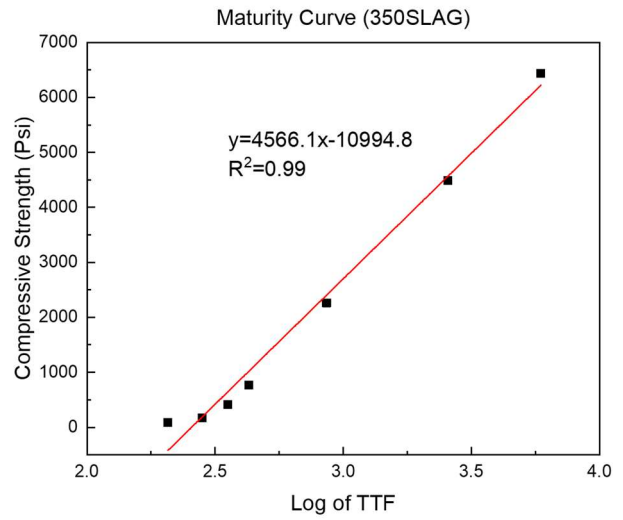
(a) 515 type I



(b) 564 type I

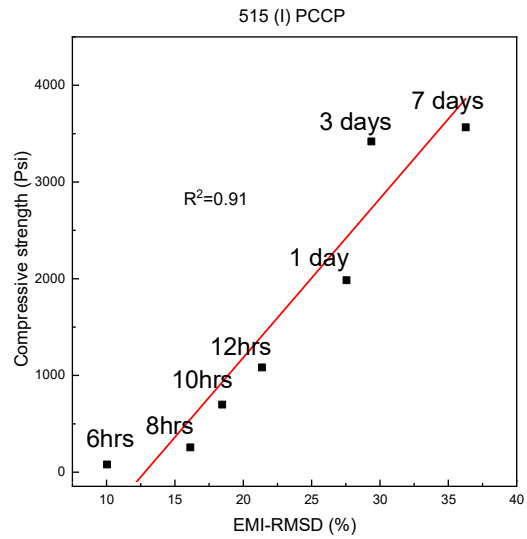


(c) 440FA

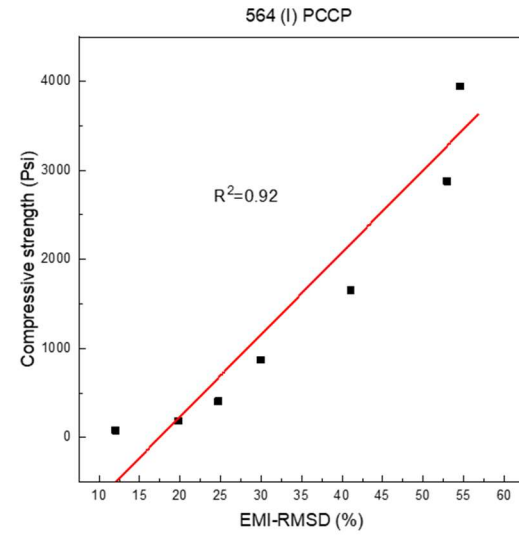


(d) 350 SLAG

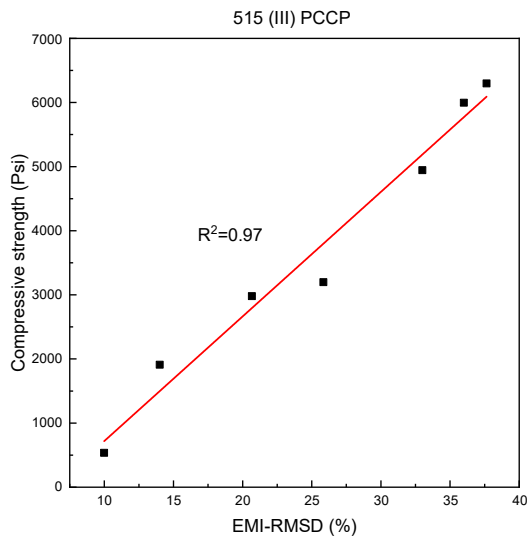
Figure A.9 Maturity curve of concrete.



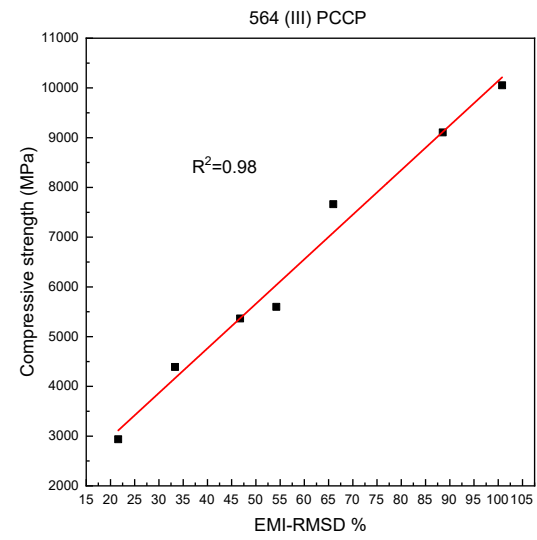
515 (I) PCCP



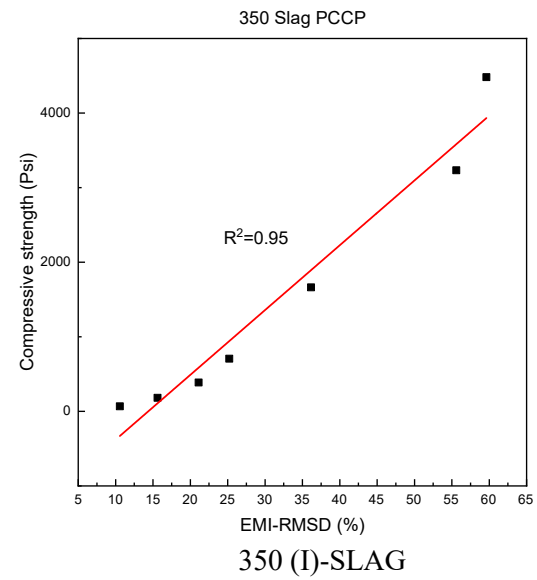
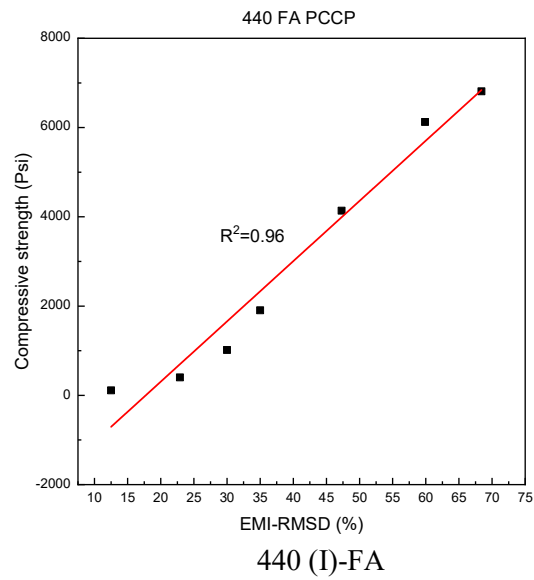
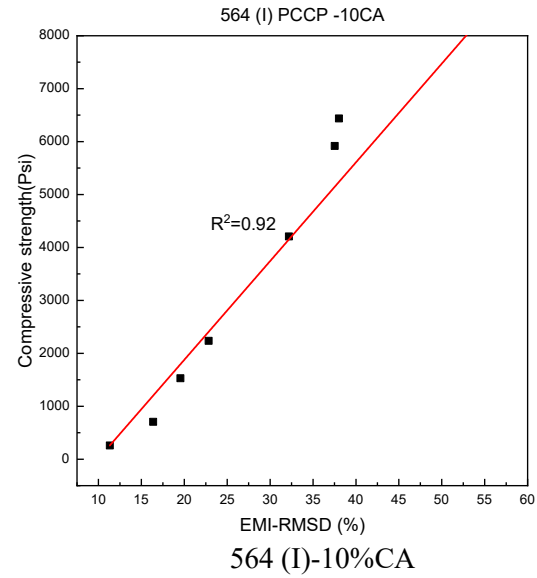
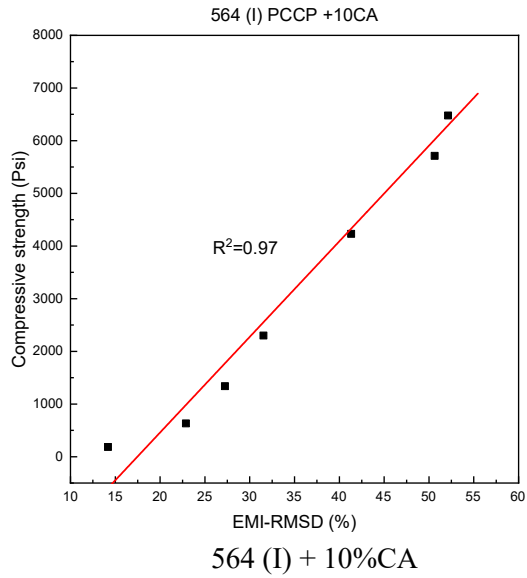
564 (I) PCCP



515 (III)



564 (III)



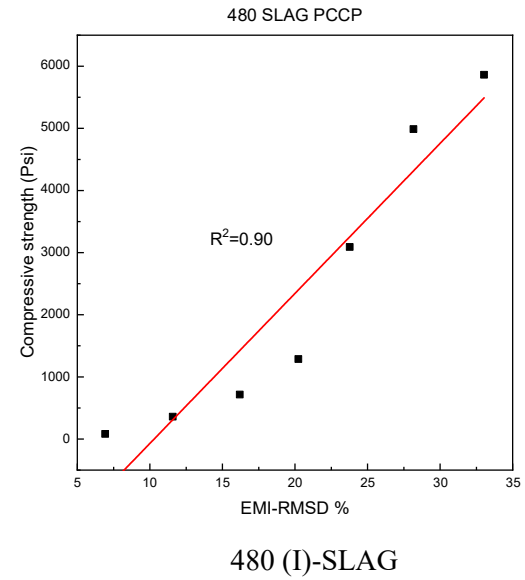
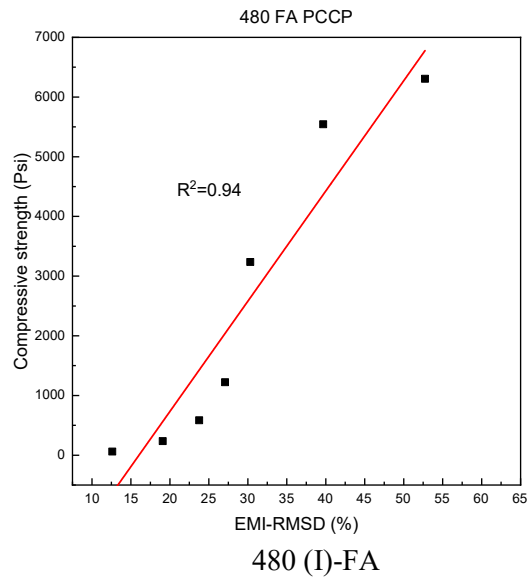


Figure A.10 Regression results of all concrete mixes.

Table A.5 Regression results of different concrete

| Mixes | EMI- R ² |
|---------------|---------------------|
| 515 (I) | 0.91 |
| 515 (III) | 0.97 |
| 564 (I) | 0.92 |
| 564 (III) | 0.98 |
| 564 (I)+10%CA | 0.97 |
| 564 (I)-10%CA | 0.92 |
| 440 (I)-FA | 0.96 |
| 350 (I)-SLAG | 0.95 |
| 480 (I)-FA | 0.94 |
| 480 (I)-SLAG | 0.90 |

Table A.6 Flexural strength of PCCP with different mix design

| Age (day) | 515 Type I (psi) | 564 Type I (psi) | 515 Type III (psi) | 564 Type III (psi) |
|-----------|------------------|------------------|--------------------|--------------------|
| 1 | 625.3 | 375.8 | 937.2 | 795.0 |
| 3 | 719.6 | 1000.0 | 1034.4 | 783.4 |
| 7 | 760.2 | 988.0 | 1089.6 | 811.1 |
| 28 | 773.3 | 1104.1 | 1044.6 | 866.1 |



Figure A.11 Field test location map on I-70.



Figure A.12 Field test location map on I-74.

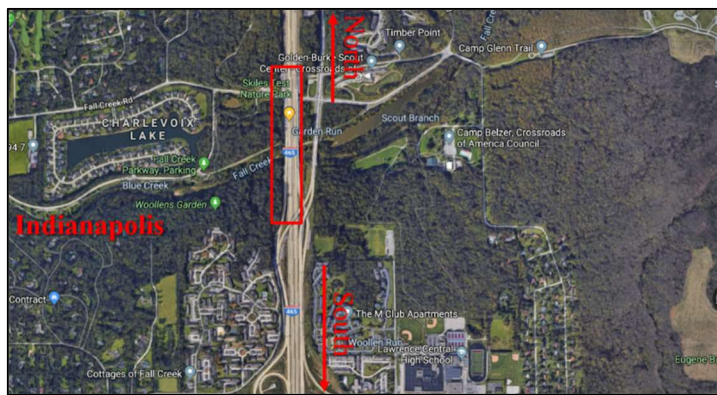


Figure A.13 Field test location map on I-465.



(a) Bonding sensor



(b) Concrete pour



(c) Spraying the curing compound



(d) EMI measuring

Figure A.14 Field test on I-465 concrete patching.

APPENDIX B. PUBLICATION LIST

Journal articles:

Ghafari, E., Yuan, Y., Wu, C., Nantung, T., & Lu, N. (2018, May 20). Evaluation the compressive strength of the cement paste blended with supplementary cementitious materials using a piezoelectric-based sensor. *Construction and Building Materials*, 171, 504–510. <https://doi.org/10.1016/j.conbuildmat.2018.03.165>

Su., Y.-F., Han, G., Amran, A., Nantung, T., & Lu, N. (2019). Instantaneous monitoring the early age properties of cementitious materials using PZT-based electromechanical impedance (EMI) technique. *Construction and Building Materials*, 225, 340–347

Conference presentations:

Su, Y.-F., Han, G., Nantung, T., & Lu, N. (2020). Field implementation of using piezoelectric sensor-based sensing technique for in-situ concrete compressive strength evaluation [Poster presentation]. *TRB 99th Annual Meeting*, Washington, DC.

Su, Y.-F., Han, G., & Lu, N. (2019). Machine learning guided modeling for concrete strength prediction using electromechanical impedance (EMI) technique [Poster presentation]. *The ACI Concrete Convention and Exposition*, Cincinnati, OH.

Su, Y.-F., Han, G., Kong, Z., & Lu, N. (2019). In-situ concrete early age strength monitoring using piezoelectric based sensors [Poster presentation]. *The ACI Concrete Convention and Exposition*, Cincinnati, OH.

Han, G., Su, Y.-F., & Lu, N. (2019). Temperature effect on electromechanical impedance (EMI) method for very early age concrete properties monitoring [Poster presentation]. *The ACI Concrete Convention and Exposition*, Cincinnati, OH.

Su, Y.-F., Han, G., & Lu, N. (2019). A machine-learning based electromechanical impedance (EMI) method for concrete slab strength monitoring [Poster presentation]. *10th Advances in Cement-Based Materials Conference*, Urbana-Champaign, IL.

Han, G., Su, Y.-F., & Lu, N. (2019). Temperature and humidity effect on piezoelectric materials based electromechanical impedance (EMI) method for concrete properties monitoring [Poster presentation]. *10th Advances in Cement-Based Materials Conference*, Urbana-Champaign, IL.

Su, Y.-F., Han, G., Amran, A., Graham, S., & Lu, N. (2019). Investigating polymer coated piezo-ceramic sensor for the very early strength monitoring of cementitious materials [Oral presentation]. *Proceeding of SPIE Smart Structure and NDE*, Denver, CO

Su, Y.-F., Amran, A., Nantung, T., & Lu, N. (2019). Systematically investigation of using electromechanical impedance (EMI) technique for monitoring the very early age properties of cementitious materials [Poster presentation]. *98th TRB Annual Meeting*, Washington DC.



Evaluation the compressive strength of the cement paste blended with supplementary cementitious materials using a piezoelectric-based sensor



Ehsan Ghafari^a, Ying Yuan^{a,b}, Chen Wu^c, Tommy Nantung^d, Na Lu^{a,*}

^a Lyles School of Civil Engineering, School of Materials Engineering, Purdue University, USA

^b Key Laboratory of Road and Traffic Engineering of Ministry of Education, Tongji University, Shanghai 200092, PR China

^c School of Civil Engineering, Fujian University of Technology, Fujian 350118, PR China

^d Indiana Department of Transportation, Office of Research and Development, 1205 Montgomery St, West Lafayette, IN 47906, USA

HIGHLIGHTS

- PZT sensors is effective to monitor the compressive strength gain of cement.
- RMSD and CC index exhibited qualitative trends of strength gain of cement.
- The RMSD is more efficient than CC index in estimating the compressive strength of cement paste.
- The EMI is a reliable NDT method to enable in-situ monitoring strength gain of cement.

ARTICLE INFO

Article history:

Received 19 January 2018

Received in revised form 19 March 2018

Accepted 21 March 2018

Keywords:

Nondestructive testing (NDT)

Piezoelectric sensor

PZT

Electro-mechanical impedance

RMSD

CC

ABSTRACT

This paper aims to investigate the feasibility of using piezoelectric-based sensors to characterize the compressive strength gain process of cement paste blended with supplementary cementitious materials. The electromechanical impedance technique was used for in-situ monitoring of the strength gain of cement pastes. Two different indices of root mean square deviation (RMSD) and correlation coefficient (CC) have been used to establish a quantitative correlation between the conductance signature obtained by lead zirconate titanate (PZT) sensors and the compressive strength of cement paste. Both indices exhibited a reasonable qualitative trend which was compatible with the trend of strength gain of cement pastes. However, the RMSD was found to be more efficient than CC index in estimating the compressive strength of cement paste over time. The experimental results indicate that EMI can be used as a nondestructive testing (NDT) method to enable in-situ measurement of strength gain process of cement paste with supplementary cementitious materials.

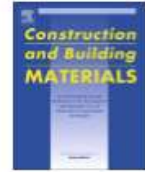
Published by Elsevier Ltd.



Contents lists available at ScienceDirect

Construction and Building Materials

journal homepage: www.elsevier.com/locate/conbuildmat



Instantaneous monitoring the early age properties of cementitious materials using PZT-based electromechanical impedance (EMI) technique



Yen-Fang Su^a, Guangshuai Han^a, Adlan Amran^a, Tommy Nantung^b, Na Lu^{a,c,d,*}

^a Lyles School of Civil Engineering, Sustainable Materials and Renewable Technology (SMART) Lab, Purdue University, 550 Stadium Mall Drive, West Lafayette, IN 47907-2051, USA

^b Office of Research and Development, Indiana Department of Transportation, USA

^c School of Materials Engineering, Purdue University, USA

^d Birck Nanotechnology Center, Purdue University, USA

HIGHLIGHTS

- The comprehensive study of using PZT based EMI method to monitor the properties of cement mortar.
- Experiments were conducted on mortar with various w/c ratio on different cements.
- RMSD is the most efficient index to reflect the stiffness growth of cement mortar.
- The EMI-RMSD index might be independent from the various w/c ratio of cement mortar.

ARTICLE INFO

Article history:

Received 13 March 2019

Received in revised form 11 May 2019

Accepted 17 July 2019

Keywords:

Electromechanical impedance (EMI)

Early age property

Very early age property

Cementitious materials

Compressive strength

Piezoelectric materials

ABSTRACT

The use of piezoelectric materials based Electromechanical Impedance (EMI) technique for monitoring the hydration of cementitious materials has caught much attention recently. However, very few literatures have explored the feasibility of using this method on monitoring the stiffness development and compressive strength gain at the very early age properties (4th–8th h) of cementitious materials. This research serves as a comprehensive study to verify the reliability of using lead zirconate titanate (PZT) based EMI method in monitoring the compressive strength gain and elastic modulus of mortar at both very early age (4th–8th h) and early age (1st, 3rd, and 7th day). Extensive experiments and data analysis have been done on ten different mixes with various water-to-cement ratio and Type I & III cement. The EMI signatures are measured for each sample at the period of interest, and post-processed with three statistical model including the root mean square deviation (RMSD), correlation coefficient deviation (CCD), and mean absolute percentage deviation (MAPD) as indices. To examine the correlation and linearity between the compressive strength/elastic modulus obtained via conventional cubic testing using ASTM C109 and the EMI indices, a linear least square regression analysis is performed. As the authors postulated, all the mixes display a good linear correlation of R^2 . Among all three statistical indices, RMSD index is proved as the most accurate statistical index on strength gain monitoring of cementitious materials. The results indicated the feasibility of using piezoelectric-based EMI method for monitoring the cementitious material's strength gain at very early age, regardless the concrete mix design.

© 2019 Elsevier Ltd. All rights reserved.

About the Joint Transportation Research Program (JTRP)

On March 11, 1937, the Indiana Legislature passed an act which authorized the Indiana State Highway Commission to cooperate with and assist Purdue University in developing the best methods of improving and maintaining the highways of the state and the respective counties thereof. That collaborative effort was called the Joint Highway Research Project (JHRP). In 1997 the collaborative venture was renamed as the Joint Transportation Research Program (JTRP) to reflect the state and national efforts to integrate the management and operation of various transportation modes.

The first studies of JHRP were concerned with Test Road No. 1 — evaluation of the weathering characteristics of stabilized materials. After World War II, the JHRP program grew substantially and was regularly producing technical reports. Over 1,600 technical reports are now available, published as part of the JHRP and subsequently JTRP collaborative venture between Purdue University and what is now the Indiana Department of Transportation.

Free online access to all reports is provided through a unique collaboration between JTRP and Purdue Libraries. These are available at <http://docs.lib.purdue.edu/jtrp>.

Further information about JTRP and its current research program is available at <http://www.purdue.edu/jtrp>.

About This Report

An open access version of this publication is available online. See the URL in the citation below.

Su, Y.-F., Han, G., & Lu, N. (2020). *Determining the optimal traffic opening timing through an in-situ NDT method for concrete early age properties* (Joint Transportation Research Program Publication No. FHWA/IN/JTRP-2020/02). West Lafayette, IN: Purdue University. <https://doi.org/10.5703/1288284317113>